
Traffic Jams

Cluster Formation in Low-Dimensional Cellular Automata Models for Highway and City Traffic

Der Fakultät für Naturwissenschaften
der Universität Duisburg-Essen
(Standort Duisburg)
zur Erlangung des akademischen Grades eines
Doktors der Naturwissenschaften
genehmigte Dissertation von

Robert Barlović
aus Mönchengladbach

Referent: Prof. Dr. rer. nat. Michael Schreckenberg
Korreferent: Priv. Doz. Dr. rer. nat. Ulrich Nowak
Datum der mündlichen Prüfung: 27.10.2003

Contents

1	Preface	9
1.1	Introduction	9
1.2	Outline	10
2	Empirical Findings and Model Approaches	13
2.1	Experimentally Observed Traffic Phases	13
2.1.1	Free-Flow	13
2.1.2	Wide Moving Jams and Stop-and-Go Traffic	14
2.1.3	Synchronized Flow	16
2.2	Phase Transitions: Jam Formation and Pinch Effect	16
2.3	CA Models for Traffic Flow	17
2.3.1	Nagel-Schreckenberg Model	18
2.3.2	Improved Models	20
2.3.3	Krauss Model	21
3	Jamming Dynamics in the VDR Model	23
3.1	VDR Model	23
3.1.1	Update Rules	23
3.1.2	Phase Separation and Fundamental Diagram	24
3.1.3	Jam Formation	25
3.2	Jamming Dynamics	26
3.2.1	Analyzed Scenario – Single Jam	26
3.2.2	Random Walk Theory of Jamming	27
3.2.3	Comparison with Numerical Results – Damage Spreading	30
3.3	Discussion	32
4	Impact of Local Defects in the VDR Model	35
4.1	Definition of the Defect	35
4.2	Occurring Phases	36
4.2.1	VDR Phase – Small Defect Noise: $p_d \ll p$	37
4.2.2	Stop-and-Go Phase – Large Defect Noise: $p_d \gg p$	38
4.2.3	Transition Regime: $p_d \approx p$	39
4.3	Density Autocorrelation	39
4.4	Relevance for Systems with Ramps	41
4.5	Discussion	41
5	Open Boundaries in the VDR Model	43
5.1	Extremal Current Principle	43
5.2	Definition of the Boundaries	44
5.3	Analytical Results for the Inflow	45
5.4	Simulation Results	46

5.4.1	Fundamental Diagram	47
5.4.2	NaSch Model: $p_0 = p$	48
5.4.3	Partially Deterministic VDR Model: $p_0 > 0, p = 0$	50
5.4.4	Stochastic VDR Model: $p_0 > p > 0$	55
5.4.5	Application: Flow Optimization	57
5.5	Discussion	58
6	Modelling City Traffic with Cellular Automata	61
6.1	Traffic States in City Networks – Two-Fluid Model	61
6.2	Cellular Automata Models for City Traffic	62
6.2.1	BML Model	62
6.2.2	CA Online Simulation	64
6.3	Chowdhury-Schadschneider Model	65
6.4	Traffic Light Control	68
6.4.1	Fixed Signal Control	68
6.4.2	Adaptive Signal Control	69
7	Global Traffic Light Control in the ChSch Model	71
7.1	Synchronized Traffic Lights	71
7.1.1	One Single Street ($N = 1$)	72
7.1.2	Low Density – Phenomenological Approach	73
7.1.3	Extension to Large Networks ($N \times N > 1$)	77
7.1.4	High Density	77
7.1.5	Optimal Fundamental Diagram	79
7.2	Green Wave Strategy	81
7.2.1	Offset Parameter	81
7.2.2	Low Densities	82
7.2.3	High Densities – Red Wave	83
7.2.4	Optimal Fundamental Diagram	84
7.3	Random Offset	86
7.3.1	Low Densities	86
7.3.2	High Densities	86
7.3.3	Optimal Fundamental Diagram	87
7.4	Comparison with the Two-Fluid Model	89
7.5	Discussion	90
8	Adaptive Traffic Light Control in the ChSch Model	93
8.1	Switching Based on Queue Length	93
8.2	Switching Based on Waiting Time	95
8.3	Switching in Analogy to a Neural Network	97
8.4	Discussion	99
9	Traffic Light Control in the ChSch Model with Inhomogeneous Densities	101
9.1	Impact of Turning	101
9.1.1	Synchronized Traffic Lights	102
9.1.2	Green Wave	104
9.1.3	Random Offset	105
9.1.4	Switching Based on Queue Length	106
9.1.5	Switching Based on Waiting Time	107
9.1.6	Switching in Analogy to a Neural Network	108

9.2	Inhomogeneous Densities	108
9.2.1	Synchronized Traffic Lights	109
9.2.2	Switching Based on Queue Length	110
9.2.3	Switching Based on Waiting Time	111
9.2.4	Switching in Analogy to a Neural Network	112
9.3	Discussion	113
10	Summary and Outlook	115
	Bibliography	119
	Zusammenfassung und Ausblick	131
	Kurzfassung	135
	Danksagung	137
	Lebenslauf	139
	Erklärung	141

Abstract

Cellular automata (CA) models are quite popular in the field of traffic flow. They allow an effective implementation of real-time traffic computer-simulations. Therefore, various approaches based on CA models have been suggested in recent years.

The first part of this thesis focuses on the so-called VDR (velocity-dependent randomization) model which is a modified version of the well known Nagel-Schreckenberg (NaSch) CA model. This choice is motivated by the fact that wide phase separated jams occur in the model. On the basis of random walk theory an analytical approach to the dynamics of these separated jam clusters is given. The predictions are in good agreement with the results of computer simulations and provide a deeper insight into the dynamics of wide jams which seem to be generic for CA approaches and are therefore of special interest. Furthermore, the impact of a localized defect in a periodic system is analyzed in the VDR model. It turns out that depending on the magnitude of the defect stop-and-go traffic can occur which can not be found in the VDR model without lattice defects. Finally, the VDR model is studied with open boundaries. The phase diagrams, obtained by Monte-Carlo simulations, reveal two jam phases with a stripped microscopic structure and for finite systems the existence of a new high-flow phase is shown.

The second part of this thesis concentrates on CA models for city traffic with the focus on the Chowdhury-Schadschneider (ChSch) model.

In the context of jam clusters the model reveals interesting features since two factors exert influence on the jamming behavior. On the one hand, jams are induced at crossings due to the traffic lights, i.e., cars are forced to stop at a “red light”, and, on the other hand, the dynamics of such induced jams is governed by the NaSch model rules. One part of the investigations covers global (fixed) traffic light strategies. These are found to lead to strong oscillations in the global flow except for the case of randomly switching lights. Furthermore, the impact of adaptive (local) traffic light control is analyzed. It is found that the autonomous strategies can nearly match the *global* optimum of the ChSch model. In order to provide a more realistic vehicle distribution, the ChSch model is enhanced by a stochastic turning of vehicles and by inhomogeneous densities. Here, the autonomous strategies can outperform the global ones in some cases.

1 Preface

1.1 Introduction

From a theoretical and practical point of view traffic jams are one of the most interesting phenomena of vehicular traffic, but for all they are annoying for the everyday driving experience and have an immense negative economic impact. These days big cities like Tokyo, Paris, or New York suffer from heavy traffic congestion that can not be managed offhand. Also preferred highways often operate beyond their capacities. In Europe for example during the holiday seasons jams may grow up to more than 100 km in size. However, since mobility is substantial for a modern society a further growing traffic volume is expected. In the most cases this additional amount of traffic can not be compensated by the extension of infrastructure due to financial, environmental, and social constrains. Thus, it is eligible to use existing structures as effective as possible. For this purpose a proper understanding of the jamming processes is indispensable.

In regard to the formation of traffic jams two cases can be distinguished: Most of the jams are induced by external influences, e.g., bottlenecks, lane reductions, intersections, and in urban areas by traffic lights or signs. Additionally, jams can emerge spontaneously without any obvious external influence. This effect was first observed by Treiterer [151] who analyzed a series of aerial photographs. These so-called “phantom jams” may be formed due to spontaneous velocity fluctuations or lane changes, leading to an avalanche-like cascade of braking maneuvers. Traffic jams are easily identifiable localized patterns (compact clusters) of almost standing vehicles that move upstream, i.e., against the driving direction. Experimentally, several characteristic properties and even “universal” parameters were observed [84]. One of the most astonishing facts is that the upstream propagation velocity of the jam front is approximately constant at about 15 km/h, independent of the road conditions. This can lead to peculiar jam patterns like the parallel movement of two wide jams over long time periods and road sections.

In 1935, Greenshields [49] started to study vehicular traffic maybe anticipating the upcoming traffic demand. Then in the 1950s, there was a huge amount of publications motivated by the rapidly growing traffic demand leading more and more frequently to jams. The engineers at that time put much effort into understanding the dynamics of traffic flow and formulating mathematical descriptions of the occurring phenomena.

Also for physicists the understanding of transportation processes within the framework of complex many particle systems represents an challenging problem. The concepts and techniques of statistical physics can be used in this context to develop efficient traffic models incorporating the most essential ingredients which are necessary to describe the features of real traffic. Moreover, the theoretical analysis and computer simulations of these models provide a deep insight not only into the properties of the models, but also into the complex phenomena observed in real traffic.

There are two different concepts for modelling vehicular traffic. In the “macroscopic” fluid-dynamical description, traffic is viewed as a compressible fluid formed by vehicles that do not appear explicitly in the theory. In contrast, in the “microscopic” models traf-

fic is treated as a system of interacting particles focussing mainly on individual vehicles and the interactions between them. Both approaches are based on methods used for the description of classical many-particle systems.

Many of the “microscopic” approaches developed in recent years are formulated using cellular automata (CA). Among them, the NaSch model is the most popular one. This model is minimal since it only describes basic features of real traffic flow. However, various modifications have been suggested to obtain a more realistic description. Recent models are even able to reproduce empirical single-vehicle data.

1.2 Outline

The outline of this thesis is as follows: The first part focuses on cluster formation in one-dimensional CA models, investigated with the help of Monte-Carlo simulations. In order to provide a point of reference to real traffic for the results obtained a brief overview of the empirical facts concerning traffic states and especially traffic jams is given in chapter 2. Furthermore, the most common CA models are introduced and discussed with regard to their jamming properties.

A main part of this thesis considers the jamming dynamics in the VDR (velocity-dependent randomization) model. Therefore, in chapter 3 the VDR model is presented and its most important features are illustrated. In this context an analytical approach is given to determine characteristic dynamical quantities of wide jams in the model. These results are of further interest since the jamming dynamics of the VDR model is generic for other CA approaches.

The impact of a localized defect in the VDR model is investigated in chapter 4. This can be described as the competition between two mechanisms of phase separation. On the one side, a high-density regime (congested traffic) pinned at the defect and free-flow in the rest of the system is formed. On the other side, compact clusters are generated at the defect moving upstream. The interplay between these two elements of congestion leads, besides other effects, to stop-and-go traffic which can not be found in the VDR model without lattice defects.

To complete the investigations on the VDR model the effects of open boundaries are further studied. This is presented in chapter 5. The VDR model exhibits metastable high-flow states. These can not be analyzed with the standard vehicle insertion procedure since such high flows can not be prepared. Therefore, a new insertion strategy is defined that allows to access all states, i.e., the complete phase diagram of the model. The analysis presented reveals a lot of new features with regard to the jamming dynamics. As a new result the existence of a new phase with a very high flow, dominated by one single large jam, is shown. Another important aspect is that the results are in agreement with an extremal current principle for the flow which relates the phase diagram of an open system to the fundamental diagram of a periodic system.

The second part of this thesis is primarily concerned with the traffic of city networks. In chapter 6 some basic empirical facts of city traffic are discussed and a brief overview about CA models for city traffic is given. In this context the Chowdhury-Schadschneider (ChSch) model for city traffic is introduced. The ChSch model exhibits two features concerning the jam dynamics: Jams are induced at crossings due to the red traffic lights or spontaneously due to the model dynamics. However, once they are formed, these jams move through the system according to the model rules and have an immense impact on the overall network flow.

To obtain some insight into these interactions the impact of global traffic light control is analyzed in chapter 7 with the aim to optimize the flow in the network. It turns out that the global flow strongly oscillates in the ChSch model. These strong oscillations can be explained by a heuristic approach in good agreement to the numerical results.

In order to allow a greater flexibility, the ChSch model is enhanced by an offset parameter so that traffic lights are not enforced to switch simultaneously anymore. The offset parameter is used to implement a two-dimensional “green wave” in the network. This leads to an improved flow, surprisingly also for high densities. Furthermore, the impact of a “random offset” in the switching between the intersections is considered. This completely suppresses the oscillations and seems applicable if a control strategy is required which is not sensitive to the adjustment of cycle times.

For the investigated strategies the optimal cycle times are obtained by a systematical analysis. Thereby, the most important result is that the “green wave” strategy matches the *global* optimum of the ChSch model. Thus, it can be used as a performance reference for any investigated strategy.

In addition, in chapter 8 the influence and benefits of an autonomous traffic light control, i.e., traffic lights are able to react to the local traffic demand, is analyzed. It turns out that the suggested strategies are very valuable since in some cases they can nearly match the “system optimum”. Moreover, the suggested algorithms are kept simple, i.e., the parameters used can easily be obtained in real traffic so that the results may be transferred to real networks.

In order to provide a more realistic vehicle distribution in the network inhomogeneous density distributions are also analyzed in chapter 9. These are realized in one case by allowing a stochastic turning of vehicles and in another case by fixed density differences along the two directions of the network. It is found that in the most cases the flow is situated below the system optimum for the global as well as for the adaptive strategies. Nevertheless, it is shown that in some cases the adaptive strategies can outperform the global strategies and nearly match the system optimum even for inhomogeneous densities.

2 Empirical Findings and Model Approaches

Traffic jams can be distinguished into two classes: Those induced by external influences, e.g., bottlenecks, lane reductions, or intersections (see [27, 58, 59, 62, 101]), and spontaneous jams, sometimes called phantom jams, caused by velocity fluctuations. The later effect was first shown empirically by Treiterer [151] who examined a series of aerial photographs of a highway. More recent measurements on German highways by Kerner and coworkers [84] revealed the existence of phase separated wide moving jams in conjunction with homogeneous metastable states with a high throughput. Experimentally, they observed several characteristic features of wide moving jams. These quantities are nowadays regarded as important parameters of highway traffic which can be used, for example, to calibrate theoretical models. In addition to homogeneous states and wide traffic jams a further phase of vehicular traffic on highways was found. Empirical observations showed the existence of so-called synchronized traffic states [74, 86]. It must be mentioned that the nature of these traffic states is still under a vivid debate. For an overview see [53, 54, 61, 76, 79, 144, 163].

In the following a brief introduction of the empirically observed traffic phases is given and common CA models are discussed with the focus on jamming in highway traffic. The origin of jamming in city networks is different and will be discussed in chapter 6.

2.1 Experimentally Observed Traffic Phases

The analysis of traffic flow data reveals the existence of three different traffic states. These are (a) free-flow, (b) wide moving jams, and (c) synchronized traffic. This arrangement into three different traffic states, the so-called “Three Phase Traffic Theory”, was proposed by Kerner [80, 81]. These three traffic phases are briefly discussed in the following with regard to their relevance concerning traffic jams. In a historical context, the first attempts to characterize traffic, carried out by Greenshields [49] in 1935, allow only a rough distinction between free flowing vehicles and congested traffic. Much effort has been made in recent years to complete the picture of traffic dynamics.

Nowadays, a huge amount of traffic data from highways is available. This allows a statistically relevant analysis of traffic flow, giving insight even into the microscopic driving behavior of single vehicles. However, some caution seems necessary keeping in mind that the empirical data are collected from complex traffic networks. This complicates the interpretation of the results and may be a reason for controversial opinions concerning the different traffic states. Further, it must be considered that most of the results discussed here were obtained from German highways so that country specific corrections may be expected.

2.1.1 Free-Flow

In traffic theory the free-flow phase is characterized by free moving vehicles with a high average velocity. Obviously, in this phase no jams occur. It is represented in the funda-

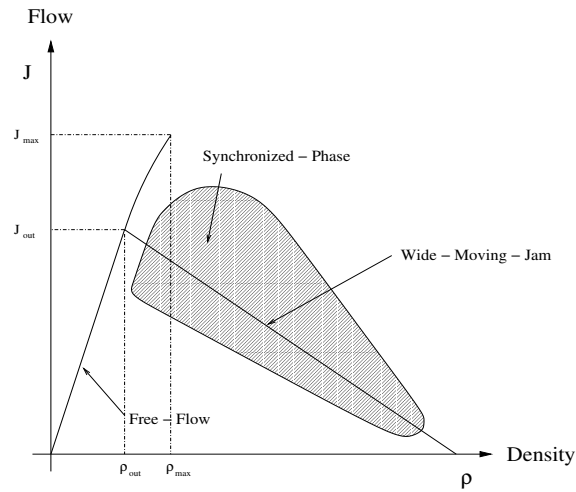


Figure 2.1: Sketch of the FD for a multi-lane road. The free-flow phase is represented by a line with a positive slope. In contrast, wide moving jams are given by the solid line with negative slope. The synchronized states are located in the hatched area. Traffic states above the line corresponding to wide moving jams are assumed to be metastable while traffic states below are stable.

mental diagram (FD) by a line with a positive slope. This line can easily be identified in the FD as shown in Fig. 2.1. The slope of the line is connected to the mean vehicle velocity via the hydrodynamical relation $J = \rho \bar{v}$. Since on German highways cars are not allowed to overtake righthandside, it is more probable that slow cars drive on the right lane. Therefore, the slope of the free-flow line may vary for different lanes.

In respect to the formation of jams within the free-flow phase two different regimes must be distinguished. Up to densities ρ_{out} no jams can evolve on the streets and small jams formed due to disturbances dissolve quickly. Above ρ_{out} , the free-flow state is assumed to be metastable, i.e., a local disturbance may lead to a breakdown of the free-flow traffic so that a phase transition into a congested traffic state occurs [75–77, 80, 84]. The metastable free-flow states are characterized by a high maximum flow J_{max} with a typical ratio of $J_{\text{max}}/J_{\text{out}} = 1.5$ compared with the jam outflow J_{out} . The transition from the metastable free-flow state to a jammed traffic state will be discussed in this chapter below.

2.1.2 Wide Moving Jams and Stop-and-Go Traffic

In contrast to free-flow traffic (jam free) congested traffic is characterized by different kinds of jams and does not belong to the free-flow line of the FD.

One of the well known phenomena of congested traffic are stop-and-go waves. Their empirical properties have been studied by many authors [33, 57, 93, 99, 107]. It can be assumed that stop-and-go waves are nonlinear since no characteristic frequency is present. In detail, an analysis of the power spectrum of the wavelength reveals white noise at high frequencies ω and a power law ω^θ with $\theta \approx 1.5$ for low frequencies [108, 109]. The power law is interpreted as *self-organized criticality* in respect to the formation of traffic jams [121]. However, it has been found empirically that the average wavelength of jams

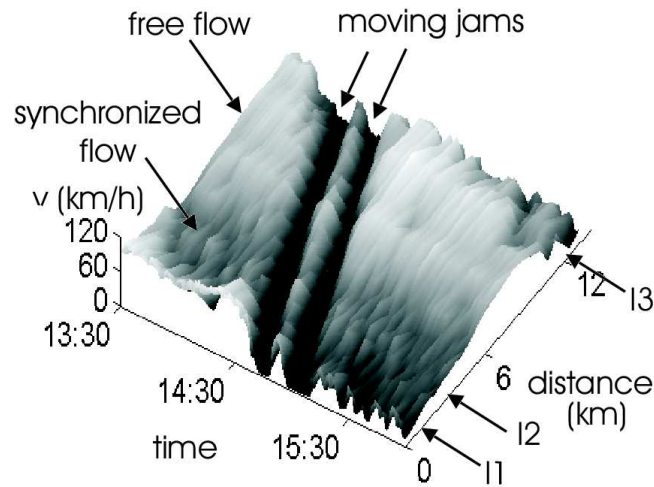


Figure 2.2: The coexistence of wide moving jams, due to the universality of the jam outflow, is shown for a section of the German highway A5. The two jams move through synchronized traffic and free-flow either without disturbing these states. The figure is taken from [78].

corresponding to their width varies between 2.5 km and 5 km. The corresponding wave period (lifetime) is between 4 min and 20 min.

Recently, the emergence of stop-and-go traffic was traced back to the so-called pinch effect in synchronized traffic [74, 80], i.e. the compression of synchronized traffic can lead to stop-and-go traffic in the course of a phase transition from synchronized flow to the formation of a wide moving jam. Therefore, the phenomenon of stop-and-go traffic is not itemized more explicitly here but rather seen in the context of jam formation in synchronized traffic in correspondence to the “Three Phase Traffic Theory”.

A wide moving jam is an upstream moving compact cluster that is restricted by two jam fronts. Inside the jam the velocity of vehicles and hence the flow is negligibly small. Moreover, due to the sharp decline of the flow the two jam fronts are decoupled so that there is no correlation between the jam inflow and the jam outflow. Wide moving jams are represented in the FD (see Fig. 2.1) by a characteristic line with a negative slope. The slope is equal to the velocity of the downstream moving jam front. This propagation velocity seems to be a “universal constant” of traffic with a typical value of 15 km/h for German highways. Apart from the propagation velocity of wide jams Kerner and Rehborn [84] found several further characteristic parameters that only slightly depend on the external conditions, e.g., average vehicle length, truck fraction, or weather. These parameters are the density ρ_{jam} inside of jams, the outflow J_{out} from jams, and the density ρ_{out} downstream of jams when propagating through free traffic. An characteristic feature of wide moving jams is the unhindered propagation through either free-flow or synchronized flow [79, 80, 90]. If a wide jam propagates through synchronized traffic, the downstream density of the jam front takes on the density of the surrounding traffic leading to complex movements in the FD. Moreover, the universality of the jam outflow can lead to the coexistence of several wide jams moving as a sequence along the road [84] (see Fig. 2.2).

2.1.3 Synchronized Flow

A further common form of congestion is the so-called synchronized traffic. Although, synchronized traffic is jam free in the sense that all vehicles move, it is anyhow important in the context of jamming since traffic jams mostly emerge out of synchronized traffic. The notation “synchronized traffic” was chosen by Kerner and coworkers [85] because of the synchronization of the velocity and the flow among neighboring lanes. However, since this synchronization can also take place in other traffic states, this criterion can not be used solely for the characterization. Mostly, synchronized traffic is observed at bottlenecks like on- and off-ramps [54, 75–77, 80, 84]. Whereas, the velocity variance in the synchronized states is in general lower than in free-flow traffic, probably due to an aggregation of vehicles, three different kinds of synchronized flow can occur: (a) Homogeneous and stationary states where the flow and the velocity are almost stationary; (b) homogeneous-in-speed states where only the velocity is stationary while the flow and the density strongly fluctuate; (c) non-homogeneous and non-stationary states are the most common manifestation. Interestingly, in synchronized traffic no functional flow-density relation can be found but rather flow and density covers a wide area of the FD (see Fig. 2.1). This area is divided by a solid line, this is denoted J , corresponding to the wide moving jams. It is assumed that synchronized states below the line are stable, i.e., no transition to wide moving jams can occur, whereas states above the J line are metastable in the sense that a disturbance can lead to the formation of wide moving jams. Remind that this is also the case for the free-flow phase where states above the intersection point with J are metastable.

2.2 Phase Transitions: Jam Formation and Pinch Effect

It was observed empirically that the transitions between the given traffic phases are “first-order transitions” since they come along with a discontinuous change of traffic observable [74, 78, 85, 86]. Considering the focus of this thesis especially the transition to jams is discussed in the following. The direct formation of jams in free-flow (transition: free-flow \Rightarrow wide jam) is hardly observed [76, 77, 80]. In fact, most jams emerge indirectly out of free-flow, namely out of synchronized states through a sequence of transitions (free-flow \Rightarrow synchronized state \Rightarrow wide jam). Furthermore, the transition from free-flow to synchronized traffic is mainly observed at bottlenecks. Therefore, wide jams also emerge in most cases in the vicinity of bottlenecks, e.g., on- or off-ramps. One possible explanation for the formation of jams in synchronized flow is the so-called pinch effect (transition: synchronized traffic \Rightarrow wide jams). The pinch effect [79, 80] describes a process of local self-compression in synchronized regions, i.e., the pinch region, which can finally lead to the formation of small narrow jams. This small jams can evolve into a wide jam or simply dissolve after a while. This can be compared with a gas-liquid transition where a gas becomes super-critical, if compressed beyond a certain critical density so that even small fluctuations can lead to droplet formation [31, 100]. Note that narrow jams do not show the universal parameters valid for wide jams. As mentioned before, the phase transitions only occur in the region of unstable states above the solid line representing wide moving jams. It is remarkable that the synchronized traffic states are pinned at the bottlenecks while wide jams formed in such a pinch region can leave it moving backwards without disturbing the synchronized area [79, 90]. This is illustrated in Fig. 2.2 where two parallel wide jams move through either synchronized and free-flow.

A hypothesis by Kerner [78] about the nucleation effect, related to the formation of jams, should be mentioned since it matches the empirical observations. It is assumed that dif-

ferent dynamic processes on the road, as overtaking or braking, can lead to the nucleation of vehicles. If a critical amplitude is exceeded this local perturbation can finally initiate a phase transition. The critical amplitude itself depends on the given traffic state. Kerner assumed that the critical amplitude in free-flow traffic is much higher than in synchronized flow, thus wide jams mostly evolve from the synchronized flow state.

2.3 CA Models for Traffic Flow

During the last half of the century various approaches for the description of traffic flow theory have been suggested. These approaches can be separated into coarse grained macroscopic models and into microscopic models where attention is paid explicitly to each single vehicle. In the following, the most common approaches based on CA are introduced since this model class is investigated in this thesis. For a more detailed overview please refer to [20, 58, 61, 144, 163].

CA are discrete dynamical systems whose behavior is completely specified in terms of local relations. More precisely, a CA consists of a regular grid of cells (discrete space), each of them can be in one of a finite number of possible discrete states, updated synchronously (parallel) in discrete time-steps. Obviously, this is an extreme idealization of physical systems, however, well suited for computer simulations.

The concept of CA models was introduced in the 1940's by von Neumann [156]. He was working on a theory of self-replicating computing machines and invented an "universal" computer¹ based on a CA consisting of two hundred thousand cells, each in any of twenty-nine states. However, many years should pass by until CA had their breakthrough due to the huge successes in the development of microcomputers. In 1970 John Horton Conway devised "the game of life" introduced in [45]. The game of life is a simple two-dimensional analogue of basic processes in living systems. The game consists of tracing changes of patterns in time formed by sets of "living" cells arranged in a two-dimensional grid. Any cell in the grid may be in either of two states: "alive" or "dead". The state of each cell changes from one generation to the next depending on the state of its immediate neighbors. The rules governing these changes are designed to mimic population change. Note that the rule-set of "the game of life" is completely deterministic.

Finally, CA became popular in the late 1980's by Wolfram [164] who introduced a family of one-dimensional deterministic CA models by means of a systematic analysis. This CA consist of binary cells (state 1 or 0) allowing only next neighbor interactions. Consequently, there are $2^3 = 8$ possible states (the cell itself and the left and the right neighbor) for the ancestors of any given cell, and these states may result in one of two states (1 or 0), leading to 256 possible rule-sets for this type of CA. Although, the investigated rule-sets are deterministic, Wolfram found a class of rule-sets among them that displayed complex and sometimes long-lived behavior.

In recent years the theory of CA was extended by stochastic rule-sets in order to enlarge the concept to a wider variety of systems [18, 105, 131]. Indeed, the most fascinating aspect of CA models, especially the stochastic ones, is that they can show complex dynamic behavior, including such phenomena as *self-organized criticality* [3, 4, 147, 165], only based on a set of a few simple local update rules.

Due to their simplicity, CA models can be used efficiently for computer simulations. In particular, the investigation of traffic flow systems with its huge complex road networks

¹By the use of logical rules an "universal" computer could emulate any describable function of any other machine.

and enormous number of interacting particles (vehicles) seems to be predestinated for the use of such effective methods. Nowadays, one of the main interests in applications to real traffic is to perform real-time simulations of large networks with access to individual vehicles [161]. Therefore, in the recent years CA models have become quite popular for traffic flow simulations (see [20, 142] for an overview). The first CA model for vehicular traffic was introduced by Cremer and Ludwig [23].

2.3.1 Nagel-Schreckenberg Model

In the spirit of modelling complex phenomena in statistical physics Nagel and Schreckenberg (NaSch) have chosen a minimal set of rules for their model [119] to describe the basic phenomena of real traffic flow, e.g., the occurrence of phantom jams. In the NaSch model the road is divided into cells of length 7.5 m. Each cell can either be empty or occupied by at most one car. The speed v_n of each vehicle $n = 1, 2, \dots, N$ can take one of the $v_{\max} + 1$ allowed integer values $v_n = 0, 1, \dots, v_{\max}$. The state of the road at time $t + 1$ can be obtained from that at time t by applying the following rules for all cars at the same time (parallel dynamics):

- Step 1: *Acceleration*:
 $v_n \rightarrow \min(v_n + 1, v_{\max})$
- Step 2: *Braking*:
 $v_n \rightarrow \min(v_n, d_n - 1)$
- Step 3: *Randomization with probability p* :
 $v_n \rightarrow \max(v_n - 1, 0)$
- Step 4: *Driving*:
 $x_n \rightarrow x_n + v_n$

Here, x_n denotes the position of the n -th car and $d_n = x_{n+1} - x_n$ the distance to the next car ahead. The density of cars is given by $\rho = N/L$, where L is the length of the system, i.e., the number of cells. One time-step corresponds to approximately 1 s in real-time.

In particular, with regard to jam formation the stochastic element p in *Step 3* plays an integral part. It reflects the overreaction of drivers when braking, accelerating, or even cruising. Thereby, the overreaction during the breaking process can lead in a chain reaction to the formation of a traffic jam. If a spontaneously decelerated vehicle does not manage to return to its previous velocity, the next car may approach and has to brake as well and so on. Consequently, this process strongly depends on the density $\rho = \frac{N}{L}$ in the system. If the density is high enough, the overreacting successors may get slower and slower, until finally a vehicle has to stop and a jam emerges “spontaneously” without any obvious external reason only due to the internal dynamics.

Jamming Transition

Several attempts [25, 34, 47, 103, 135, 137, 143, 154] have been made to explain the nature of the transition between the free-flow phase and the jammed phase of the NaSch model. Eisenblätter *et al.* [34] studied an order parameter $m(\rho)$ that was introduced by [154]. They investigated spatial correlations in order to obtain a consistent picture for the jamming transition. The order parameter describes the density of nearest-neighbor pairs

$$m = \frac{1}{L} \sum_{i=1}^L n_i n_{i+1} \quad (2.1)$$

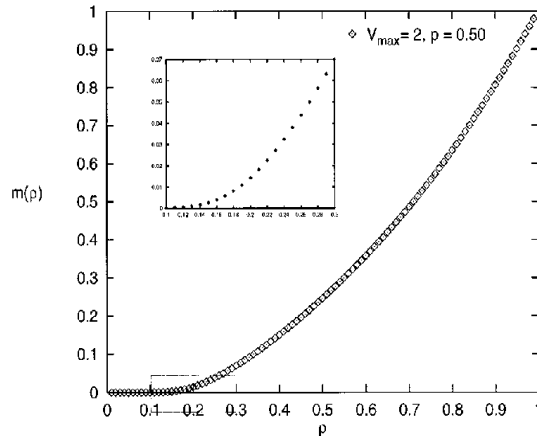


Figure 2.3: The density dependence of the order parameter for the NaSch model (taken from [34]). Here, no clear identification of a transition density is possible.

with $n_i = 0$ for an empty cell and $n_i = 1$ for a cell occupied by a car. Their measurements revealed that only in the deterministic limit $p = 0$ the transition shows critical behavior, i.e., a sharp transition of the order parameter $m(\rho)$ and a diverging correlation length, whereby the critical transition density in this special case is equal to the density of maximum flow given by $\rho_c = \frac{1}{v_{\max}+1}$. Note that in the deterministic limit of the NaSch model no spontaneous jams emerge. However, in the presence of noise $p > 0$ the transition of the order parameter $m(\rho)$ is smeared out (see Fig. 2.3) and shifted towards smaller densities with increasing values of p . Furthermore, it was found that the maximum correlation length diverges as $1/\sqrt{p}$ independent of the velocity. Therefore, the long-range correlations are destroyed by the noise even for small p . This suggests that the jamming transition in the NaSch model is not critical except for its deterministic limit. Another aspect supporting the absence of critical behavior for $p > 0$ is the fact that the transition density ρ_c is smaller than the density corresponding to the maximum flow although one should expect that the state with the strongest correlations is also the state with the highest flow. Gerwinski and Krug [47] derived an approximation for the transition density for $p > 0$. By taking into account that fluctuations might add up they calculated the following expression for the transition density: $\rho_c \approx \frac{1-p}{v_{\max}+1}$. This expression is clearly below the point of maximum deterministic flow.

Jam Formation

Nagel and Paczuski [121] studied the formation of traffic jams far downstream of a megajam in the “cruise control limit” of the NaSch model where vehicles move deterministically after they reach their maximum velocity. Here, the outflow from a large jam self organizes to the maximum throughput. They showed that small perturbations in the outflow can lead to jams of all sizes. This is an example for *self-organized criticality* (SOC). The emerging jams show a power law distribution $P(t) \approx t^{-3/2}$ of lifetimes t , where the number of jammed vehicles n scales as $t^{1/2}$. In fact, this exponent corresponds to the first return time exponent for an one-dimensional random walk.

Moreover, they analyzed the branching of jams in terms of a cascade equation. This leads

to the suggestion that random walk theory is valid up to logarithmic corrections for the cruise control limit of the NaSch model.

In this context it should be reminded that criticality is absent in the original NaSch model. Here, one finds a pure exponential decay for the jam cluster size distribution [34]. This is also supported by an earlier investigation of Nagel [118], where it was shown that a cutoff in the lifetime distribution of jams near $\tau_c = 10.000$ exists in the NaSch model. Only for times smaller than the cutoff time the lifetime distribution appears to decay algebraically. At this point it must be mentioned that also controversy views exist. Roters *et al.* [135] investigated the dynamical structure factor of the NaSch model for $p > 0$ and found some evidence for critical behavior. However, their results are anyhow consistent with the statements from above since the investigated lifetimes, contributing to the structure factor, are much smaller than the cutoff and lie well in the region where an algebraic decay was found.

Jam Dynamics

So far the transition from free-flow to jammed vehicles in the NaSch model and its cruise control variant was briefly discussed. However, for sufficiently large densities jams are surely present moving backwards through the system. Neubert *et al.* [124] investigated density correlations in order to determine the velocity of such upstream moving jams in several CA models for traffic flow including the NaSch model. The method used is suitable to calculate this value without the necessity to define a jam. This is beneficial for models with complex density profiles. Furthermore, their results can be used to calibrate the models since the velocity of wide moving jams is a known quantity of real traffic as discussed in the beginning of this chapter.

2.3.2 Improved Models

As mentioned before, the NaSch model is the simplest known CA that can reproduce the basic phenomena encountered in real traffic, e.g., the occurrence of spontaneous traffic jams. On the other hand, the NaSch model is not able to explain all phenomena found in traffic flow. Therefore, modifications have been suggested to obtain a more realistic description. The main part of this thesis is about the jamming dynamics in the NaSch model with velocity-dependent randomization (VDR model [9]) introduced in the next chapter. The VDR model exhibits metastable free-flow states and large phase separated jams that are understood to be an important ingredient for realistic traffic flow models. However, further approaches were suggested in the last years to enhance the degree of realism of CA traffic models. Recently Knospe *et al.* [87, 89] proposed a high fidelity CA model (BL model) for highway traffic being able to reproduce even empirical single-vehicle data [91, 125]. In order to allow a more realistic modelling of car characteristics like different acceleration capabilities and car lengths they reduced the standard NaSch cell length from $l = 7.5$ m to $l = 1.5$ m. Additionally, a slow-to-start rule was implemented as in the VDR model and a velocity anticipation term was introduced. Furthermore, dynamical long-range interactions were included by braking lights (therefore the notation BL model). A recent CA approach by Kerner *et al.* [83] introduces a new kind of speed adaption between vehicles. This model seems to be consistent with the “Three Phase Traffic Theory” discussed in the beginning of this chapter. Concerning the VDR model it is important to point out that the formation of wide jams in the BL model as well as in the CA approach by Kerner *et al.* is implemented using the same mechanisms as the VDR model.

2.3.3 Krauss Model

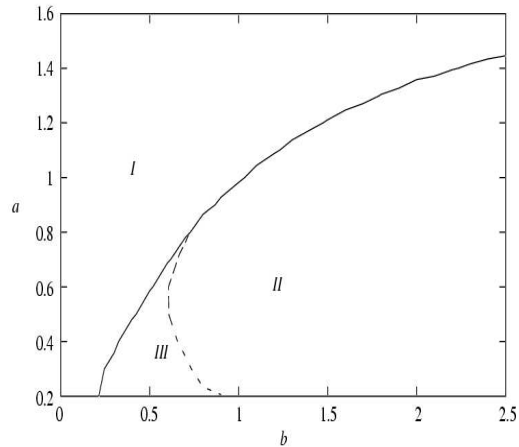


Figure 2.4: The variation of the parameters a , b leads to three different types of models.

An interesting class of models with respect to metastability and jam formation was introduced by Krauss *et al.* [94, 95]. Although this model class does not belong to the CA models, it is briefly discussed here since it shows some similarities to the NaSch and the VDR model. The Krauss model is continuous in space but discrete in time. Besides a maximum velocity v_{\max} the vehicles have certain acceleration a and deceleration b capabilities. Due to the limited braking capability a vehicle has to choose a safe velocity $v < v_{\text{safe}}$ allowing collision free motion. This leads to the following set of update rules:

- Step 1: *Determine safe velocity:*

$$v_{\text{safe}} \rightarrow v_p + 2b \frac{g - v_p}{2b + v_p + v}$$
- Step 2: *Determine desired velocity:*

$$v_{\text{des}} \rightarrow \min(v_{\max}, v + a, v_{\text{safe}})$$
- Step 3: *Randomization:*

$$v \rightarrow \max(0, \text{rand}(v_{\text{des}} - a\epsilon, v_{\text{des}}))$$
- Step 4: *Movement:*

$$x \rightarrow x + v$$

Here, v_p is the velocity of the preceding vehicle and $g = x_p - x - 1$ the corresponding headway. The function $\text{rand}(v_{\text{des}} - a\epsilon, v_{\text{des}})$ denotes a random number in the interval $[v_{\text{des}} - a\epsilon, v_{\text{des}})$, where ϵ measures the degree of randomness. Depending on a , b three different types of models can be distinguished (see Fig. 2.4).

Type I: These models are similar to the VDR model primarily investigated in this thesis. They exhibit phase separation and metastability. Furthermore, the transition from free-flow to the jammed phase seems to be of first order.

Type II: These models display jam formation but no metastable states or phase separation is observable. The jamming transition is not a true phase transition but rather a crossover one as in the NaSch model discussed above.

Type III: Refers to models without spontaneous jamming, these are not of relevance here.

Recently Nagel *et al.* [120] argued that the characterization of Krauss *et al.* is incomplete. It is assumed supported by numerical results that the high-flow states at maximum flow can in addition also be stable instead of unstable (metastable). As a further characteristics they investigated the interface² between jam and jam-outflow and found that the interface can be as well unstable or stable, i.e., the density in the jam outflow area can grow due to branching or stay constant. Thus, the authors proposed to extend the characterization by means of two more criteria. Summarizing, traffic models can be divided by the property of a stable or an unstable maximum flow and in addition by a stable or an unstable interface. In regard to this characterization, it is found that the Krauss model has a stable interface while the VDR model has an unstable. Thus, it must be stressed that, concerning the stability, the Krauss model behaves differently from the VDR model.

²The interface is the position which divides a high-density area belonging to the jam from a low-density area corresponding to the jam outflow (see [120] for more details).

3 Jamming Dynamics in the VDR Model

3.1 VDR Model

In CA models for traffic flow the space, speed, acceleration and even the time are treated as discrete variables. Also the motion of vehicles is realized through a simple set of rules. Obviously, such a description of a physical system is in general an extreme simplification of the real world conditions. Therefore, the aim of Nagel and Schreckenberg (NaSch) by choosing a minimal set of rules for their model [122] was to describe basic phenomena of traffic flow and not to be accurate on a microscopic level. This is also the case for the VDR model [9] which is discussed in the following. The VDR model is a simple generalization of the NaSch model leading to a completely different jam dynamics, i.e., the existence of wide phase separated jams and metastable free-flow states. Due to the distinct jams occurring in the model it is predestinated for the investigation of the jamming dynamics. The circumstance that even recent CA models [83, 89], with a high degree of realism, use the procedure of the VDR model to generate wide jams makes a thorough understanding of its jamming dynamics important. Beyond it, the jamming dynamics of NaSch like traffic models seems to be generic anyhow, emphasizing this relevance.

3.1.1 Update Rules

As mentioned before, the VDR [9] model represents a simple generalization of the NaSch model. The update rules of the NaSch model were given in Sec. 2.3.1. In the VDR model a velocity-dependent randomization (VDR) parameter $p = p(v(t))$, in contrast to the constant randomization in the NaSch model, is introduced. This parameter must be determined before *Step 1*. The update rules of the VDR model read as follows:

- Step 0: *Randomization parameter:*
determination of $p_n = p(v_n)$
- Step 1: *Acceleration:*
 $v_n \rightarrow \min(v_n + 1, v_{\max})$
- Step 2: *Braking:*
 $v_n \rightarrow \min(v_n, d_n - 1)$
- Step 3: *Randomization:*

$$v_n \rightarrow \begin{cases} \max(v_n - 1, 0) & \text{with probability } p_n, \\ v_n & \text{with probability } 1 - p_n \end{cases}$$

- Step 4: *Driving:*
 $x_n \rightarrow x_n + v_n$

One finds that the dynamics of the model strongly depends on the randomization. It is focused on the so-called slow-to-start case [11, 43, 141, 149]

$$p(v) = \begin{cases} p_0 & \text{for } v = 0, \\ p & \text{for } v > 0, \end{cases} \quad (3.1)$$

with two stochastic parameters p_0 and p already containing the expected features, i.e., metastable states and wide phase separated jams. Thereby, p controls the velocity fluctuations of moving cars while p_0 controls the fluctuations of cars that have not moved in the previous time-step and thus determines the velocity of a jam. In the slow-to-start case the randomization p_0 for standing cars is much larger than the randomization p for moving cars, i.e., $p_0 \gg p$. This leads to a reduction of the jam outflow compared to the maximum possible flow as suggested by empirical observations [84].

3.1.2 Phase Separation and Fundamental Diagram

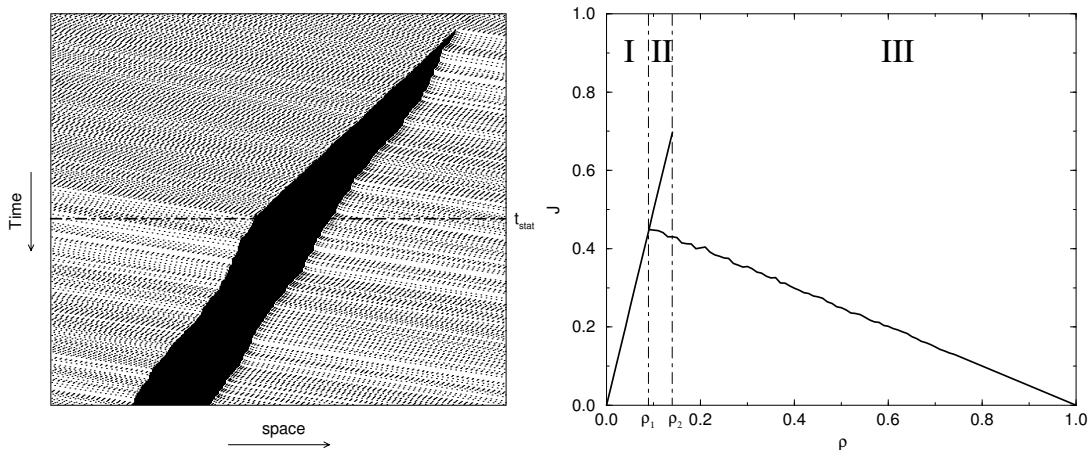


Figure 3.1: **Left:** Space-time diagram of a spontaneously emerging jam in the VDR model for $\rho = \frac{1}{7}$, $p_0 = 0.5$, $p = 0.01$. The jam is growing monotonously from its first appearance until inflow and outflow are equal due to the periodic boundary conditions. After t_{stat} time-steps the average jam length fluctuates around its mean value. **Right:** Typical FD of the VDR model. The fluctuation parameter of standing cars is set to $p_0 = 0.5$ and for free flowing vehicles to $p = 0.01$. The metastable branch in regime II can clearly be identified.

The microscopic structure of the jammed states in the VDR model differs from the one found in the NaSch model. While jammed states in the NaSch model contain clusters with an exponential size distribution [121, 138, 139] (see also the previous chapter), one finds phase separation in the VDR model (one single cluster). The reason for this different behavior is the reduction of the outflow of a jam compared to the maximal possible free-flow. A large stable jam can only exist if the outflow from it is equal to the inflow. If the outflow is the maximal possible flow, a stable jam can only exist at the corresponding density ρ_{max} but will easily dissolve due to fluctuations. If the outflow of a jam is reduced, the density in the free-flow regime is smaller than the density ρ_{max} of maximal free-flow where interactions between vehicles lead to jams so that cars can propagate freely (for $p \ll p_0$) through the low-density part of the road. Therefore, no spontaneous jam formation is observable. It is obvious that no phase separation can occur in the NaSch

model due to the fact that the outflow of a jam is in the area of maximal flow. Figure 3.1 (left) shows the typical structure of the jammed state in the VDR model.

In Fig. 3.1 (right) a typical FD of the VDR model is shown. For densities $\rho_1 < \rho < \rho_2$ the flow $J(\rho)$ can take on two different states depending on the initial conditions. One of them is a homogeneous high-flow branch. This is metastable and shows an extremely long life-time¹. The other is a jammed branch showing phase separation between jammed and free flowing cars. The phase separation can clearly be identified in the left plot of Fig. 3.1. Neglecting interactions among free flowing vehicles the FD of the model can be derived on the basis of heuristic arguments in good agreement with numerical results. Obviously, the flow in the homogeneous branch is given by

$$J_{\text{hom}}(\rho) = \rho(v_{\text{max}} - p) = \rho v_{\text{free}}, \quad (3.2)$$

because every car can move with the free-flow velocity v_{free} . Since the jammed state (stationary) of the VDR model is phase separated also here the flow can be obtained. The jammed branch consists of a large jam and a free-flow regime where each car can move with velocity v_{free} . The density in the free-flow regime ρ_{free} is determined by the average waiting time

$$T_w = 1/(1 - p_0) \quad (3.3)$$

of the first car in the jam. Neglecting interactions between cars, the average distance of two consecutive cars is given by $\Delta x = T_w v_{\text{free}} + 1 = 1/\rho_{\text{free}}$. Using the normalization $L = N_J + N_F \Delta x$, the flow in the jammed branch of the FD is given by:

$$J_{\text{jam}}(\rho) = (1 - p_0)(1 - \rho). \quad (3.4)$$

N_F is the number of cars in the free-flow regime and N_J the number of jammed cars. Obviously, ρ_{free} is precisely the lower branching density ρ_1 (see Fig. 3.1 (right)) because for densities below ρ_{free} the jam-length is zero. Note that this approach is only valid for $p_0 \gg p$.

3.1.3 Jam Formation

The FD of the VDR model with periodic boundary conditions can be divided into three different regimes according to the formation of jams. For densities up to ρ_1 no jams with long lifetime appear and jams existing in the initial conditions dissolve quickly since the outflow of a jam is greater than the inflow. This behavior has to be contrasted to the one found for densities above ρ_2 . Here, no homogeneous state without jams can exist. The most interesting regime lies between the two densities ρ_1 and ρ_2 where the system can be in two different states. One is a metastable homogeneous state with an extremely long lifetime where jams can appear due to internal fluctuations. Note that the homogeneous states can be destroyed by external perturbations, e.g., by stopping cars. The other state is a phase separated state with large jams which can be reached through the decay of the homogeneous state or directly owing to the initial condition. The microscopic structure of a spontaneously emerging jam can be seen in the space-time plot in Fig. 3.1 (left). The origin of the wide jam in the initially homogeneous state is a local velocity fluctuation that leads to a stopped car. Such local velocity fluctuations determine the typical density-dependent lifetime of the homogeneous states.

As one can see in Fig. 3.1 (left), the density in the outflow regime of the jam, this is equal

¹Typical life-times for the standard parameters ($p_0 = 0.5$, $p = 0.01$, $v_{\text{max}} = 5$, $L = 10000$) are in the order of $T = 10^6$ time-steps [5] for densities near ρ_2 .

to ρ_1 , is reduced compared to the average density. Therefore, the jam length is growing approximately linearly until outflow and inflow coincide due to the periodic boundary conditions. It is quite evident that interactions between vehicles in the outflow region of a jam are negligible due to the reduced density so that no spontaneous jams can appear and only one wide jam exists.

In the next chapter 4 it is shown how the strong phase separation can be broken by a localized defect in such a way that more than one jam, i.e., stop-and-go traffic, can exist. Moreover, in chapter 5 the impact of open boundaries to the phase separation of the model is investigated.

3.2 Jamming Dynamics

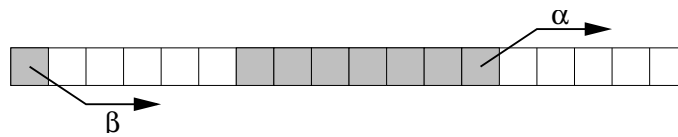


Figure 3.2: Schematic representation of a single jam. Cars are represented by grey cells and empty cells are white. α is the outflow of the jam. The inflow β is determined by the vehicle distribution behind the jam.

It can be seen in Fig. 3.1 (left) that strong fluctuations in the upstream jam front appear because of the fact that the outflow from a jam is determined by a stochastic parameter. As mentioned before, a locally emerged jam, within the density range $\rho_1 < \rho < \rho_2$, will probably grow for a certain time because the mean inflow into the jam is larger than the mean outflow. At this point it should be stressed, however, that although the inflow is larger than the outflow, these quantities are stochastic and therefore even in this growth regime a complete dissolution of the emerging jam is possible through fluctuations. The dynamics of this growth (dissolution) process of a jam is the main object in this chapter. Anyhow, assuming that the locally emerged jam does not dissolve, it will grow a certain time t_{stat} until the mean inflow and outflow are equal due to periodic boundary conditions. The average jam length then strongly fluctuates. This can also lead to a complete dissolution of the jam if these fluctuations are of the order of the jam length. The phase separation in the jammed state can be identified directly using the jam-gap distribution [29, 30]. It was shown that for $p = 0$ the jam is compact in the sense that no holes between the jammed cars appear. For $p > 0$ holes are formed due to velocity fluctuations of vehicles entering the jam. Nevertheless, it can be assumed that for $p_0 \gg p$ the jammed states are phase separated, i.e., the size of a jam is of the order of the system size.

3.2.1 Analyzed Scenario – Single Jam

Imagine a sequence of n cars at rest forming a compact jam (see Fig. 3.2). In every time-step the first car can leave the mega-jam with probability $\alpha = p_0$ according to the acceleration and randomization steps in the update algorithm (see Sec. 3.1.1). Since for $p \ll p_0$ car-car interactions can be neglected in the outflow region a car that leaves a jam can be treated as escaped for all times. Additionally, a new car is able to enter the jam at its end with probability β which is determined by the vehicle distribution behind the jam. The outflow α , realized through p_0 , is an independent identically distributed (i.i.d.) ran-

dom variable. For simplicity, the case that β is also an i.i.d. random variable is focused at in the following. Therefore, a stochastic theory of the jamming dynamics of such a single jam based on arguments from random walk theory is presented. The relevance of this special case is demonstrated in Sec. 3.2.3 where several scenarios are investigated by numerical means. It turns out that the approach gives the exact solution for open boundaries and a vehicle distribution generated by a mega-jam for the special case $p = 0$ where the fluctuations of free flowing vehicles are completely suppressed. For the general case $0 < p \ll p_0$, with open or periodic boundaries, the results are in good agreement with numerical results. However, a detailed description of the initial and boundary conditions as well as a discussion of the influence of deviating gap distributions in the inflow region, e.g., if β is no longer an i.i.d. variable, is also given in Sec. 3.2.3.

3.2.2 Random Walk Theory of Jamming

In the following the jam dynamics is mapped onto a random walk problem. The number of standing cars n in the jam determines the position n of a random walker. The walker moves on a discrete lattice in discrete time. A car leaving (entering) the jam then corresponds to one step to the left (right). In the following the probability $\pi_{t,n}$ that a jam of width n resolves after t time-steps will be determined. Here, a jam is considered as resolved when the last remaining car accelerates.

In random walk terminology [41] this problem is equivalent to the calculation of the first passage time of a walker starting at position $n_0 = n(t = 0)$. $\pi_{t,n}$ is the probability that a walker at position n reaches the origin $n = 0$ of the system in t time-steps. Taking into account that α and β are i.i.d. random variables one gets the following master equation for the duration of the process until the random walker reaches the origin:

$$\begin{aligned}\pi_{t+1,n>1} &= \alpha(1-\beta)\pi_{t,n-1} + \beta(1-\alpha)\pi_{t,n+1} + [(1-\alpha)(1-\beta) + \alpha\beta]\pi_{t,n}, \\ \pi_{t+1,1} &= \alpha\pi_{t,0} + \beta(1-\alpha)\pi_{t,2} + (1-\alpha)(1-\beta)\pi_{t,1}.\end{aligned}\tag{3.5}$$

It is obvious that $\pi_{0,n_0>0} = 0$ and that by definition $\pi_{1,1} = \alpha$ since a jam of length $n = 1$ resolves with probability α in one time-step independent from the inflow². Furthermore, an absorbing barrier at the origin $\pi_{0,0} = 1$ is assumed, i.e., the process stops when the random walker reaches the origin (the jam is dissolved). Note that the variable n covers the whole spectrum of possible positions of a random walker during his movement, while n_0 denotes the starting position. For a discussion of the mathematical aspects of first passage time problems see [41, 153].

As an example for the derivation of these equations consider a walker starting at position $n_0 > 1$. If the first trial results in a movement to the left, the process continues as if the initial position had been $n_0 - 1$. A movement to the left means that a jam of width n_0 evolves into a jam of width $n_0 - 1$. This event occurs if the first car leaves the jam and no additional car enters it. The probability for this is $\alpha(1 - \beta)$. Similarly, if the first trial results in a movement to the right, the process continues as if the initial position had been $n_0 + 1$. The probability for a movement to the right is given by $\beta(1 - \alpha)$, i.e., the first car remains in the jam and an additional car enters it. Furthermore, the position of the walker, and thus the jam length, are unchanged if either one car leaves and one car enters the jam (probability $\alpha\beta$) or no car leaves and enters the jam (probability $(1 - \alpha)(1 - \beta)$). From the first equation of Eqn. 3.5 it can be seen that the random walk is symmetric (for $n > 1$) if $\alpha(1 - \beta) = (1 - \alpha)\beta$. For $\alpha(1 - \beta) > (1 - \alpha)\beta$ the walker is biased to the left and the jam will dissolve quickly. For $\alpha(1 - \beta) < (1 - \alpha)\beta$ the bias is to the right and the

²This is due to the update procedure and will be discussed later.

jam will grow on average. But even in this case a complete resolution is possible through fluctuations.

In order to determine the probabilities, the following generating function is introduced:

$$\Pi_{n_0}(z) = \sum_{t=0}^{\infty} \pi_{t,n_0} z^t. \quad (3.6)$$

At this point it has to be taken into account that the case $n = 1$ must be viewed separately. For a jam consisting of only one standing car the probability for resolving is equal to α (the standing car accelerates) even if a new car enters the mini-jam at its end. Therefore, it is first looked at the special case of a random walker starting at position $n_0 = 1$. A typical process in which the jam resolves after $t > 1$ time-steps may be described as follows.

- (a) The walker does not move for μ time-steps.
- (b) Then the random walker moves one unit to the right.
- (c) After the step to the right the walker first has to return to $n = 1$ before the jam resolves, i.e., before the walker reaches $n = 0$. The return to the initial position $n = 1$ will take $\nu - 1$ further time-steps ($\nu = 2, 3, \dots$).
- (d) Now there are $t - \nu - \mu$ further time-steps left for the walker to reach the origin at last.

These three events are mutually independent and so the probability of the simultaneous realization of the three events is given by the product of the single probabilities.

First, the case $\mu = 0$ is considered. The cases $\mu > 0$ will later be taken into account iteratively. It seems useful to start with the solution of event (c). Since in this case the position of the walker is always larger than one so that only the first equation of the system Eqn. 3.5 has to be considered. In contrast to the general solution for event (c) the hopping probabilities do not depend on the position anymore. A random walker has to return to the origin (in this case $n = 1$) starting from a position shifted one step to the right (here $n = 2$). The solution of this homogeneous first passage time problem is described in [41, 153]. Assuming an absorbing barrier and introducing a separate generating function for event (c),

$$\tilde{\Pi}(z) = \sum_{t=0}^{\infty} \tilde{\pi}_{t,1} z^t, \quad (3.7)$$

where $\tilde{\pi}_{t,1}$ is the probability that a walker starting at $n = 2$ reaches $n = 1$ for the first time after t time-steps, the following solution for part (c) of the problem can be obtained:

$$\begin{aligned} \tilde{\Pi}(z) = & \frac{1 - [\alpha\beta + (1 - \alpha)(1 - \beta)] z}{2\beta(1 - \alpha)z} \\ & - \sqrt{\left[\frac{1 - [\alpha\beta + (1 - \alpha)(1 - \beta)] z}{2\beta(1 - \alpha)z} \right]^2 - \frac{\alpha(1 - \beta)}{\beta(1 - \alpha)}}. \end{aligned} \quad (3.8)$$

The return probability, i.e., the probability that the walker reaches $n = 1$ at an arbitrary time, is then given by

$$\tilde{\Pi}(1) = \begin{cases} \frac{\alpha(1-\beta)}{\beta(1-\alpha)} & \text{if } \alpha(1 - \beta) \leq \beta(1 - \alpha) \\ 1 & \text{if } \alpha(1 - \beta) \geq \beta(1 - \alpha). \end{cases} \quad (3.9)$$

As already discussed above, for $\alpha(1 - \beta) > \beta(1 - \alpha)$ the walker is biased to the left and will always reach $n = 1$. For $\alpha(1 - \beta) < \beta(1 - \alpha)$, on the other hand, the walker is biased

to the right and will only return with probability $\frac{\alpha(1-\beta)}{\beta(1-\alpha)} < 1$.

Now the complete event (a)–(d) occurs for some $\nu < t$. Summing over all possible ν one gets:

$$\begin{aligned} \pi_{t,1} = & \beta(1-\alpha) [\tilde{\pi}_{1,1}\pi_{t-2,1} + \tilde{\pi}_{2,1}\pi_{t-3,1} + \dots + \tilde{\pi}_{t-2,1}\pi_{1,1}] \\ & + (1-\alpha)(1-\beta)\pi_{t-1,1}. \end{aligned} \quad (3.10)$$

The last term takes into account event (a) for $\mu \neq 0$ since $(1-\alpha)(1-\beta)$ is the probability that a walker at site n will not move. In the first term, $\beta(1-\alpha)$ is the probability of event (b). The quantity within the brackets is the probability of events (c) and (d) for the allowed values of ν . Note that is the $(t-1)$ -st term of the convolution $\{\pi_{t,1}\} * \{\tilde{\pi}_{t,1}\}$ (see [41]). After multiplying Eq. 3.10 with z^t and summing over all times one finds an expression for the generating function Eq. 3.6 for $n_0 = 1$:

$$\Pi_1(z) = \frac{\alpha z}{1 - (1-\alpha)(1-\beta)z - \beta(1-\alpha)\tilde{\Pi}(z)z}. \quad (3.11)$$

The probability for the complete return is given by $\Pi_1(1)$. Using Eq. 3.9 it is easy to obtain this quantity explicitly. The solution for the nontrivial case $\alpha(1-\beta) < \beta(1-\alpha)$ is given by

$$\Pi_1(1) = \frac{\alpha}{\beta}. \quad (3.12)$$

Now the general case where one has to deal with starting positions greater than one, i.e., initial conditions consisting of more than only one standing car, $n_0 > 1$ is considered. Similarly to the foregoing approach the process of reaching the origin can be seen as the realization of mutually independent events. For instance, the probability that a random walker starting at position $n_0 = 2$ reaches the origin is given by the event that the walker reaches first position $n = 1$ and thereafter reaches position $n = 0$.

The general resolving process of a jam with an initial width n_0 standing cars can be described as a chain of processes leading finally to the case $n = 1$. Thus, using the generating functions Eq. 3.6 and Eq. 3.7 this convolution of events can be expressed through

$$\Pi_{n_0}(z) = \tilde{\Pi}(z)^{n_0-1} \Pi_1(z). \quad (3.13)$$

With Eq. 3.9 and Eq. 3.12 the following relation for the resolving probability of a jam of width n can be obtained:

$$\Pi_{n_0}(1) = \frac{\alpha}{\beta} \left[\frac{\alpha(1-\beta)}{\beta(1-\alpha)} \right]^{n_0-1}. \quad (3.14)$$

Besides the resolving probability there is also another quantity that is directly accessible through the generating function Eq. 3.13, namely the average lifetime T_{n_0} of a jam of initial length n_0 :

$$T_{n_0} = \sum_{t=0}^{\infty} t \pi_{t,n_0} = \Pi'_{n_0}(1). \quad (3.15)$$

Using Eq. 3.13 one can obtain an explicit result for T_{n_0} .

Figure 3.3 shows the results for the resolving probability Eq. 3.14 and for the lifetime Eq. 3.15 of a jam for various initial widths n_0 . The outflow parameter (fluctuation parameter of standing cars) is chosen such that $\alpha = 0.5$ in both diagrams. In the left figure a strong dependence on the starting position of the walker (initial width of the jam) can be seen. Furthermore, one can observe directly an outstanding difference between the case $n_0 = 1$ and $n_0 > 1$. While for $n_0 > 1$ the resolving probability rapidly converges to zero

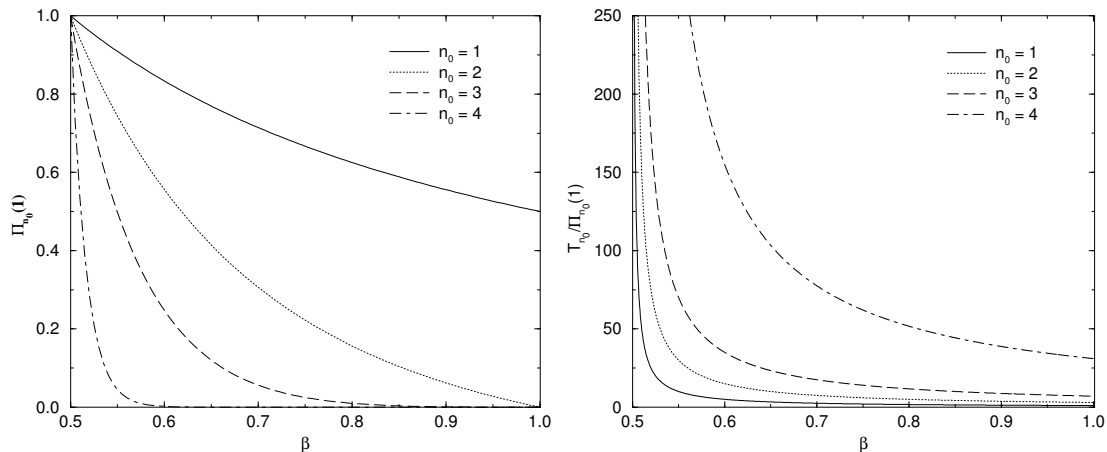


Figure 3.3: **Left:** The dissolving probability of a jam Eq. 3.14 is illustrated for different n_0 . It can clearly be seen that the dissolving probability strongly depends on the initial width n_0 of the jam and that for the special case $n_0 = 1$ this quantity will never fall below α . **Right:** The conditional mean dissolving time $T_{n_0}/\Pi_{n_0}(1)$ is shown for the set of n_0 used in the left part of the diagram. Note that the higher the inflow β the lower the mean dissolving time but the probability for dissolution on short times will shrink drastically. The outflow rate in both diagrams is set to $\alpha = 0.5$.

for increasing β , this value is shifted to α for $n_0 = 1$. This shift can be explained through the update procedure of the model discussed above. A jam consisting of only one standing car resolves with probability α even if a new car enters the mini-jam at its end. The right part of Fig. 3.3 shows the mean dissolving time for different n_0 . It is obvious that this quantity grows with increasing n_0 due to the fact that the resolving process of a jam with n_0 standing cars can be described as a chain of resolving processes of smaller jams. Additionally, a higher inflow β leads to lower dissolving times but it must be taken into account that the dissolution of a jam under a high inflow β is a rather rare event.

3.2.3 Comparison with Numerical Results – Damage Spreading

In order to compare the analytical predictions with simulation results a damage scenario by initializing a finite jam into an undisturbed system is considered. The reaction of the system to such disturbances can be characterized by the sensitivity $S = 1 - \Pi_{n_0}(1)$. The sensitivity is simply the probability that a cluster of n_0 standing cars causes a wide jam (for open boundary conditions) or leads to the jammed state of the system (for periodic boundary conditions).

In the analytical investigations presented above it is assumed that β can be treated as an i.i.d. random variable. This assumption is exactly fulfilled if fluctuations of free flowing vehicles are completely suppressed, i.e., for $p = 0$, and when the vehicle distribution behind the considered jam is generated by the outflow of a mega-jam. Focusing on open boundary conditions with an (infinite) mega-jam at the left end and an empty system at the right end the density in the free-flow regime is determined by the waiting times of each first car in the mega-jam. However, for this special case the gaps between the free-flowing vehicles, generated by the outflow of the mega-jam, are always a multiple of their maximum velocity v_{\max} since the waiting times are discrete and no interactions between cars occur in the outflow region for $p = 0$. For example, a waiting time of t_w time-steps leads to a

gap of $t_w v_{\max}$ cells. Thus, a car with this gap will reach the investigated damage exactly t_w time-steps after the arrival of its predecessor. Obviously, the waiting times of the first car in the mega-jam determine directly the inflow β into the analyzed jam which therefore can be treated as an i.i.d. variable in this case. Note that the randomization parameter \tilde{p}_0 of cars standing in the mega-jam is considered as a control parameter for the vehicle distribution in the free-flow regime, i.e., the inflow $\beta = \beta(\tilde{p}_0)$. Therefore, it is in general different from the p_0 of the cars that have already left the mega-jam, i.e., the p_0 governing the resolution of the jam under consideration. In this way $\alpha \neq \beta$ for open system can be realized.

Furthermore, two cases of deviating gap distributions in the inflow region of the damage, e.g., β is no longer an i.i.d. variable, are also investigated here. The deviations are realized by means of periodic boundary conditions and by allowing fluctuations of free flowing vehicles $p > 0$. In this way all occurring free-flow vehicle distributions of the VDR model are captured.

Summarizing, the following initial conditions are considered to produce an area of free flowing vehicles in the density regime $\rho_1 < \rho < \rho_2$. Remember that the mean inflow into the induced mini-jam will always be greater than the mean outflow in this area.

(a) Here, the randomization parameter p of moving cars is zero, i.e., fluctuations in free-flow are suppressed. An open system with a sufficiently large mega-jam at the left boundary is used in this scenario. The gap distribution is then realized through the outflow of this mega-jam and fluctuations of free flowing vehicles are completely suppressed. The randomization parameter \tilde{p}_0 of standing cars in the mega-jam is used as control parameter for β . After a car has left the mega-jam it is therefore reset to p_0 . Thus, the distance between two consecutive cars is always a multiple of v_{\max} whereby the inflow into the damage is an i.i.d. random variable in that case in correspondence to the theory.

(b) Also in the second case the free-flow car distribution is generated through a mega-jam but fluctuations are permitted, i.e., $p > 0$. Hence, the gap distribution contains values deviating from nv_{\max} due to velocity fluctuations or braking events.

(c) Finally, a homogeneous initialization of cars in a periodic system is considered. Simulations for this situation are performed until the system has relaxed into its free-flow steady state. As a result of the dynamics this steady state shows large deviations in the gap distribution in comparison to the mega-jam initializations.

Note that the inflow into the induced mini-jam is controlled in the cases (a)+(b) by the randomization parameter of standing cars at the left boundary (mega-jam) while in case (c) the inflow is controlled indirectly through the density of the homogeneous initialization. The inflow β can be obtained easily in the simulations.

After the free-flowing vehicles are initialized according to the scenarios described above a damage is induced into the system by setting the velocity of a randomly chosen vehicle to zero. The acceleration of this stopped car is suppressed in the following update steps until the damage grows to n_0 cars. Now, the system is updated according to the update rules without any further external influences. The damage considered can either grow to a large jam or dissolve.

In Fig. 3.4 the numerical results for the sensitivity $S = 1 - \Pi_{n_0}(1)$ and the mean resolving time for the different initial conditions are compared to the analytical predictions of Sec. 3.2.2. It is clear that for scenario (a) the analytical results are exact.

Even scenario (b) shows an excellent agreement with the analytical curve but small deviations occur due to the fact that the inflow is no i.i.d. random variable anymore although the mean inflow is still identical to that of scenario (a). Furthermore, it should be noted that for the considered dissolution of a small *damage* the time scale is small so that local

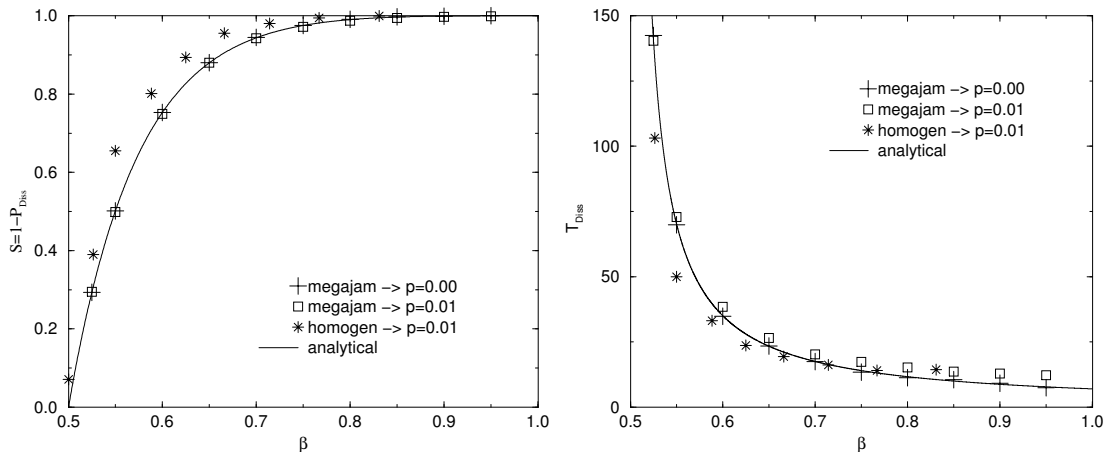


Figure 3.4: The outflow rate in both diagrams is set to $\alpha = 0.5$ and a width of $n_0 = 4$ is chosen for the induced mini-jam. 10^5 simulation runs (induced mini-jams) are performed for every data point. **Left:** The probability that the initial mini-jam grows to a wide jam is illustrated for different starting conditions. The analytical curve is given by $S = 1 - \Pi_{n_0(1)}$ (see Eq. 3.14). **Right:** The mean dissolution time of the initial mini-jam is shown in the left part of the diagram.

deviations in the gap distribution can play an important role.

In the case of the homogeneous initialization (c) larger deviations from the analytical curve are obtained. The origin of this discrepancy is also the gap distribution which, in contrast to the mega-jam initializations, is not generated through a stochastic outflow parameter. Instead, it is determined by vehicle interactions due to the model dynamics (simulation runs until relaxation). Hereby, repulsive forces between the cars lower the probability of finding large gaps. Therefore, the theory overestimates the dissolving probability in the case of a periodic system with homogeneous starting conditions (c). Note that for large p spontaneous jams can appear in the free-flow region before a car is able to enter the induced mini-jam (starting condition (b)) or in the case of homogeneous initialization (c) jams can appear in the system before the steady state is reached. Therefore, initializations with higher p are not considered since the aim is to analyze the dynamics of a single jam and the VDR model exhibits phase separation only for $p_0 \gg p$. Nonetheless, the random walk approach for the dynamics of a single jam seems to be generic for the VDR model even for case (c) since the shape of the curve matches the numerical results well.

3.3 Discussion

The results presented in this chapter are of practical relevance for various applications of traffic flow using stochastic CA models. Complex networks usually contain many bottlenecks such as crossings, lane reductions, traffic lights, or traffic signs. Therefore, induced jams often play an important role in realistic traffic scenarios and a proper understanding of the jamming process and dynamics is beneficial. An analytical approach in terms of random walk theory was suggested in order to determine characteristic quantities of wide jams, especially resolving probabilities and lifetimes. The analytical predictions were compared to simulation results by the help of a damage scenario in the context of different

boundary conditions. It was shown that the random walk approach renders the jamming dynamics of the model. Nagel and Paczuski [121] (see also chapter 2) also analyzed the lifetime of jams in another stochastic CA model for traffic flow, the cruise control limit of the NaSch model, and found also good agreement with random walk theory. Therefore, it can be assumed that the jamming behavior is generic for a lot of the stochastic CA models for traffic flow, especially the model types mentioned in Sec. 2.3.2 that use the VDR slow-to-start rule for the generation of wide phase separated jams.

time*

4 Impact of Local Defects in the VDR Model

In the previous chapter it was shown that compact wide jams occur in the VDR model. Because of the strong phase separation it turns out that the VDR model is an interesting candidate for further investigating the influence of external perturbations on the internal jamming dynamics. Due to the fact that only wide jams appear in an undisturbed system, any additional high-density pattern induced by external forces can be identified easily. This allows to study the occurring interplay between two very different mechanisms for phase separation, i.e., one driven by the dynamics of the particles, and one driven by the defect.

The investigations reveal the occurrence of three different phases whereby one of them shows the characteristics of stop-and-go traffic. These phases can not be obtained in the model without lattice defects. Moreover, concerning the question whether certain jam patterns found in real traffic are induced by local defects or due to the internal behavior of the drivers, the findings allow a deeper insight into possible methods of modelling such traffic states since mostly the occurrence of traffic states with high density like wide moving jams or synchronized traffic (see chapter 2) can be linked to external (localized) influences, e.g., on- and off-ramps, bottlenecks, lane reductions or road works (see [27, 60, 74, 86, 101, 125, 127]).

However, the impact of defects in other CA models, e.g., the asymmetric simple exclusion process (ASEP) [96] or the NaSch model, is by now well understood. Basically, two types of defects can be distinguished. These can be characterized as particle-wise and site-wise disorder. In the first case the defect may be realized, e.g., by particles with a smaller maximal velocity [38, 39, 88, 97, 98]. Such defects are not localized in space, in contrast to those corresponding to site-wise disorder where in a localized region certain parameters of the model take on different values, e.g., by imposing a speed limit or increasing the deceleration probabilities [24, 35, 72, 73, 116, 117, 136, 166]. In both cases a parameter regime exists where the global behavior of the system is controlled by the defect acting as a bottleneck. Generically it induces phase separation into a high- and a low-density region separated by a sharp discontinuity (shock). In the case of particle-wise disorder, with one slow car (and no overtaking), the faster cars tend to pile up behind the slow one. This behavior has certain similarities with Bose-Einstein condensation [38]. For a spatially localized defect one also finds a separation into a high- and a low-density regime but with the high-density region pinned to the defect. This behavior has been found in a variety of models and for different defect realizations. However, none of the models investigated exhibits phase separation through the existence of high-flow metastable states, which is an important ingredient for any realistic traffic model.

4.1 Definition of the Defect

For the purpose of keeping the set of model parameters manageable (see Sec. 3.1.1 for the update rules of the VDR model) the local defect is implemented in a simple straightforward manner. Since the model contains a stochastic parameter, which is needed to implement

various phenomena found in real traffic, e.g., spontaneous jam formation, reduced outflow from a jam, it seems obvious to implement a local defect by increasing this parameter in a limited area. As mentioned before, other types of localized defects have been studied in the NaSch model and related models, e.g., reducing the maximal velocity of the cars locally. Introducing a local lower speed limit in the VDR model should have the same effect as the enhanced deceleration probability since one expects also phase separation into high- and low-density regions in a certain regime of the global density. However, the microscopic details of the states may be different for the various defect types.

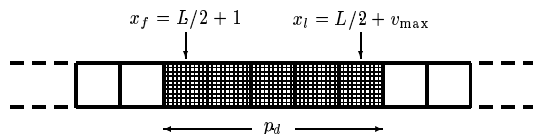


Figure 4.1: Schematic representation of the local defect. The defect itself is placed at a fixed position on a periodic one lane street. Its width is chosen to v_{\max} cells.

The length of the defect is chosen to L_d cells and the stochastic noise $p(v)$ is replaced by a defect noise p_d . The defect length L_d itself is set to $L_d = v_{\max}$ to ensure that each car will participate at least once in an update with the enhanced breaking probability p_d . Note that this also implies that slow vehicles undergo a stronger influence. They need more than one time-step to cross the defect region and thus the defect deceleration rule has to be applied more often than for fast cars which can cross the defect in one time-step. Given that the stochastic noise in the VDR model depends on the velocity of vehicles the choice of the stochastic parameter inside the defect must be seen with respect to this. The strategy is to choose the stochastic noise in a way that it is maximal. Thus, the stochastic noise can be written as:

$$p(x, v) = \begin{cases} \max(p(v), p_d) & \text{for } x \in D \\ p(v) & \text{for } x \notin D \end{cases}, \quad (4.1)$$

with $D = \{x | x_f \leq x \leq x_l\}$ denoting the cells belonging to the defect. Here, x_f is the first cell of the defect and x_l the last one. In Fig. 4.1 a schematic representation of the local defect with all its parameters is depicted. Obviously, the defect width as well as p_d control the strength of the defect. For the sake of simplicity the width of the defect is fixed and p_d is chosen as control parameter. The influence of different spatial extensions of the defect is explored in [129] in detail.

4.2 Occurring Phases

In the following the impact of the defect is discussed on the basis of numerical results. The stochastic noise p_d inside the local area belonging to the defect is used as control parameter. The other parameters of the model are kept fixed ($L = 3000$, $v_{\max} = 5$, $p_0 = 0.5$, $p = 0.01$). Starting from low p_d , three different phases can be distinguished in the system.

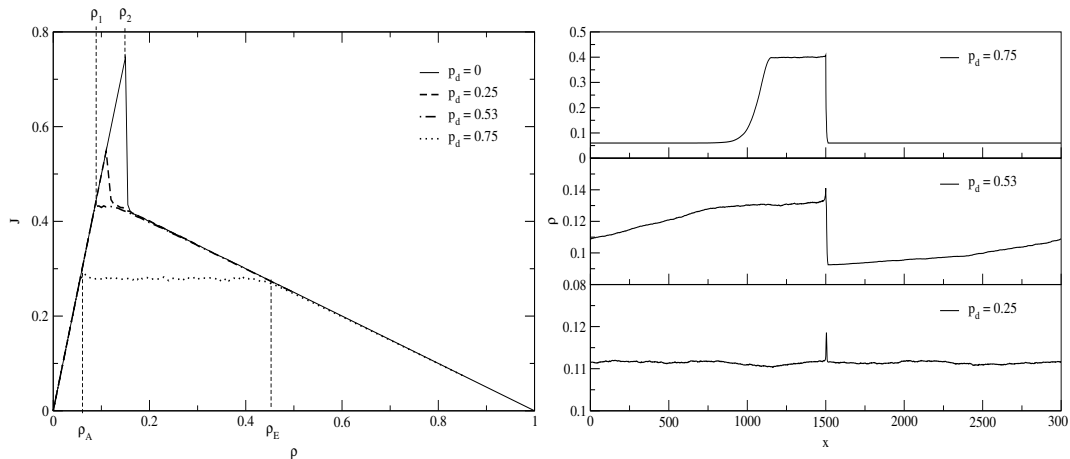


Figure 4.2: **Left:** Typical FD of the VDR model with a lattice defect. The different defect noise parameters p_d cover the occurring phases. The remaining model parameters are: $L = 3000$, $v_{\max} = 5$, $p_0 = 0.5$, and $p = 0.01$. **Right:** Density profiles of the analyzed system for the density $\rho = \frac{1}{3}$. Starting from bottom to top: The case $p_d = 0.25$ corresponds to the “VDR phase”. Only a small peak at the defect is observable representing the interactions between the defect and the vehicles. For an intermediate defect noise, here $p_d = 0.53$, the density profile is almost linear due to the different lifetimes of the small jams emerging at the defect. In the high defect noise case, with $p_d = 0.75$ (“stop-and-go phase”), the system self-organizes into macroscopic high- and low-density regimes similar to the NaSch model with defect.

4.2.1 VDR Phase – Small Defect Noise: $p_d \ll p$

For a low stochastic noise inside the defect $p_d \ll p$ the influence on the overall dynamics of the system is negligible. The only exception is the decreasing lifetime of the metastable states which are known to be sensitive in regard to perturbations. Remind that in chapter 3 an analytical expression for the sensitivity was given. As one can see in Fig. 4.2 (left) the maximal possible flow of the metastable branch is reduced extremely for $p_d = 0.25$, which is chosen as a typical value for a small defect noise. Obviously, other values for p_d lead to different lifetimes. However, the term small noise should not be related to the lifetimes of the metastable states but rather to the impact on the systems dynamics after the transition from a metastable high-flow state to a jammed state. Thus, a defect noise is small if the jammed state of the system is nearly unaffected by it. This phase is denoted as the “VDR phase” since it matches with the jammed state of the VDR model. It is characterized by a wide jam, which moves backwards and is able to pass the defect area uninfluenced, and free flowing vehicles. The distribution of head-ways in the free-flow area is completely determined by the outflow from the jam. The distance between the free flowing vehicles is large enough to absorb additional velocity fluctuations in the area of the defect without the emergence of new jams. In Fig. 4.2 (right) the density profile of the system considered is shown for various p_d . The “VDR phase” shows a constant density profile with a small peak in the area of the defect. This peak is created by the additional velocity fluctuations leading to an increased travel times. Besides this peak there is no prominent difference to the jammed state of the VDR model.

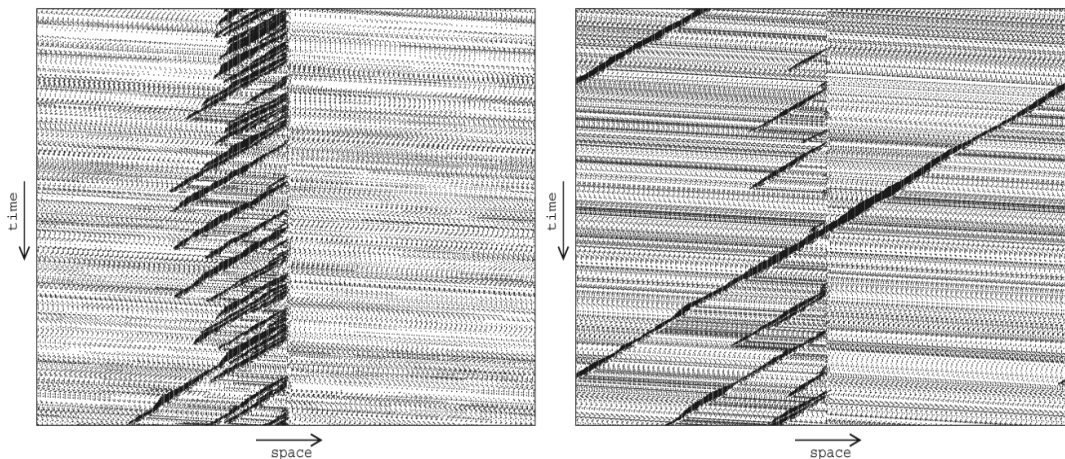


Figure 4.3: Space-time plot of the analyzed system for a density of $\rho = \frac{1}{8}$. **Left:** For a high defect noise ($p_d = 0.75$) a high-density region consisting of small compact jams, which are separated by small free-flow regions, is observable at the defect. **Right:** For an intermediate defect noise ($p_d = 0.53$) a mixture of a wide jam moving nearly undisturbed through the system and small jams, formed at the defect, is observable. The different lifetimes of the small jams lead to an approximately linear density profile as shown in Fig. 4.2 (right).

4.2.2 Stop-and-Go Phase – Large Defect Noise: $p_d \gg p$

As expected, large defect noises p_d have a significant influence on the flow of the system. Three different density regimes can be distinguished, corresponding to the ones found in the NaSch model under the same circumstances [136]. At low densities, the average distance between the vehicles is large enough to compensate velocity fluctuations induced by the defect. Similarly, for high densities the system is dominated by jams whose movement is nearly unhindered. Thus, the FD in Fig. 4.2 coincides for these two density regimes with the undisturbed one. However, the most interesting density regime is situated in the middle of the FD and can be identified by a plateau. This plateau is formed since the capacity of the defect limits the global flow in the system. It can not exceed the maximal flow J_d through the defect which therefore cuts off the FD at J_d and leads to the formation of the plateau. The plateau value decreases almost linearly with an increasing defect noise. As one can see in the corresponding space-time plot Fig. 4.3 (left) a considerable amount of vehicles is gathered at the defect forming a high-density region. The width of this high-density region itself grows linearly with increasing density as long as densities corresponding to the plateau are considered ($\rho_A < \rho < \rho_E$). Figure 4.2 (right) shows the density profile for a density within the plateau region. The system self-organizes into a macroscopic high-density region pinned at the defect and a low-density region determined by the capacity of the defect. So far the macroscopic properties are comparable to results obtained by the NaSch model with a local defect [136].

However, a look at the microscopic structure of the high-density region reveals some important differences. In contrast to the NaSch model, where the high-density region at the defect consists of a compact congested region, the high-density region in the VDR model is characterized by small compact jams separated by free-flow regimes (see Fig. 4.3 (left)). The term “small compact jams” means that the jams at the defect are significantly smaller than the width of the high-density region. This specific jam pattern shows some similarities with stop-and-go traffic. Therefore, the large defect noise regime is called

“stop-and-go phase”. However, the correspondence to real-world traffic patterns should be viewed in a qualitative sense here (see Sec. 2). The “stop-and-go phase” is characterized by a relatively large congested region consisting of jams alternating with free-flow sections. It is important to keep in mind that the high-density region is not distinguishable from the one occurring in the NaSch model if considering only macroscopic quantities. The microscopic structure shows a new high-density state which cannot be found in the NaSch model. Moreover, it must be stressed that the local defect is an essential ingredient for the occurrence of stop-and-go traffic in the VDR model (an undisturbed system shows only free-flow or one single wide jam) while in the NaSch model jams of various sizes can occur even in an undisturbed system [20].

4.2.3 Transition Regime: $p_d \approx p$

In the following the focus is on an intermediate defect noise parameter p_d . The space-time plot in Fig. 4.3 (right) shows the typical microscopic structure for this parameter region. In particular, a wide jam moves backwards through the system and additionally some small jams with a limited lifetime are formed at the defect. Note that for all cases, the impact of the defect is most distinct for intermediate global densities.

In Fig. 4.2 it can be seen that the described mixture of a wide jam and small jams does rarely influence the FD. The flow is almost identical to the case without defect, except for the missing metastable branch. This is rather different from the case of large p_d where a plateau is formed in the FD. Therefore, it can be assumed that for an intermediate p_d the capacity of the defect is close to the maximum possible flow in the system. Furthermore, taking a look at the density profile for a corresponding intermediate defect noise ($p_d = 0.53$) another difference to the large p_d case is observable. For a large p_d the system self-organizes into a macroscopic high-density region pinned at the defect and a low-density region. In contrast, for intermediate values of p_d the density profile decreases approximately linearly in upstream direction at the defect. This behavior can be traced back to the different lifetimes of the small compact jams. The dynamics of such a small jam can be described analytically as was shown in chapter 3.

The coexistence of a wide moving jam and small jams pinned at the defect may also be interesting for the interpretation of empirical results. Traffic states consisting of wide jams passing a localized congested region with a flow comparable to free-flow and small mean velocity are observable in real traffic [76, 77, 90] (see also chapter 2). However, the system state for intermediate p_d has to be interpreted as a “crossover phase”. For small p_d it was shown that only one single wide jam moves undisturbed through the system while for a high p_d no single wide jam can exist. In contrast, a region with many small jams is formed at the defect. Starting from small p_d without any small jams in the system one can observe the occurrence of small jams at the defect with an increasing frequency if increasing the defect noise p_d . Further increasing the defect noise finally leads to the complete dissolution of the large jam. Now the system shows only stop-and-go traffic in the vicinity of the defect. To identify this transition between the “crossover phase” containing one large and various small jams and the “stop-and-go phase” (large p_d) the autocorrelation function is investigated in the following.

4.3 Density Autocorrelation

The density autocorrelation function \mathcal{C} is defined as

$$\mathcal{C}(\Delta T) = \frac{1}{T} \frac{\sum_{\tau=1}^T \rho_n(\tau) \rho_n(\tau + \Delta T) - \frac{1}{T} \sum_{\tau=1}^T \rho_n(\tau) \sum_{\tau=1}^T \rho_n(\tau + \Delta T)}{\langle \rho^2 \rangle - \langle \rho \rangle^2}, \quad (4.2)$$

with the local density¹ $\rho_n(\tau)$ of a site at position n at time-step τ is used to distinguish between the phase with stop-and-go traffic (pinned at the defect) and the intermediate p_d region where crossover behavior is observed. The autocorrelation function is able to detect periodically moving structures, i.e., large moving jams. For small p_d (“VDR phase”), as well as for intermediate p_d (“crossover phase”), the system is characterized by a wide jam recurring periodically due to the periodic boundary conditions. The autocorrelation function specifies the vanishing point of this wide jam, i.e., the transition point to the pinned “stop-and-go phase”. Remember that in the case of crossover behavior additional small jams are formed at the defect. However, these small jams do not affect the autocorrelation function at all since their lifetime is not large enough to move through the whole system. In Fig. 4.4 (left) the density autocorrelation function is plotted against the time lag ΔT . The curve shows peaks with a regular distance, representing the wide jam, moving backwards through the periodic system. It can clearly be seen that the height of the peaks decreases with increasing p_d until they finally vanish completely, i.e., the wide jam dissolves and the transition to the pinned phase occurs.

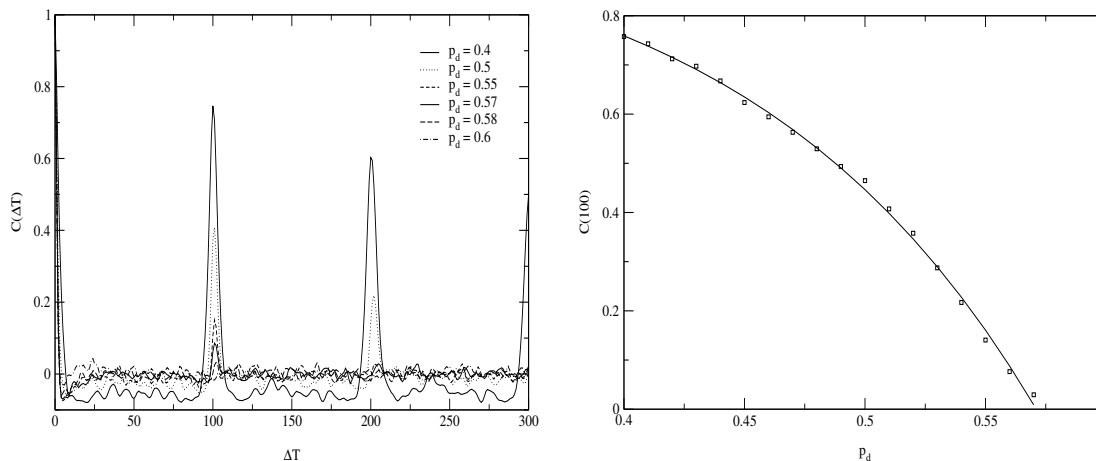


Figure 4.4: **Left:** The autocorrelation function shows peaks at a regular distance representing the wide backward moving jam in the system. The height of the peaks decreases with increasing p_d until the peak vanishes completely because the transition to the “stop-and-go phase” occurs. **Right:** Plot of the maximum of the first peak as function of the defect noise p_d . The vanishing point of the peak is determined through an extrapolation using an exponential fit function.

In order to determine the transition point the absolute value of the first peak is plotted as function of the defect noise parameter p_d (Fig. 4.4). This curve is extrapolated to zero, i.e., vanishing peak values, with the help of a fit function $f(x) = 1 - \alpha e^{-\beta x}$, this reproduces the shape of the curve quite accurately. For the parameters used in Fig. 4.4 the best fit is given with $\alpha = 0.01$ and $\beta = -7.9$. The crossing through zero is obtained for a defect noise of $p_d = 0.57$.

¹The local density is averaged over 60 sec. Therefore, one time-step τ in Eq. 4.2 corresponds to 1 min.

4.4 Relevance for Systems with Ramps

It has been realized recently [60, 101, 102, 127] that inhomogeneities like on- and off-ramps play an important role in real traffic. They might be the origin of a variety of different traffic states observed empirically. For the NaSch model it was found in [30] that the effects of ramps are similar to those of localized defects. The presence of an on-ramp leads to a local increase of the density and a restriction of the maximal possible flow. The FD shows a plateau and the plateau value is determined by the inflow from the ramp. Also the microscopic structure of the states in systems with defects and ramps is similar. For the case of the VDR model with ramps considered here one finds also for small ramp flows a phase similar to the VDR phase in defect systems [129, 130]. However, the width of the jam varies close to the on- and off-ramp where it becomes larger or smaller, respectively. For large ramp flows a phase similar to the “stop-and-go phase” in the defect model is realized. It is characterized by a high-density region of stop-and-go traffic pinned to the ramp. Furthermore, a transition region can be identified where a large moving jam coexists with smaller jams pinned at the ramps. This shows that also the VDR models with defects and ramps exhibit a rather similar behavior.

4.5 Discussion

The presented results pointed out that defects do have a strong influence on the system dynamics and that even new system states like stop-and-go traffic can emerge through the introduction of defects. Concerning the question whether certain system states, like stop-and-go traffic or synchronized traffic, found in reality are induced by topological aspects or the drivers behavior, the findings could be beneficial since they imply a strong influence of defects.

In detail, the competition between two mechanisms of phase separation was observed due to the defect leading to three different system states (phases), if the defect noise p_d is varied. Small defect noises p_d reduce the lifetimes of the metastable states in the VDR model, which show a strong sensitivity to disturbances. The vehicles in the jammed state of the system consisting of a single wide jam and a free-flow region can pass nearly undisturbed through the defect. This phase was denoted as “VDR phase” since there is almost no difference to the jammed state of the VDR model without a defect. In contrast to the low p_d case for a large p_d a pinned high-density region is formed at the defect limiting the overall system flow. The microscopic structure of this high-density region reveals the occurrence of small compact jams separated by small free-flow regions. This phase was denoted as “stop-and-go phase” since the jam pattern shows strong similarities to stop-and-go traffic. The most important result was that stop-and-go traffic cannot be found in the VDR model without a lattice defect.

Furthermore, crossover behavior was found for an intermediate defect noise p_d . Here, a wide jam moves backwards through the system. Additionally, small jams with a limited lifetime are formed at the defect. In order to determine the transition point between this “crossover phase”, containing one wide jam and various small jams, and the “stop-and-go phase”, where no wide jam can be found, the density autocorrelation function was investigated.

5 Open Boundaries in the VDR Model

It is well known that the boundary conditions of CA models can have an immense impact on the overall system dynamics. In the following the influence of open boundaries in the VDR model as well as in the NaSch model is investigated systematically. Note that CA models for transport with open boundaries are often denoted as driven lattice gas models (DLG) in statistical physics [32], i.e., a lattice connected to particle reservoirs at its boundaries whereby the particles have a preferred hopping direction. One of the most interesting features of driven lattice gases are boundary-induced phase transitions. These have been studied intensively so that even exact results exist for some models, e.g., the asymmetric simple exclusion process (ASEP) [96, 104]. The ASEP has originally been introduced to provide an explanation for the kinetics of protein synthesis [104] but several extensions were proposed to enlarge the potential field of applications. For instance, the approach of [70, 71], which allows a multiple occupation of sites, is able to reproduce even the complex dynamics of data transport along paths in the Internet.

In [2] a special case of the VDR model, i.e., $v_{\max} = 1$ and suppressed fluctuations, was analyzed. A striped microscopic structure appears and the existence of high-flow states instead of a maximal-current phase, which occurs in the ASEP as well as in the NaSch model under open boundary conditions, was observed. It will be shown here that these results are transferable to the $v_{\max} > 1$ case. Furthermore, a phenomenological approach capable of explaining the occurrence of high-flow states is given in good agreement with numerical results. Allowing fluctuations of free flowing vehicles can lead to interesting effects due to spontaneous jamming. In this context a surprising result, namely, the flow optimization by a systematic reduction of the inflow is presented.

Besides the modelling aspects, there is much evidence [125, 127] that non-equilibrium phase transitions occur in traffic flow on highways in the vicinity of on- and off-ramps.

5.1 Extremal Current Principle

For models with a *unique* FD a rather general phenomenological theory for boundary-induced phase transitions was developed in [1, 52, 92, 128]. This theory is able to predict the phase diagram of open systems even for complex models. It can be summarized by the extremal current principle

$$J = \begin{cases} \max_{\rho \in [\rho_R, \rho_L]} J(\rho) & \text{for } \rho_L > \rho_R \\ \min_{\rho \in [\rho_L, \rho_R]} J(\rho) & \text{for } \rho_L < \rho_R \end{cases}, \quad (5.1)$$

relating the current J in the open system to the flow-density relation ($J(\rho)$) of the periodic system. $\rho_{L/R}$ are the typical densities at the left and right boundary, respectively.

In [127, 136] it is pointed out that the phase diagram of the NaSch model is similar to the one of the ASEP which supports the extremal current principle. Contrary to these results, e.g., Cheybani *et al.* [16, 17] as well as Huang [69] found large deviations in the phase diagram of the NaSch model in comparison to the ASEP. Due to this discrepancies

it is emphasized in Sec. 5.4.2 that these deviations are related to the special boundary conditions considered and that the phase diagram of the NaSch model is well comparable to the one of the ASEP. Remind that the NaSch model can be seen as a special case of the VDR model with $p(v) = p$. Therefore, the NaSch model is a good starting point for the analysis of open boundaries. So one can see systematically what additional effects occur due to the non-unique flow-density relation (metastability) when considering $p \neq p(v)$. Note that such models with non-unique flow-density relations have not been discussed in the context of the above mentioned phenomenological theory yet.

5.2 Definition of the Boundaries

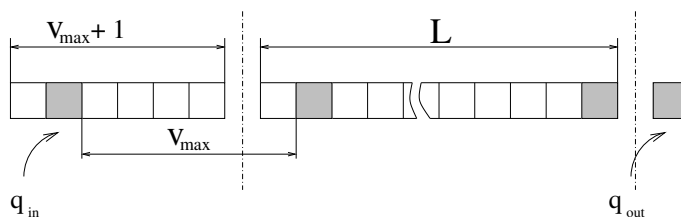


Figure 5.1: Schematic representation of the analyzed system. Cars move from left to right and are represented by dark cells whereas empty cells are white. The left boundary is given by a small system consisting of $v_{\max} + 1$ cells. This particle reservoir is occupied by at most one car with probability q_{in} . The right boundary consists of a single cell occupied with probability q_{out} .

A schematic representation of the analyzed system is depicted in Fig. 5.1. The width of the left boundary is expanded from one single cell to a mini system of width $v_{\max} + 1$. This is done to provide a proper insertion strategy allowing to investigate the whole spectrum of possible system states. The maximum inflow into the system should correspond to the maximum possible flow of the deterministic VDR model¹. The allocation of the mini system (left boundary) has to be updated every time-step. The update procedure consist of two steps. If one cell of the mini system is occupied it has to be emptied first. Then a vehicle with initial velocity v_{\max} is inserted with probability q_{in} . Its position has to satisfy the following conditions: (a) The headway to the first car in the main system is at least equal to the maximum velocity v_{\max} and (b) the distance to the main system has to be minimal, e.g., if no vehicle is present in the main system within the first v_{\max} cells the first cell of the boundary is occupied. The benefits of this insertion strategy are illustrated briefly for the case of the maximum insertion rate $q_{\text{in}} = 1$, i.e., in every time-step one vehicle with velocity v_{\max} is inserted. The initial position of these vehicles will circulate within the boundary from the right to the left end. This is due to the fact that inserted vehicles will occupy a position v_{\max} cells ahead so that the initial position of the next vehicle must be shifted about one cell back to satisfy condition (a). After a while all vehicles move with maximum velocity v_{\max} and the minimal headway of v_{\max} cells. This corresponds to the maximum flow pattern of the model. For smaller values of q_{in} the system is adjusted into states with lower densities and flows.

¹This is also equal to the maximum flow in the deterministic NaSch model. The maximal flows in the stochastic versions of the models are always smaller.

At this point it should be stressed that the maximum flow state of the VDR and NaSch model with $v_{\max} > 1$ and moreover even a large spectrum of system states can not be obtained with the help of the standard insertion procedure, where just the first cell of the system is occupied with a certain probability. For example, for $q_{\text{in}} = 1$ and only one single cell used as boundary the velocity of inserted cars v_{in} forms a sequence corresponding to a circulating pattern, i.e., $v_{\text{in}} = (5, 4, 3, 2, \dots)$, instead of the circulating positions in the case of the enhanced boundary. As a consequence, one finds an artificial phase diagram and unusual dynamics especially for small p . Further, there is a lack of obtainable system states (high-flow) since continuous small gaps can not be generated within this standard strategy. For details see [16, 17] where the NaSch model $v_{\max} > 1$ is studied in the context of the standard boundary conditions.

The right boundary is realized by a single cell linked to the end of the system. Here, the update is applied similar to the case of the left boundary before the general vehicle update procedure. First the right boundary is cleared (if necessary) and then occupied with probability q_{out} . This corresponds to an outflow probability of $1 - q_{\text{out}}$. At last cars are removed if their velocity is large enough to reach at least the (empty!) boundary cell.

5.3 Analytical Results for the Inflow

In this section an analytical expression for the inflow of the enhanced insertion strategy is presented. This expression is valid for all cases investigated in this chapter, even for the NaSch model. Note that the inflow into the system is equal to the flow in the free-flow phase. As shown above, the initial position of vehicles circulate from the right end of the boundary to the left end for $q_{\text{in}} = 1$. Finally, if the last cell of the boundary is occupied, this vehicle is not able to enter the system anymore but will move to the first cell within the boundary instead. Therefore, the first cell has to be refreshed in the next update step before a new vehicle may be inserted so that effectively five cars are inserted in six time-steps (for $v_{\max} = 5$). In general, one has to consider an arbitrary insertion rate q_{in} . Obviously, when calculating the inflow one has to subtract from the vehicle insertion rate q_{in} just the events that lead to an occupation of the last cell of the boundary. That are in detail all events where $v_{\max} + 1$ vehicles are inserted consecutively into the boundary. Note that if a series of insertion events is interrupted (no insertion), the process restarts at the first cell of the boundary. In the language of a stochastic process this can be formulated as follows. The vehicle insertion can be seen as a sequence of Bernoulli trials (it is referred to [41] for details), i.e., an insertion of a vehicle corresponds to a “success” S (probability q_{in}) while a non occupation corresponds to a “failure” F (probability $1 - q_{\text{in}}$). Now a “success run” of length r within a sequence of trials will be defined as follows. A sequence of n letters S and F contains as many “success runs” of length r as there are non-overlapping uninterrupted blocks containing exactly r letters of S each. For example, the sequence $F|SSS|SF|SSS|SSS|SSF$ contains three “success runs” of length three. The probability that a “success run” occurs at the n -th trial will be denoted as u_n in the following. Obviously, the probability that a series of r successes occurs at the trials $n, n - 1, \dots, n - r + 1$ is equal to $(q_{\text{in}})^r$. In this case the “success run” occurs at one among these trials². Then the probability that a “success run” occurs at trial number $n - k$ ($k = 0, 1, \dots, r - 1$) and the following k trials are successes is equal to $u_{n-k}(q_{\text{in}})^k$. Since these events are independent one gets the following relation

²One has to take into account here that successes may occur before trial $n - r + 1$.

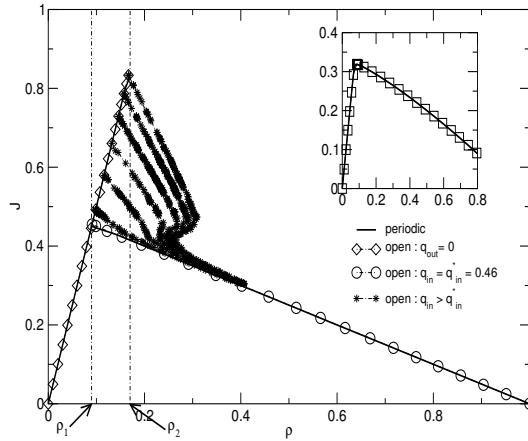


Figure 5.2: FD of the partially deterministic VDR model and the NaSch model (inset). The full lines correspond to periodic boundary conditions while the symbols represent system states, i.e., global density and global flow, obtained by open boundaries. The fluctuation parameter is set to $p_0 = 0.5$ for cars at rest and $p = 0$ for driving cars. In the NaSch model (inset) $p = 0.5$ for all velocities. For high inflows the FD shows an interesting shape, i.e., there are densities where the system can take on three different states. Note, the FD of the stochastic VDR model is the same [9] except for the position of ρ_2 , which takes on a lower value

$$u_n + u_{n-1}q_{\text{in}} + \dots + u_{n-r+1}(q_{\text{in}})^{r-1} = (q_{\text{in}})^r \quad (5.2)$$

with $u_1 = u_2 = \dots = u_{r-1} = 0$. This relation can be solved with the help of a generating function (see [41] for details). The following solution for the probability that the considered trial corresponds to a “success run” can be derived:

$$u = \frac{(q_{\text{in}})^r}{1 + \sum_{n=1}^{r-1} (q_{\text{in}})^n} = \frac{(q_{\text{in}})^r}{\sum_{n=0}^{r-1} (q_{\text{in}})^n}. \quad (5.3)$$

Returning to the considered boundary with a length of $v_{\text{max}} + 1$ cells (whereby v_{max} is set to 5) the following expression for the inflow into the system (flow in the free-flow phase) is obtained:

$$J_{\text{free}}(q_{\text{in}}) = q_{\text{in}} - u = q_{\text{in}} - \frac{q_{\text{in}}^6}{\sum_{n=0}^5 q_{\text{in}}^n} = \frac{q_{\text{in}}(q_{\text{in}}^5 - 1)}{q_{\text{in}}^6 - 1}. \quad (5.4)$$

Note that the analytical expression Eq. 5.3 for the inflow can be used for any v_{max} .

5.4 Simulation Results

Now the most relevant results of the system investigated are discussed on the basis of numerical simulations. Three different cases of the model dynamics are considered. At first it is focused at the standard NaSch model which can be viewed as a special case of the VDR model with $p_0 = p$. It provides a point of reference for the cases with metastability

and helps to clarify whether the phase diagram of the NaSch model is comparable to the one of the ASEP. Then generic parameter combinations of the VDR model, including slow-to-start behavior and thus metastability, are treated for two different cases. In the first case fluctuations in the movement of vehicles are suppressed so that only the jam outflow is stochastic. This case is comparable to the system investigated in [2] except for the higher velocity $v_{\max} > 1$. Moreover, the case of stochastic vehicle movement such that phase separation is still ensured is investigated. For this parameter combination it is pointed out that characteristic additional features can occur due to spontaneous jamming.

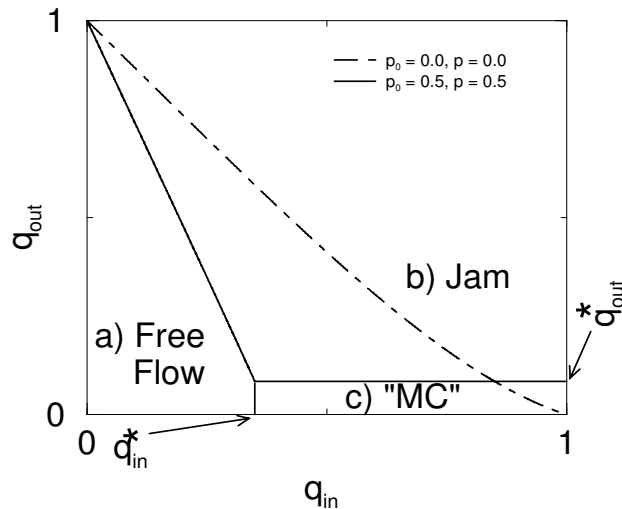


Figure 5.3: Phase diagram of the NaSch model derived from Monte-Carlo simulations. In the free-flow phase (a) the flow is determined by particle injection at the left boundary whereas in the jam phase (b) the particle outflow at the right boundary is the determining factor. On the contrary, the flow in the maximum-current phase (MC) (c) is given by the maximal possible flow due to the model dynamics. The full lines corresponds to the parameter combination $p_0 = p = 0.5$ while the dotted line represent a deterministic system $p_0 = p = 0$. Note that the MC phase vanishes for the deterministic case.

5.4.1 Fundamental Diagram

In Fig. 5.2 the FD of the partially deterministic VDR model ($p_0 > 0, p = 0$) is plotted. As can be seen, the complete FD of the periodic system is reproduced within the scope of open boundaries for an arbitrary choice of inflow rates. Note that global values for the flow and density are considered in the diagram. In detail, if the inflow is below $q_{\text{in}} < (q_{\text{in}}^* = 0.46)$, i.e., this value corresponds to the jam outflow, the FD except for the metastable branch can be obtained via the extremal flow principle. For greater inflows and a small outflow restriction $q_{\text{out}} \ll 1$ some caution is necessary. This is due to the fact that high-flow states may occur in finite systems. Here, system states (\star) may be measured lying outside the lines of the periodic FD as can be seen clearly in the figure. The FD shows a interesting shape in a certain density regime where the system can take on three different states. However, besides the new states (\star) that are ascribed to a new phase, as discussed in Sec. 5.4.3, the boundaries of the phase diagram can easily be related to the periodic FD of

the VDR model if proper parameter combinations are chosen (\circ) so that in this sense the extremal current principle is fulfilled. In the inset of Fig. 5.2 the FD of the NaSch model is plotted. This can be obtained easily by varying the boundary densities in correspondence to the extremal flow principle.

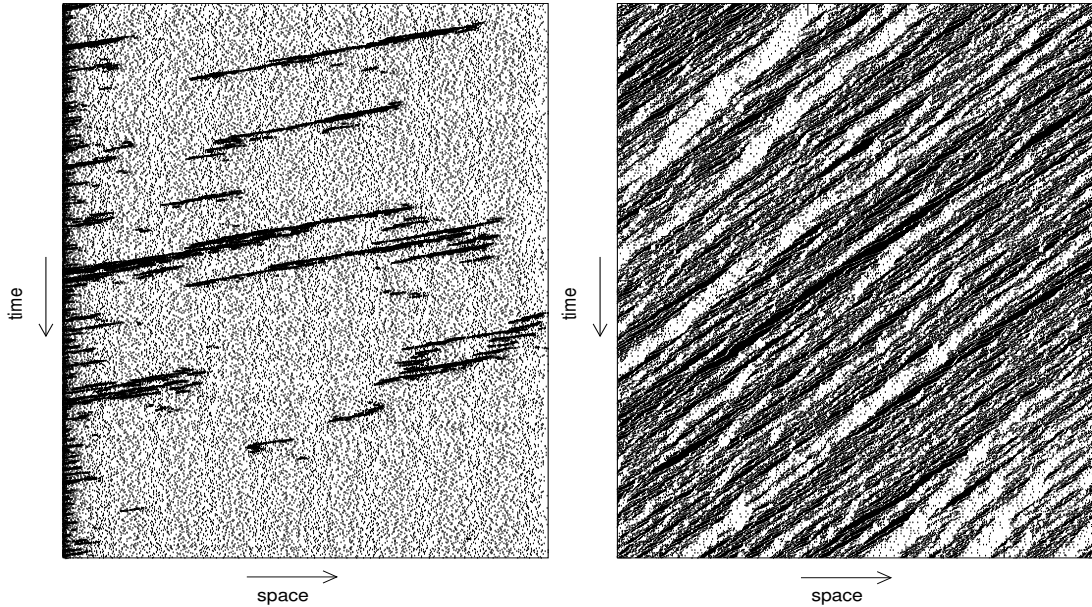


Figure 5.4: Typical space-time plots of the NaSch model with open boundaries. The model parameters are $L = 500$, $p_0 = p = 0.5$. The left part of the figure represents the MC phase ($q_{\text{out}} = 0.01$, $q_{\text{in}} = 1.0$). Spontaneously occurring large jams can easily be identified at erratic positions in the whole system. Further, jams are formed at the left boundary due to the overfeed of vehicles hindering the inflow into the system. The right part of the figure shows the jam phase ($q_{\text{out}} = 0.5$, $q_{\text{in}} = 0.3$). Here, the system is dominated by backwards moving jams generated at the right boundary because of the restricted outflow.

5.4.2 NaSch Model: $p_0 = p$

As already mentioned, the special case $p_0 = p$ of the VDR model is equal to the NaSch model. The corresponding phase diagram obtained by numerical simulations is plotted in Fig. 5.3 (see also [127, 136]). In the free-flow phase the system is jam free except for some small jams formed at the right boundary. Hence, the flow is given by the particle inflow. For $v_{\text{max}} = 5$ this is equal to $J_{\text{free}}(q_{\text{in}}) = q_{\text{in}}(q_{\text{in}}^5 - 1)/(q_{\text{in}}^6 - 1)$ in correspondence with Eq. 5.3. On the contrary, in the jam phase the system is dominated by large jams of various sizes mostly generated at the right boundary due to the restricted outflow. Consequently, the flow is determined by the outflow parameter q_{out} . A typical space-time plot of a system in the jam phase is shown in the right part of Fig. 5.4. The backwards moving jams, mostly generated at the right boundary due to the restricted outflow, can easily be identified in the diagram. In the maximum-current (MC) phase the flow is not restricted by the boundaries but rather by the maximum possible bulk flow of the given model. The MC phase spans a rectangle in the phase diagram. The boundaries are given by the outflow parameter q_{out}^* corresponding to the density in the jam outflow area $\rho_R(q_{\text{out}}^*)$

and the probability q_{in}^* according to the maximum flow of the model $J_{\text{free}}(q_{\text{in}}^*) = J_{\text{max}}$. If the inflow $J_{\text{free}}(q_{\text{in}})$ exceeds this value, jams are formed most likely directly in front of the boundary so that the inflow into the system is hindered. This is shown in the left part of Fig. 5.4. Given that the maximum flow in the NaSch model is restricted by the fluctuation parameter it is clear that the area of the MC phase shrinks with decreasing p until it vanishes completely for the deterministic case $p = 0$.

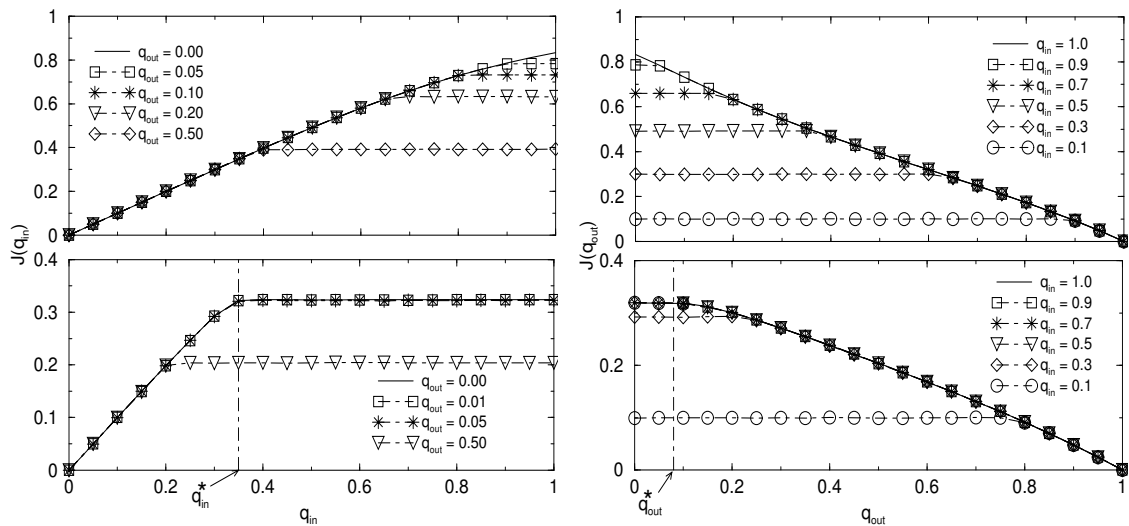


Figure 5.5: The left part of the figure shows the dependence between system flow J and inflow parameter q_{in} for the deterministic case (top) of the model and for the stochastic version $p_0 = p = 0.5$ (bottom) for different values of q_{out} . In the right part of the figure the global system flow is plotted against the outflow parameter q_{out} for different q_{in} . As in the left part, the deterministic case is represented by the upper picture and the stochastic case by the lower one. In all cases the system size is $L = 1000$.

Up to here, the phase diagram of the NaSch model is qualitatively in complete agreement with that of the ASEP ($v_{\text{max}} = 1$) which is known exactly [28, 39, 40]. This result coincides with the argumentation of Kolomeisky *et al.* (see Sec. 5.1), i.e., models with one single maximum in the FD (periodic system) exhibit the same phases for open boundaries. In order to determine the FD from the open system global flow and densities are measured. These global quantities are obtained by averaging over all cells. For low inflow and restricted outflow the bulk density is just ρ_R whereas for the free-flow case it is given by ρ_L . By varying the inflow q_{in} and the outflow q_{out} all possible bulk densities and thus the full FD (see Fig. 5.2 (inset)) can be generated. This FD agrees with that of a periodic system as predicted by the extremal flow principle Eq. 5.1.

In Fig. 5.5 the impact of the boundary parameters q_{in} and q_{out} is illustrated. As one can see for the deterministic case $p_0 = p = 0$ (top left) obviously the maximum possible system flow $J_{\text{max}} = v_{\text{max}}/(v_{\text{max}} + 1)$ (see [122] for details) is achieved for $q_{\text{in}} = 1$. Therewith, it is ensured that the whole spectrum of possible system states can be scanned. Furthermore, it can be seen (top right) that a plateau is formed immediately when the inflow exceeds the capacity of the right boundary given by the restricted outflow $q_{\text{out}} > 0$. Hence, the plateau value, equal to the capacity, decreases continuously with an increasing q_{out} . A

major difference with regard to this can be seen when turning to the stochastic (NaSch) model (bottom figures). Even for $q_{\text{out}} = 0$, i.e., no restriction of the outflow, a wide plateau is build (see Fig. 5.5 (bottom left)). This is due to the fact that if the inflow exceeds the maximum possible flow of the system $J_{\text{free}}(q_{\text{in}}) > [J_{\text{free}}(q_{\text{in}}^*) = J_{\text{max}}]$, no further vehicles are able to enter (“overfeeding”). The system is now in its MC phase. As long as the capacity determined by the right boundary (q_{out}) does not fall below the maximum flow all curves are on the same plateau level independent of q_{out} . If q_{out} is further increased to $q_{\text{out}} > q_{\text{out}}^*$ so that the capacity falls below the maximum system flow after all, the plateau value decreases continuously as in the deterministic case. This picture is confirmed in the right part of Fig. 5.5 where the global system flow is plotted against q_{out} . For the stochastic case (bottom) the MC phase can clearly be identified. As long as $q_{\text{out}} < q_{\text{out}}^*$ holds the flow does not change for a wide range of different q_{in} , while in the deterministic case (top) no plateau is formed where the flow stays fixed.

5.4.3 Partially Deterministic VDR Model: $p_0 > 0, p = 0$

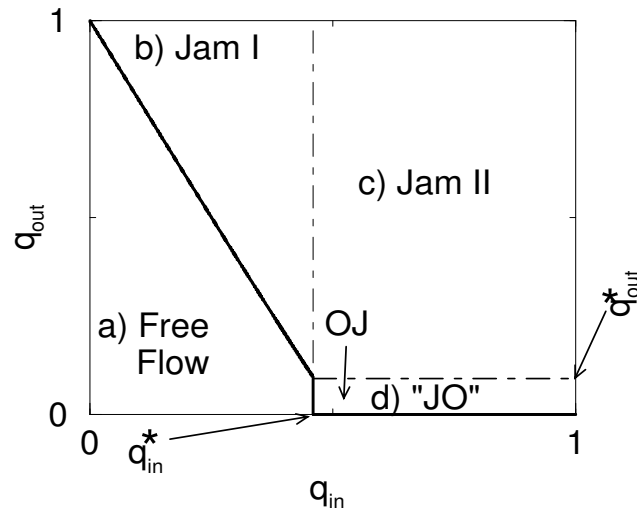


Figure 5.6: Phase diagram of the VDR model with deterministic movement ($p = 0$) of free flowing vehicles. The phase diagram is similar to the one of the NaSch model. However, there are some differences most notably on the $q_{\text{out}} = 0$ line. Furthermore, two different regions (b) and (c) in the jam phase have to be distinguished with respect to their microscopic structure. The JO phase (d) is characterized by wide continuously growing jams. In this phase high flows can be observed in finite systems.

This section proceeds with characterizing the typical properties of the VDR model with metastable states and phase separated large jams when considering open boundaries. Fig. 5.6 summarizes the results of our Monte-Carlo simulations for a VDR model where fluctuations of free flowing vehicles are suppressed. If not stated otherwise, the stochastic parameter for standing cars is set to $p_0 = 0.5$ in the following. As in the NaSch model three different phases can be distinguished. The free-flow phase is similar to the free-flow phase of the deterministic NaSch model since the vehicles move deterministically through the system. No jams are formed except for some small ones occurring at the right bound-

ary. However, these small jams dissolve quickly since the flow in the free-flow phase is smaller than the jam outflow. One peculiarity which can not be found in the NaSch model occurs in the case $q_{\text{out}} = 0$, i.e., maximal outflow. Here, even for inflows greater than the outflow of a jam $J_{\text{free}}(q_{\text{in}}) > [J_{\text{free}}(q_{\text{in}}^*) = J_{\text{out}}]$ the system is in the free-flow phase. This is indicated by the thick black line in the phase diagram. The origin of this line can be explained quite simply taking into account that vehicles inserted into the system move deterministically and no perturbations are present. Again the flow within the free-flow phase $J_{\text{free}}(q_{\text{in}})$ is given by Eq. 5.3.

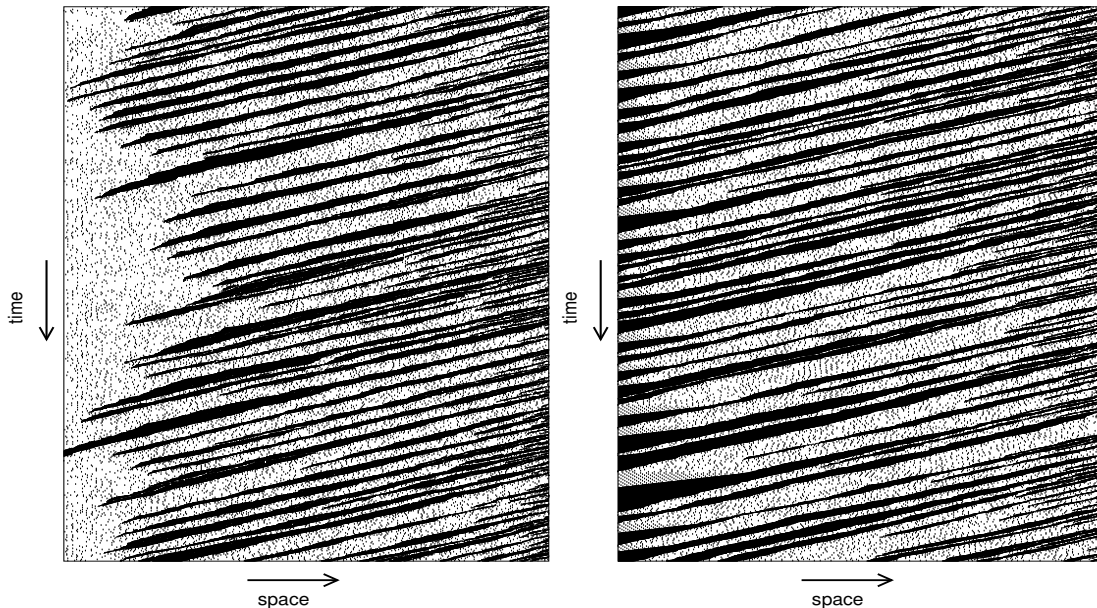


Figure 5.7: Typical space-time plots of the two different jam phases of the VDR model for a system consisting of $L = 500$ cells. The left part of the figure represents the jam I phase ($q_{\text{out}} = 0.4$, $q_{\text{in}} = 0.3$). Here, jams formed at the right boundary rarely reach the left boundary of the system. The width of the clusters most close to the entrance decreases. On the contrary, in the jam II phase (right, $q_{\text{out}} = 0.4$, $q_{\text{in}} = 1.0$) most jams reach the entrance and their width increases rapidly close to the entrance.

The microscopic structure of the two different jam phases of the VDR model is characterized briefly in the following. A look at typical space-time plots in Fig. 5.7 reflects that both phases produce a striped structure, i.e., compact jam clusters alternating with free-flow regions. At the right boundary free-flow segments as well as compact clusters are injected into the system. Both regions stay most likely separated due to the model dynamics and move backwards. The inflow into a single cluster is produced by the outflow of the preceding cluster. Hence, both flows are equal and stochastic. The width of the clusters follows a non-biased random walk [10] until the clusters are far enough from the left boundary, i.e., there is a preceding cluster present. However, due to the underlying stochastic process there is a non-vanishing probability that a cluster dissolves leading to the fusion of two neighboring free-flow segments. If a cluster arrives finally near the left boundary, it becomes the first one in the system so that its inflow gets equal to the system inflow. The cluster width now follows a biased random walk. If the inflow is smaller than the outflow of a jam $J_{\text{free}}(q_{\text{in}}) < [J_{\text{free}}(q_{\text{in}}^*) = J_{\text{out}}]$ (jam I phase), the width decreases in

average while it increases for $J_{\text{free}}(q_{\text{in}}) > [J_{\text{free}}(q_{\text{in}}^*) = J_{\text{out}}]$ (jam II phase). Note that in the jam I phase the clusters vanish often before they reach the left boundary (left part of Fig. 5.7).

High-Flow States – Phenomenological Approach

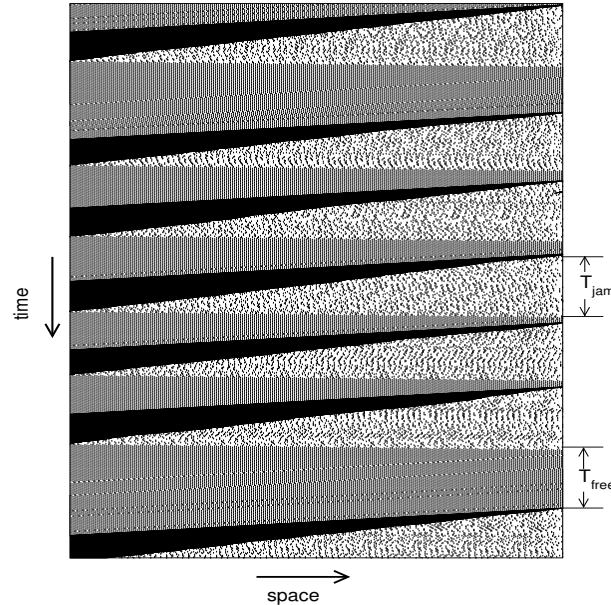


Figure 5.8: Space-time plot of the JO phase. The system is dominated by one large jam which does not vanish until it reaches the left boundary. The model parameters are $p_0 = 0.5$, $p = 0$, $q_{\text{out}} = 0.01$, $q_{\text{in}} = 1.0$, $L = 500$.

The most important result is that a new phase with a non-stationary oscillating density pattern and high flows in finite systems can be found in the VDR model for $q_{\text{in}} > q_{\text{in}}^*$ and $q_{\text{out}} < q_{\text{out}}^*$. The new phase will be denoted as JO phase in the following. This notation is motivated by the fact that in the thermodynamic limit the system flow is only determined by the jam outflow (JO), i.e., the high-flow states fade out with increasing system size. Moreover, the microscopic pattern reveals that in the JO phase the system is dominated by one single large jam³ as can be seen in Fig. 5.8. This peculiarity has its origin in the metastability of the model leading to the so-called local-cluster effect [66, 82], i.e., a small local disturbance of the system can lead to the formation of a global wide jam. Due to this effect the global density in the JO phase can not be related to one of the boundary densities. In fact, the left boundary density (inflow) directly determines the global density and the high flows during the time interval T_{free} (see Fig. 5.8). On the contrary, the right boundary (outflow) only acts as the local seed that causes the formation of wide global jams. However, it exerts an indirect influence to the global density since it determines how often wide global jams occur. The density within the corresponding jammed time interval T_{jam} depends on the jam outflow, which is a fixed parameter of the model.

Shortly before the transition to the jam phase, i.e., increasing q_{out} , additional small jams are formed at the right boundary. These small jams constrict the formation of wide global jams so that the global density slightly decreases before it increases again in the jam

³This is indicated by OJ (one jam) in Fig. 5.6.

phase. In fact this sequence of density changes (increase - decrease - increase) combined with the high flows are the origin for the shape of the curve (\star) corresponding to the JO phase in the FD (see Fig. 5.2) where the system can take on three different states. Note that in Fig. 5.2 the global densities instead of the bulk densities are considered due to the oscillating density pattern. This may lead to small differences compared to the bulk density in the middle of the system.

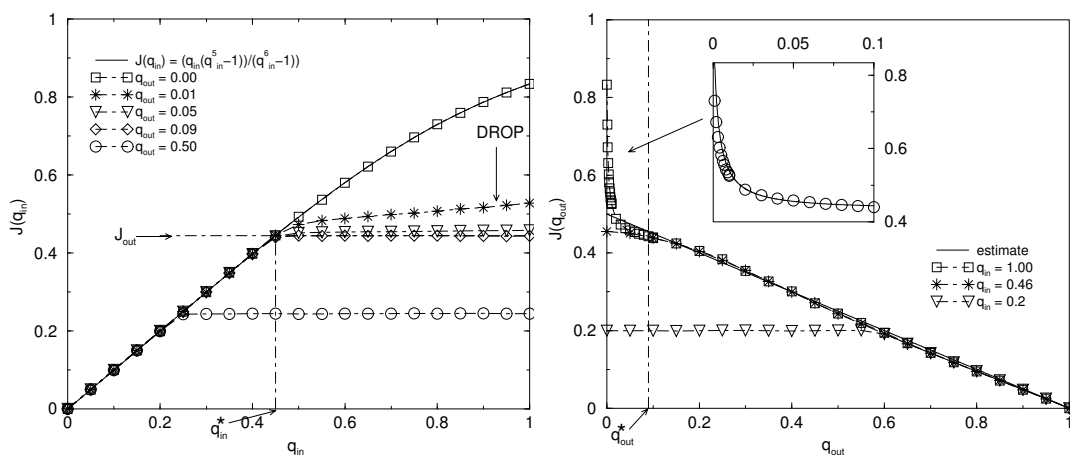


Figure 5.9: The dependence between system flow and inflow parameter q_{in} (left), respectively outflow parameter q_{out} (right), is shown for the VDR model with deterministic movement of free flowing vehicles. The inset in the right part of the figure is ought to emphasize the existence of high-flow states in the JO phase. The model parameters were chosen as follows: $L = 1000$, $p_0 = 0.5$, $p = 0$.

In the following a phenomenological approach for the flow in the JO phase is given. The jam front, which originates from the right boundary, moves backwards with a velocity of $v_{jam} = 1 - p_0$ [9] until it reaches the left boundary. In the meanwhile, i.e., for the time interval T_{jam} , the jam outflow determines the system flow. The duration time T_{jam} is proportional to the system size L . It is the average time interval L/v_{jam} needed for the jam front to move from the right to the left boundary plus the time L/v_{max} the last car of the jam needs to move from the left to the right boundary. This leads to $T_{jam} = L [1/v_{jam} + 1/v_{max}]$ for the mean duration time where the system flow is dominated by the jam outflow. Note that the inflow $J_{free}(q_{in})$ does not influence this time interval T_{jam} at all. In contrast, the duration T_{free} , where the flow is given by the inflow, does not depend on the system size but only on the probability that a jam emerges. Assuming that the right boundary is blocked, the first car in front of it has to slow down if the distance to the boundary is smaller than the maximum velocity. The probability to find a car within the scope of v_{max} cells at the blocked boundary is equal to q_{in} . Note that this assumption holds since deterministic movement of free flowing vehicles is considered so that the inflow at the left boundary can directly be mapped to the right boundary. Thereof, only the fraction of about $(\frac{1}{v_{max}+1} = \frac{1}{6})$ of cars has to brake completely to zero, namely, the cars that are directly in front of the boundary (no more free cell left). This fraction of stopped cars will cause a large jam, taking into account that the average flow in the JO phase is larger than the jam outflow. The rest of the slowed down cars will only brake down to zero (cause a jam) if the boundary is blocked even in the next time-step.

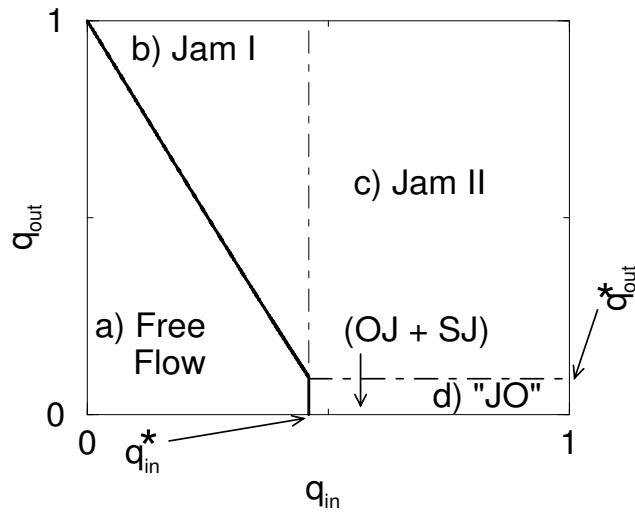


Figure 5.10: Phase diagram of the VDR model with stochastic vehicle movement. The phase diagram is similar to the deterministic case (Fig. 5.6). However, in contrast, the JO phase has to be distinguished in respect to q_{in} . For relatively small q_{in} the microscopic pattern is dominated by one large jam marked by “OJ” (one jam). If larger q_{in} are considered in addition spontaneous jams occur at erratic positions most likely near the left boundary.

The probability for this is equal to q_{out}^2 . Neglecting the less probable events one gets the estimation $T_{free} = 1 / [q_{in}(\frac{1}{6}q_{out} + \frac{5}{6}q_{out}^2)]$ for the time duration that the system flow is determined by the inflow, i.e., the mean time duration until a wide jam is formed at the right boundary. The flow in the JO phase can then be estimated by

$$J_{JO} = \frac{T_{jam}J_{out} + T_{free}J_{free}}{T_{jam} + T_{free}}. \quad (5.5)$$

The jam outflow can be approximated as $J_{out} = v_{max} / [v_{max} / (1 - p_0) + 1]$. Consequently, the reason for the strong size dependence of the high-flow states in the JO phase becomes clear. For small systems the fixed, i.e., independent of the system size L , time periods T_{free} play an integral part in the overall flow while for larger systems these regions can be more and more neglected since T_{jam} grows proportional to L . Finally, in the thermodynamic limit only the jam outflow determines the system flow. At this point it should be mentioned that for growing q_{out} , even in the jam outflow region (within T_{jam}), additional small jams are formed at the right boundary so that the microscopic structure merges into the striped pattern of the jam phases. As an side effect, these small jams can enlarge the time duration T_{jam} .

The comparison of the predictions for the flow within the JO phase shows a good agreement with simulation results (inset Fig. 5.9). The left part of the figure points out the characteristic properties with respect to the system inflow. The $q_{out} = 0$ line of the phase diagram corresponds to the free-flow phase. As soon as the outflow is restricted, i.e., $q_{out} > 0$, the global flow drops to a significantly lower level even for small $q_{out} < q_{out}^*$ (JO phase). Remind that the sharp decline of the flow with growing q_{out} is predicted by estimation Eq. 5.5 as can be seen in Fig. 5.9 (inset). Further, it can be seen in the curve for $q_{out} = 0.01$ that the global flow grows with an increasing inflow $J_{free}(q_{in})$, if low q_{out}

are chosen so that high-flow states are present. Obviously, this effect is caused by the increased free-flow within the time periods T_{free} . However, the flow rapidly converges to the jam outflow J_{out} when further increasing q_{out} . If q_{out} exceeds q_{out}^* , the capacity of the right boundary determines the system flow once the inflow is larger than the capacity of the right boundary. These states can be identified by a large plateau on a level below J_{out} (Fig. 5.9 (right)). The system is now in the jam phase. In the left part of the figure the dependency between the global flow and the outflow restriction q_{out} is shown. This confirms the results discussed above.

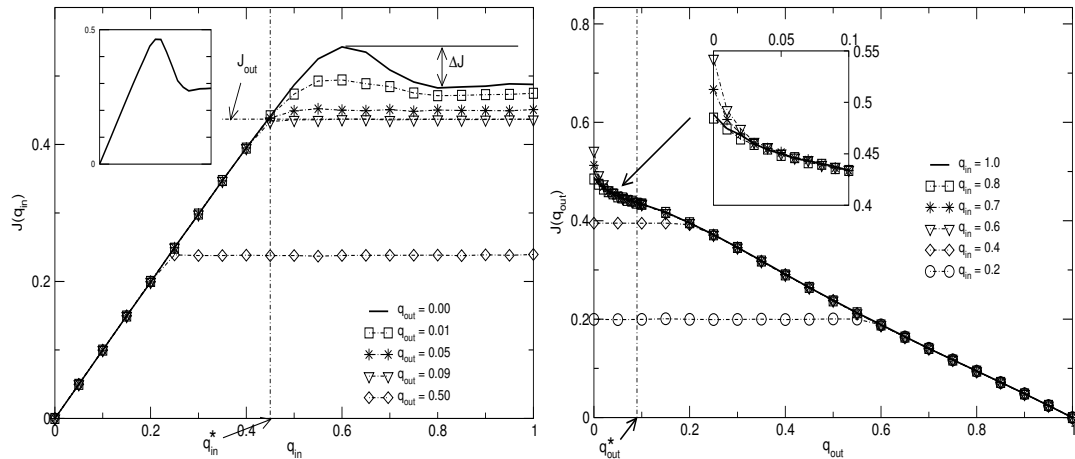


Figure 5.11: **Left:** Global flow vs. inflow parameter q_{in} . For $q_{\text{out}} = 0$ a wide maximum exists for inflows noticeable smaller than the maximal possible inflow. The maximum vanishes rapidly with increasing q_{in} . This is different to the deterministic case which has its maximum flow for maximum inflow. **Right:** For capacities (right boundary) above the jam outflow (JO phase $q_{\text{out}} < q_{\text{out}}^*$) high-flow states are observable as in the deterministic case but they are not so distinct. The model parameters are chosen as $p_0 = 0.5$, $p = 0.1$, $L = 1000$.

5.4.4 Stochastic VDR Model: $p_0 > p > 0$

So far a particular case of the VDR model, where vehicles move deterministically if once started up, was considered. A substantial property of this model variant is that the only stochasticity comes from the jam outflow. However, due to the fact that jams are formed only because of the outflow restriction $q_{\text{out}} > 0$ the generation of jams within the different phases is determined by the right boundary. Now the VDR model with stochastic movement of free flowing vehicles as an additional element is investigated. The focus is on the so-called slow-to-start case with $p_0 \gg p$, for which the expected features as phase separation and metastable states (see [5, 8, 9] for further details) are retained. If not stated otherwise, p_0 is set to 0.5 and p to 0.1 in the following. The stochastic movement of vehicles leads to an additional feature, in comparison to the deterministic case, namely the occurrence of spontaneous jams at sufficiently high flows. A look at the phase diagram (see Fig. 5.10) reveals strong similarities with the deterministic case. The free-flow phase is not influenced at all by the additional fluctuations, except for some small jams. Moreover, even the two different jam phases are indistinguishable since spontaneous jamming does not play a relevant role within the free-flow segments of the striped jam patterns. In the

following the focus is on additional effects based on the spontaneous jamming in the JO phase.

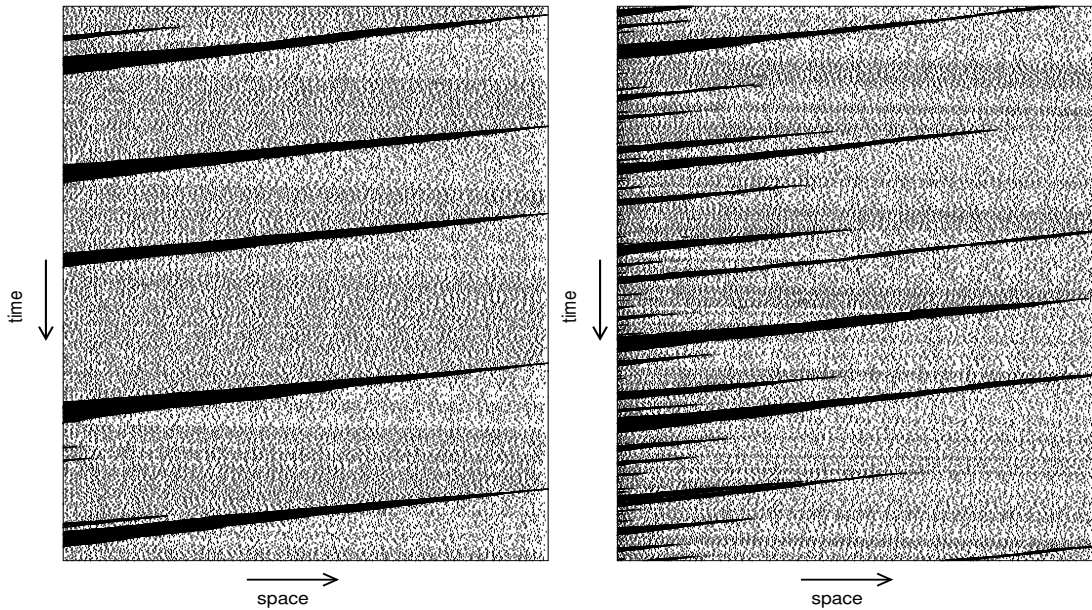


Figure 5.12: Typical space-time plots of the two distinguishable states in the JO phase. In the left figure a state with an optimal inflow is shown, i.e., the inflow is not so high that spontaneous jams are formed often and the flow is still remarkable higher than the jam outflow. The microscopic pattern is similar to the deterministic case so that the assumptions for the flow from the previous section still hold. The right figure shows a state where the inflow is relatively high. This leads to spontaneous jam formation due to the stochastic vehicle movement. Therefore, the flow is mostly determined by the jam outflow. The parameters are $q_{\text{out}} = 0.01$, $L = 500$, $T = 10000$, $p_0 = 0.5$, $p = 0.1$ with $q_{\text{in}} = 0.65$ for the left figure and $q_{\text{in}} = 1.0$ for the right one.

The most eye-catching difference in comparison to the VDR model with deterministic movement can be seen in Fig. 5.11 (left). The maximum possible flow can not be achieved for maximum inflow anymore, even for $q_{\text{out}} = 0$. Contrary, the curve corresponding to $q_{\text{out}} = 0$ shows a clear maximum at an intermediate inflow. The occurrence of this maximum can be explained as follows. Up to inflows smaller than the outflow of a jam $J_{\text{free}}(q_{\text{in}}) < [J_{\text{free}}(q_{\text{in}}^*) = J_{\text{out}}]$ the system is in the free-flow phase anyway. Further increasing the inflow shortens the average distance between the vehicles. This enlarges the probability that velocity fluctuations can lead via a chain reaction to the spontaneous formation of a jam. Therefore, an increasing inflow leads more and more frequently to spontaneous jams and finally to decreasing global flows. Note that the sensitivity of the high-flow states also depends on the system size since the probability to find a vehicle configuration which is capable to produce a jam is proportional to the number of vehicles (see [5] for details). If the inflow is further increased, the system is overfed and the flow converges into a plateau. Here, the global flow is mainly determined by the outflow of jams, occurring mostly near the left boundary, but also spontaneously at erratic positions in the system. In addition, if switching on the outflow restriction $q_{\text{out}} > 0$, the occurrence of a separated maximum levels off fast due to the additional jams generated at the

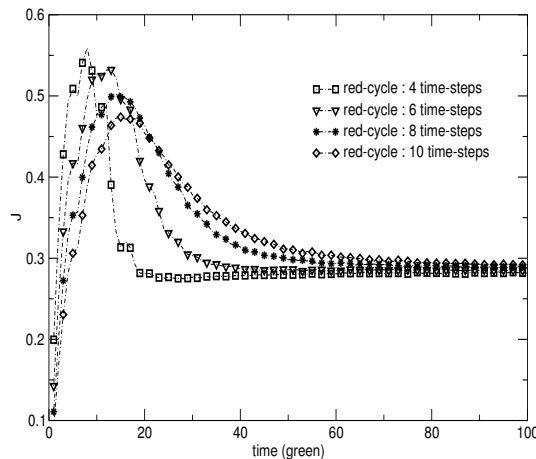


Figure 5.13: The global flow is plotted vs. the green-cycle time for some red-cycle times. Obviously, the flow is nearly twice as high for the optimal parameter combination than for a system without inflow restriction. The limit of large green-cycle times corresponds to an unrestricted system. Note that $p_0 = 0.75$ is chosen to stress the strong impact of the inflow restriction onto the overall flow. The remaining model parameters are chosen as follows: $p = 0$, $q_{in} = 1.0$, $q_{out} = 0$, $L = 1000$.

right boundary. In the right part of Fig. 5.11 the dependence of the global flow on q_{out} is plotted. The results are similar to Fig. 5.9, with the high-flow states (inset) occurring when $q_{out} < q_{out}^*$. However, while in Fig. 5.9 the high-flow states are most distinct for a maximum inflow $J_{free}(q_{in} = 1) = J_{max}$, here the maximum high-flow state is obtained for an optimal q_{in} . That is, if the inflow is too large, the spontaneous jamming levels off the flow drastically and that greatly reduces the current from the deterministic case.

As a further demonstration for the impact of spontaneous jamming within the JO phase, typical space-time plots for two different inflows are given in Fig. 5.12. In particular the interplay among spontaneous jams and jams generated due to a restricted outflow is shown. The left part of the figure corresponds to a situation with optimal inflow. This means that the inflow into the system is large enough to increase the overall flow due to an increased flow between the time interval of two consecutive large jams. In the right part of the figure a system with high inflow is depicted. Here, spontaneous jams are formed at arbitrary positions, mostly near the left boundary caused by fluctuations, in addition to the large jams generated due to the outflow restriction. In consequence, the system flow then is completely determined by the jam outflow. This is undesirable since the corresponding global flows are considerable lower than for an optimal situation. In this context in the following it will be shown in how far the overall flow can be optimized systematically by regulating the inflow into a system and therewith suppressing the emergence of spontaneous jams.

5.4.5 Application: Flow Optimization

Besides the theoretical interest in metastable states there are also real-world traffic applications for this phenomenon. The previous discussion about the existence of high-flow states shows that one can optimize the throughput if the homogeneous state is stabilized by controlling the inflow into the system. This strategy was followed for example in mini-

mizing frequent jams in the Lincoln- and the Holland-Tunnels in New York [48, 64]. Before traffic lights were installed, jams used to form spontaneously within the tunnel. The installed traffic lights at the entrance restrict the inflow so that a critical value cannot be exceeded anymore. With this strategy a remarkable increase of the overall capacity was achieved. The modelling aspect of this situation may be seen in the following manner. The inflow $J_{\text{free}}(q_{\text{in}})$ represents the traffic demand. If a high q_{in} is allowed, this leads typically to spontaneous jams inside the “tunnel” as explained in the previous section. In Fig. 5.13 a situation is depicted where a traffic light is implemented into the simulations. The inflow is set to the maximum possible value $J_{\text{free}}(q_{\text{in}} = 1) = J_{\text{max}}$ to guaranty that an uncontrolled inflow generates a multitude of jams. The traffic light itself is implemented in a way that the connecting cell between the system and the left boundary is blocked for the duration of the red-signal time period and open for the green-signal period. As one can see in Fig. 5.13, for an optimal signal combination, the possible flow is about twice as high as for an unrestricted system. In reality, i.e., the case of the Lincoln- and Holland-Tunnels, improvements of about 20% have been achieved. Note that in the case of large green-signal periods the system converges to a system without traffic light restriction. However, the flow in the JO phase for $q_{\text{in}} = 1$ is determined by the jam outflow which can easily be adjusted by p_0 . Therefore, the choice of p_0 determines the possible gain achieved by the flow optimization strategy so that the model can simply be calibrated to real traffic conditions.

5.5 Discussion

Recapitulating, a new insertion strategy was defined in this chapter that allows to analyze the complete phase diagram of the VDR model as well as of the NaSch model. One advantage of this insertion scheme has been that the corresponding inflow into the system can be determined by an analytical approach.

It was shown that the phase diagram of the NaSch model for $v_{\text{max}} = 5$ is in total agreement with that of the ASEP and that the origin of contradictory results can be related to unsuitable insertion schemes. This was confirmed by the extremal current principle of Kolomeisky *et al.* [92].

The main focus of the investigations was on the VDR model with slow-to-start behavior (see also [7]). It was shown that a striped microscopic jam pattern within the jam phases of the VDR model occur. That seems to be generic for DLG’s with metastability. For example, in [2] a similar microscopic structure was observed in a related model, i.e., $v_{\text{max}} = 1$ and suppressed fluctuations.

As another typical feature of this model class, in the area that corresponds to the MC phase of the NaSch model, a new phase denoted as JO (jam outflow) phase where metastable high-flow states can exist in finite systems was presented. This phase was also observed in [2] so that it may be seen besides the striped microscopic jam patterns as a further signature of metastability. It was shown by a simple phenomenological approach, in good agreement to numerical results, in how far the high-flow states are influenced by the boundary conditions and the system parameters.

Furthermore, the impact of spontaneous jamming and consequential the competition between induced jams at the boundary and spontaneous jams was discussed. From a practical point of view a flow optimization strategy that has been followed, for example, in the Lincoln- and the Holland-Tunnels in New York was reproduced with the help of the high-flow states occurring in the analyzed model.

Similar results [123] were also found in the Krauss-model (see Sec. 2). This model also im-

explicitly contains slow-to-start behavior. There is, however, an important difference to the VDR model since the high-flow states in the Krauss-model seem to be bistable in a certain region in contrast to the metastable states of the VDR model [120]. Furthermore, some caution is necessary for the choice of appropriate boundary conditions since the model is not intrinsically crash free.

6 Modelling City Traffic with Cellular Automata

6.1 Traffic States in City Networks – Two-Fluid Model

In chapter 2 the “Three Phase Traffic” theory was presented. Based on this theory the different traffic states occurring on highways as well as the transitions among them, including phenomena like jam formation, can be described. Unfortunately, it does not exist a theoretical framework to describe the traffic states in city networks. In contrast to the highway networks, where individual highway segments can be treated separated, the structure elements of city networks, i.e., intersections, traffic-lights, -signs, priority-rules, are maybe even more important than the dynamics of cars. Therefore, the description of city traffic in terms of a FD for a single road is inadequate. Rather the whole city network must be considered. Anyhow, some general criteria for the description of the traffic dynamics can be formulated.

Already in the 60’s a linear relationship between the flow and the mean velocity in city networks was recognized for low densities. Exemplary, in the city of London, in the time period from 1952 to 1966, the travel times of floating cars were measured once every two years [53]. It is remarkable that after these 14 years the flow was about three times as high as in the beginning of the measurements. However, so far there is no criteria to benchmark streets or regions within a city network independently of the overall traffic volume.

Based on the kinetic theory of traffic flow [132] a simple model for city traffic, the two-fluid model [53, 65], was invented. In this model the traffic volume is divided into standing and moving vehicles. The dynamics of the vehicles are related to a liquid consisting of two different types of fluids.

The model relies on two basic assumptions: (a) The mean velocity of moving vehicles V_{move} depends on the fraction of moving vehicles f_{move} as

$$V_{\text{move}} = V_{\text{max}}(f_{\text{move}})^n; \quad (6.1)$$

(b) the fraction of standing vehicles f_{stand} is given by the proportion of the total trip-time T of a vehicle and its standing time T_{stand} :

$$f_{\text{stand}} = \frac{T_{\text{stand}}}{T}. \quad (6.2)$$

Hereby, V_{max} is proposed to be the maximal reachable mean velocity of a vehicle during its trip. Obviously, the parameter n can be seen as a measure for the quality of movement in the network. Note that for smaller values of the parameter n the movement in the network becomes better, since $0 \leq f_{\text{move}} \leq 1$. A further criterion for the quality of movement in the network is the minimal mean travel time T_{min} , given by $T_{\text{min}} = \frac{1}{V_{\text{max}}}$. Empirical values for the parameters were obtained by “car chase” studies [162], i.e., the chase of randomly chosen vehicles whose observable, e.g., standing time T_{stand} or total trip time T ,

are recorded by the following car¹.

In general one is interested to get direct access to macroscopic traffic observable as the mean velocity $V(\rho)$ or the flow $J(\rho)$. Therefore, it is useful to rewrite relation Eq. 6.1. With $f_{\text{stand}} + f_{\text{move}} = 1$ one gets the following equation for the mean velocity V of all vehicles:

$$V = V_{\text{move}} f_{\text{move}} = V_{\text{max}} (f_{\text{move}})^{n+1} = V_{\text{max}} (1 - f_{\text{stand}})^{n+1}. \quad (6.3)$$

In a next step, the density dependence of one of the observable has to be determined. Often, the fraction of standing cars is expressed as:

$$f_{\text{stand}} = f_{\text{stand, min}} + (1 - f_{\text{stand, min}})^{n+1} \left(\frac{\rho}{\rho_{\text{max}}} \right)^k, \quad (6.4)$$

whereby $f_{\text{stand, min}}$ corresponds to the minimum fraction of standing vehicles in the network (independent of the density) and k represents a fit parameter with respect to real data. Combining Eq. 6.3 and Eq. 6.4 one gets a relation for $V(\rho)$, and with the hydrodynamical relation $J = V\rho$, even $J(\rho)$. However, more sophisticated flow-density relations has been used to enhance the quality of the predictions (for more details see [53] and references therein).

6.2 Cellular Automata Models for City Traffic

Obviously, city traffic is quite different from highway traffic since the structure elements as intersections exert an immense influence onto the traffic dynamics. In fact, the flow is mostly determined by traffic lights and traffic engineers are often forced to deal with the question if the capacity of the network is exploited by the chosen control strategy. A possible method to investigate such problems is the use of traffic models in control systems as well as in the planning and design. Among the traffic models known, in particular the CA models seem to be capable to perform real-time simulations of complex city road networks with an enormous number of interacting particles.

6.2.1 BML Model

The first CA model for city traffic was invented by Biham, Middleton, and Levine (BML) [13]. It is a simple two-dimensional square lattice CA model. Each cell of the lattice represents an intersection of an east-bound and a north-bound street. The spatial extension of the streets between the intersections is completely neglected. The cells (intersections) can either be empty or occupied by a vehicle moving to the east or to the north. The vehicles are initialized at random positions in the lattice. In order to enable movement in two different directions east-bound vehicles are updated at odd discrete time-steps whereas north-bound vehicles are updated at even time-steps. The velocity update of the cars is realized by following the rules of the asymmetric simple exclusion process (ASEP) [96]: A vehicle moves forward by one cell if the cell in front is empty, otherwise the vehicle stays at its current position. The alternating movement of east- and north-bound vehicles corresponds to a traffic lights cycle of one time-step. In the simplest version of the BML model lane changes are not allowed and therefore, if periodic boundaries are considered, the number of vehicles on each street is conserved. Note that the update rules in the BML model are deterministic so that the only randomness is introduced by the initial position of the vehicles.

¹“Car chase” studies yield to the parameters ($n = 0.8$, $T_{\text{min}} = 1.68\text{min/km}$) for Houston and ($n = 1.65$, $T_{\text{min}} = 1.11\text{min/km}$) for Austin.

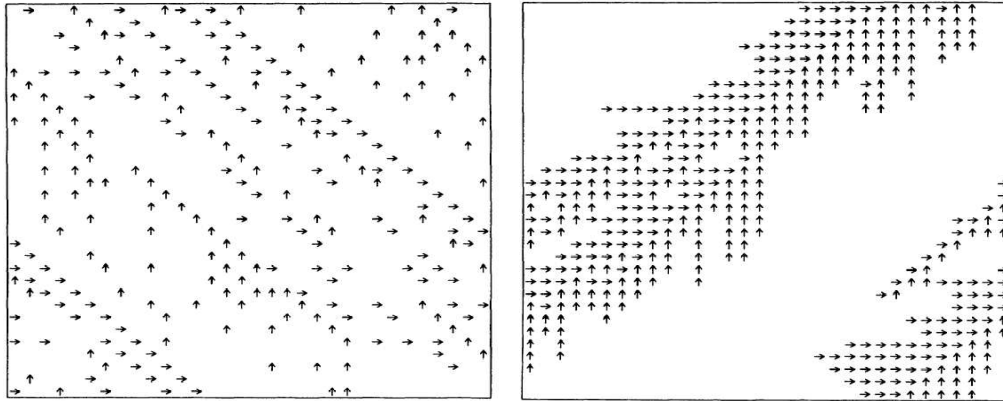


Figure 6.1: Typical dynamical configurations of the BML model. The system size is 32×32 and vehicles are represented by arrows reflecting their driving direction. The plots are taken from [13]. The left plot shows a configuration in the low-density phase below the transition to a blocked state, while in the right plot a blocked system is depicted where the vehicles are organized in a global jam cluster.

Numerical investigations of the BML model with periodic boundaries reveal that a first-order phase-transition occurs at a finite density. At this non-vanishing density ρ_c the complete traffic (global flow) breaks down, forced by the mutual blocking of the east- and north-bound traffic at crossings. The jammed vehicles are then organized in a single cluster which is more and more fractal with increasing densities. Typical configurations of the BML model below and above the transition density are shown in Fig. 6.1. Since the random like branching shows some similarity to percolation, concepts of percolation theory [148] have been used to characterize the blockage [51, 113]. However, in contrast to the random clustering in percolation, the cluster formation in the BML model emerges from the self-organization of the system. Furthermore, it is remarkable that a mean-field estimate can return proper values and even determine the transition density ρ_c [110, 160] in good agreement to numerical results. Based on a mean-field approach one gets the following equation for the mean velocity:

$$v = \frac{1}{2} \left[1 + \frac{\rho}{2} + \sqrt{\left(1 + \frac{\rho}{2}\right)^2 - 4\rho} \right]. \quad (6.5)$$

In order to get a more realistic description, various modifications and extensions of the BML model have been suggested. For example:

- The asymmetric distribution of vehicles [110], i.e., the introduction of different densities or maximum velocities for north- and east-bound vehicles [44].
- The effects of overpasses [111]. This leads to a weakening of the grid-lock effect and thus to a better movement at high densities.
- The impact of several kinds of defects, e.g., faulty traffic lights [22], static hindrances [50], or stagnant streets [112].
- The implementation of stochastic turning at crossings [26, 114, 115]. This leads to the effect that clusters, which are formed due to blocked crossings, do not cause a complete breakdown of the global flow anymore since grid-locks can dissolve.

- The implementation of streets between the intersections [14, 19, 42, 68]. This is done, for example, by locating vehicles on the bonds [14] of the lattice so that the crossings are never blocked, or by decorating the bonds with an extra lattice site in between [68].

6.2.2 CA Online Simulation

In [6, 36, 37, 159] a complete urban area, namely the inner city of Duisburg, was investigated by means of a CA approach. The microscopic dynamics used there, is based on the NaSch model which allows to simulate the whole network (≈ 22000 cells) in multiple real-time. The network itself was implemented detailed. For instance, complex crossings were modelled with all details, i.e., geometrical peculiarities like turn lanes as well as realistic traffic lights or priority rules. Furthermore, even parking capacities and the circulation of public transports were considered. The microsimulation has been used in combination with real-time (online) traffic counts. The main aim of the investigations was to provide an useful tool for designing and planning traffic management systems and to obtain or complete information about the traffic states in areas where no counting setup is present. In Fig. 6.2 the considered network is shown. Note that information about the online simulation of Duisburg are accessible via the WWW [161].

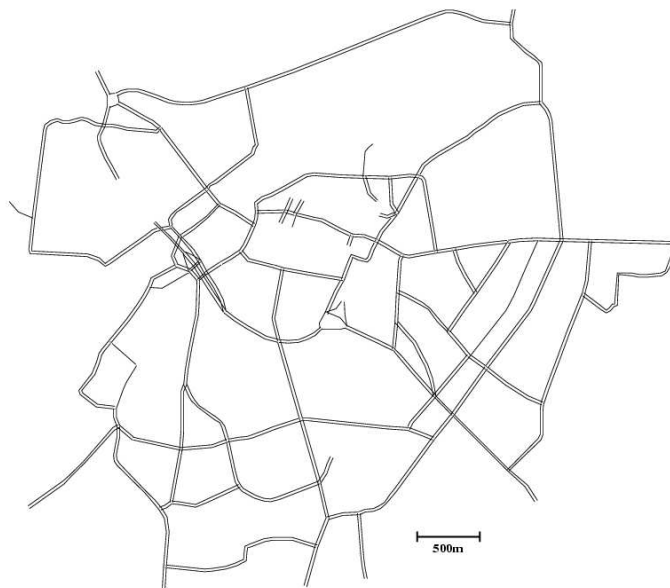


Figure 6.2: Road network for the simulation of the inner city of Duisburg [37]. The total lane length is about 165 km which corresponds to 22059 cells.

In order to clarify in how far the results from the two-fluid theory can be transferred to the considered network, the belonging quantities were obtained by computer simulations [36]. It turned out that the important quantities (T_{\min} , n) do strongly depend on the chosen model parameters²(v_{\max} , p). Furthermore, a remarkable deviation from the power-law

²For $v_{\max} = 2$ and $p = 0.2$ the following parameters: $T_{\min} = 1.178 \pm 0.004$ min/km, $n = 0.139 \pm 0.001$ min/km, were obtained in [36].

distribution which is expected in the two-fluid theory was obtained. This was explained by the fact that the ChSch model covers system states that do not appear in two-fluid theory, e.g., the transition between free-flow and jammed traffic. Therefore, a modification of the two-fluid approach may be beneficial.

Due to the strong interest in traffic management solutions various simulation tools on the basis of CA were developed in the recent years with the focus on realistic real-time traffic simulations. The first approach was made in the framework of the project **PAM-INA** (**P**aralleler **M**ikroskopischer **N**etzwerk **A**lgorithmus) [133]. This allows the simulation of a simplified representation of the German highway network. A further project is **TRANSIMS** (**T**ransportation **A**nalysis **S**imulation **S**ystem) [150]. Here, the complete area of Dallas/Fort Worth is simulated and, in addition, individual “Route” information are used to investigate the traffic demand. A recent project **BAB-NRW** (**B**undes**A**utobahn**v**erkehr -**N**ord**R**hein**W**est**f**al**e**n) focuses on the detailed simulation of the highway traffic in North Rhine-Westphalia [158, 161]. Therefore, a large amount of online data and a sophisticated model for the vehicle dynamics, the BL-model [89], which is able to reproduce single-vehicle data, are used. One aim of this project is to give a proper short-time traffic forecast for the considered area. Another interesting aspect is the analysis of the impact of informations [157] to the network. In future versions it is planned to combine the simulation of the highway network with the simulation of urban traffic of adjacent cities.

6.3 Chowdhury-Schadschneider Model

Up to now, some approaches to city traffic, based on CA models, were briefly introduced in this chapter. The considerations started with the BML model. This extremely oversimplifies city traffic in a way that the impact of streets is completely neglected. Although the BML model shows some interesting features, like a transition to a blocked state, it is not capable to answer questions like in how far traffic lights could be optimized since the light period is restricted to one update step. Furthermore, due to the lack of streets, there is no formation of queues that are known to have a strong impact to the traffic flow in cities. On the other side, some realistic simulations were presented where whole urban areas are modelled in detail. Obviously, these tools can be used and are beneficial for planning and design. But up to now they are primarily used as case studies within the considered areas, e.g., the inner city of Duisburg. However, the networks are often complex and the dependencies between the parameters are hard to manage. As a consequence, the results obtained can not be generalized. Therefore, the Chowdhury-Schadschneider (ChSch) [21, 140] model was introduced. Here, it is the intention to keep the model as simple as possible but anyhow to capture the most important features of city traffic. The obtained results are in the best case transferable to realistic scenarios.

For this purpose Chowdhury and Schadschneider combined basic ideas from the Biham-Middleton-Levine (BML) model of city traffic and the Nagel-Schreckenberg (NaSch) [122] model of highway traffic. One of the main differences between the ChSch model and the BML model is the nature of jamming. In the NaSch model traffic jams appear because of the intrinsic stochastic part of the dynamics [10, 121]. In contrast, the movement of vehicles in the BML model is completely deterministic and the stochastic element arises only from the random initial conditions. Additionally, the NaSch model describes vehicle movement and interaction with sufficiently high detail for most applications, while the vehicle dynamics on streets is completely neglected in the BML model. In order to realize a more detailed dynamics the BML model is extended by inserting streets of finite

length between the cells. On the streets vehicles drive in accordance with the NaSch rules. Further, some of the prescriptions of the BML model have to be modified concerning the interactions at the crossings. At this point it should be emphasized that in the considered network all streets are identical with respect to the processes at intersection, i.e., there are no dominant streets or directions.

Definition of the Model

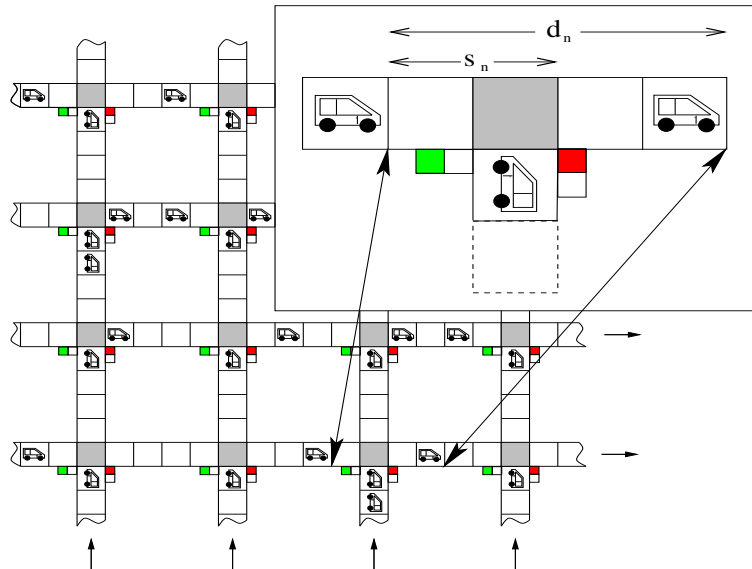


Figure 6.3: Snapshot of the model. The number of intersections in the quadratic network is set to $N \times N = 16$. The distance between neighboring intersections is given by D and the length of the streets between them is equal to $D - 1 = 4$. Note that vehicles can only move from west to east on the horizontal streets or from south to north on the vertical ones. The magnification on the right side shows a segment of a west-east street. Obviously, the traffic lights are synchronized and therefore all vehicles moving from south to north have to wait until all traffic lights switch.

As mentioned before, the main aim of the ChSch model is to provide a more detailed description of city traffic. Especially, the important interplay of the different timescales set by the vehicle dynamics, distance between intersections, and cycle times can be studied in the ChSch model. Therefore, each bond of the network is decorated with $D - 1$ cells representing single streets between each pair of successive intersections. Moreover, the traffic lights are assumed to flip periodically at regular time intervals T instead of alternating every time-step ($T > 1$). Each vehicle is able to move forward independently of the traffic light state, as long as it reaches a site where the distance to the traffic light ahead is smaller than the velocity. In this case the car is allowed to keep on moving for green traffic lights. Otherwise, it has to stop immediately in front of the signal. As one can see from Fig. 6.3 the network of streets builds a $N \times N$ square lattice, i.e., the network consist of N north-bound and N east-bound streets. The simple square lattice geometry is determined by the fact that the length of all $2N^2$ street segments is equal and that the street segments are assumed to be parallel to the x - and y -axis. In addition, all inter-

sections are assumed to be equal, i.e., there are no main roads in the network where the traffic lights have a higher priority. In accordance with the BML model streets parallel to the x -axis allow only single-lane east-bound traffic while the ones parallel to the y -axis manage the north-bound traffic. The separation between any two successive intersections consists of $D - 1$ cells so that the total length of a single street is $L = N \times D$. Note that for $D = 1$ the structure of the network corresponds to the BML model, i.e., there are only intersections without roads connecting them.

The traffic lights are chosen to switch simultaneously after a fixed time period T . Additionally, all traffic lights are synchronized, i.e., they are green for the east-bound vehicles and red for the north-bound vehicles or vice versa. The time periods for green traffic lights do not depend on the direction and thus the “green light” periods are equal to the “red light” periods. This is reasonable since there are no preferred streets. At this point it is important to mention that a large part of the investigations will consider different traffic light strategies. In the following the strategy described above will be called “synchronized strategy”. In addition the traffic lights are improved by assigning an offset parameter to them. This modification can be used, for example, to shift the switching of two successive traffic lights in a way that a “green wave” can be established in the complete network. The different traffic light strategies used are discussed in detail in the next chapters.

Update Rules

As in the original BML model periodic boundary conditions are considered and the vehicles are not allowed to turn at the intersections. Hence, the total number N_v of vehicles and also the numbers N_x and N_y of east- and north-bound vehicles are conserved. All these numbers are completely determined by the initial conditions. In analogy to the NaSch model the speed v of the vehicles can take on one of the $v_{\max} + 1$ integer values in the range $v = 0, 1, \dots, v_{\max}$. The dynamics of vehicles on the streets is given by the maximum velocity v_{\max} and the randomization parameter p of the NaSch model. The state of the network at time $t + 1$ can be obtained from that at time t by applying the following rules to all cars at the same time (parallel dynamics):

- Step 1: *Acceleration*:

$$v_n \rightarrow \min(v_n + 1, v_{\max})$$
- Step 2: *Braking due to other vehicles or red traffic lights*:
 - Case 1: The traffic light is red in front of the n -th vehicle:

$$v_n \rightarrow \min(v_n, d_n - 1, s_n - 1)$$
 - Case 2: The traffic light is green in front of the n -th vehicle:
If the next two cells directly behind
the intersection are occupied

$$v_n \rightarrow \min(v_n, d_n - 1, s_n - 1)$$
else
$$v_n \rightarrow \min(v_n, d_n - 1)$$
- Step 3: *Randomization with probability p* :

$$v_n \rightarrow \max(v_n - 1, 0)$$

- Step 4: *Movement*:

$$x_n \rightarrow x_n + v_n$$

Here x_n denotes the position of the n -th car and $d_n = x_{n+1} - x_n$ the distance to the next car ahead (see Fig. 6.3). The distance to the next traffic light ahead is given by s_n . The length of a single cell is set to 7.5 m in accordance to the NaSch model. The maximal velocity of the cars is set to $v_{\max} = 5$. Since this should correspond to a typical speed limit of 50 km/h in cities, one time-step approximately corresponds to 2 sec in real-time. In the initial state of the system N_v vehicles are distributed among the streets. In most cases the number of vehicles on east-bound streets $N_x = \frac{N_v}{2}$ is equal to the one on north-bound streets $N_y = \frac{N_v}{2}$. The global density then is defined by $\rho = \frac{N_v}{N^2(2D-1)}$ since in the initial state the N^2 intersections are left empty.

Note that *Case 2* of *Step 2* is slightly modified in comparison to the original formulation [140]. Due to this modification a driver will only be able to occupy an intersection if it is assured that he can leave it again. A vehicle is able to leave an intersection if at least the first cell behind will become empty. This is possible in most cases except when the next two cells directly behind the intersection are occupied. The modification itself is done to avoid the transition into a completely blocked state (grid-lock) that can occur in the original formulation of the ChSch model at sufficiently large densities. Further, in the original formulation [21] the traffic lights mimic effects of a yellow light phase, i.e., the intersection is blocked for both directions one second before switching. This is done to attenuate the transition into a blocked state (grid-lock). Since the blocked states are completely avoided in the modification a yellow light is not considered anymore. The reason for avoiding the grid-lock situation in the considerations is the fact that the impact of traffic light control on the network flow is analyzed in this thesis. Therefore, a transition to a blocked state would prevent from exploring higher densities. However, taking into account that situations where cars are not able to enter an intersection are extremely rare it gets clear that this modification does not change the overall dynamics of the model. Moreover, a comparison between the original formulation of the ChSch model and the modified one was done by simulations leading to no other differences except for the grid-lock situations which appear in the original formulation due to the stronger interactions between intersections and roads. Remind that a grid-lock effect, which leads to a complete breakdown of the traffic, also occurs in the BML model (see Sec. 6.2.1).

6.4 Traffic Light Control

Nowadays, traffic light control systems use complex optimization methods and simulation models to improve the overall traffic flow. The main task is to find appropriate parameters for the traffic lights. Important parameters are the cycle time (green phase and red phase), and the coordination between the traffic cycles of different traffic lights.

The traffic light control strategies can be divided into fixed and adaptive (traffic dependent) signal control, reacting more flexible on changing traffic states.

6.4.1 Fixed Signal Control

In most cities, the traffic lights are controlled by daytime dependent fixed cycle time plans. These plans are determined in the most cases with the help of certain simulation and optimization tools. In the following two different methods are briefly discussed since they are the basis for various tools.

The first one is **TRANSYT** [155], whose development started in 1969. The optimization is based on a “hill-climbing” algorithm that minimizes a defined quality factor which is a linear combination of the number of stops and the loss time in the network. For the calculation of the quality factor the vehicle movement is simulated with a waiting queue model. More precisely, vehicle pulks at the edges of a network are modelled. Thereby, vehicles can enter a pulk after a certain travel time³, coming from the preceding intersection, and leaving it with a defined outflow at “green light”. However, unfortunately the optimization is complex and highly machine time intensive. Furthermore, often only a local optimum of the network can be established.

A further optimization tool is **SIGMA** [56]. Here, two different optimization strategies, global vs. local optimization, can be applied. On one side the optimum of the whole network can be aspired, while on the other side certain streets can be preferred in the optimization. The optimization itself is also a complex task and therefore divided into three steps. In a first step, a starting solution is calculated for every intersection on the basis of the known traffic demand. Then in a second step, the starting solutions of each intersection are coordinated among each other in order to allow, for example, a “green wave”. Finally, the two solutions are systematically combined.

Obviously, the presented tools as well as other tools on the same basis reveal some serious problems. First of all, there is the problem of finding solutions in large networks with an optimization algorithm. This is an extremely hard task since many parameters must be considered. Furthermore, if a solution is found, it is not guaranteed that this one represents the *global* optimum of the complete network.

Simon and Nagel [145] found an important result for CA models with respect to traffic signals. They explored the effects of different time-dependent blockage sites in the NaSch model. Including random blockage, fixed red and green time intervals as for traffic lights, and a Dirac like (delta-peak) blockage. However, none of the methods returned a linear relationship between the fraction of green time and the throughput, which would be recommended for traffic lights optimization tools as presented above. Therefore, it is probably not advisable to simply exchange the waiting queue models by CA models.

In the next chapter the impact of fixed traffic light strategies in the ChSch model is investigated. Here, another way of optimization is adopted. Instead of using complex optimization methods the model is analyzed systematically since the number of parameters is manageable. The aim is to find optimal solutions for the model. These solutions can of course not be related directly to a realistic city network but may serve as a guideline.

6.4.2 Adaptive Signal Control

The development of adaptive signal control was evolved in two steps. In the early tools, the cycle times of traffic lights were determined by fixed algorithms using local measurements like flow or density to improve the traffic conditions. The methods have the disadvantage that they are not able to work properly in saturated networks (at high densities) since in this cases the algorithms operate at their maximum cycle times. Then the signal control behaves like a fixed signal control.

In order to avoid the fixed control, recent tools were improved by a global optimization strategy. Additionally, these tools utilize a traffic forecast algorithm within a certain time horizon.

Common adaptive signal control tools of the second generation are for example:

³The travel time only depends on the street length in this approach.

OPAC [46], a decentralized tool for single intersections that makes use of dynamic programming. The time is divided into discrete time-steps, and within a defined time horizon the signal phases are determined (optimized) on the basis of an assumed traffic volume. After every time-step the optimization must be recalculated. Note that this method can not be used for online systems since the knowledge about the traffic volume for the complete optimization time is needed.

UTOPIA [106], focusing on the optimization of public transport and individual traffic. These are organized in a hierarchical structure whereby public transport is preferred. As an extension in comparison to OPAC a rolling time horizon is used, instead of a fixed one. This qualifies UTOPIA for online (real-time) systems.

Further common adaptive signal control tools are: **PRODYN** [63], **SCATS** [146], **SCOTS** [134], and **MOTION** [12].

Obviously, the second generation of adaptive signal control tools suffer from the same problems as the fixed tools since global optimization is included. A further problem, especially of first generation adaptive signal control is the fact that it cannot be evaluated in how far the *global* optimum of a system is reached since this is unknown.

In chapter 8 the ChSch model is enhanced by an adaptive signal control. Here, the signal control reacts on local traffic conditions. The impact of three suggested adaptive signal algorithms is analyzed systematically and the results are compared to the results gained by simulations with fixed strategies. Fortunately, the performance of these algorithms can be rated since a description for the *global* optimum of the ChSch model was found in chapter 7.

7 Global Traffic Light Control in the ChSch Model

Traffic light control is usually determined by means of linear or non-linear optimization algorithms. These are applied to complex traffic models containing a huge number of parameters. The optimization procedures are known to be a hard mathematical problem, consuming an immense machine time. Unfortunately, in the most cases only local optima are obtainable and the *global* optimum, which may be much better, resides hidden.

An important feature of the ChSch model is its simplicity, i.e., the number of parameters is small and manageable. Therefore, the impact of traffic light control in the ChSch model can be systematically analyzed in the following. The aim is to find parameter combinations to establish the *global* optimum in the system and thereby improve the overall traffic conditions in the system. Such optimal strategies may serve as a guideline how to optimize the traffic flow in realistic traffic scenarios.

At this point it has to be taken into account that all streets are treated as equivalent in the ChSch model, i.e., there are no dominant streets. This makes the optimization much more difficult and implies that the green and red phases for each direction should have the same length. For a main road intersection with several minor roads the total flow can usually be improved by optimizing the flow on the main road.

7.1 Synchronized Traffic Lights

Three different global traffic light strategies are investigated. The starting point is the “synchronized traffic lights” strategy, considered in the standard formulation of the ChSch model (see Sec. 6.3). It is shown that a simple “mini network”, consisting of an one-dimensional road with one single traffic light in its middle, leads to appropriate results that are also valid for larger systems.

Furthermore, it is shown that a two-dimensional “green wave” strategy can be established in the ChSch model. The “green wave” strategy improves over the “synchronized traffic lights” strategy and even leads to the *global* optimum of the model.

Finally, it is demonstrated that switching successive traffic lights with a random shift, denoted as “random offset” strategy, can be useful in order to create a more flexible strategy that does not depend much on the model and network parameters. Throughout this chapter, it is assumed that the duration of the “green light” phase is equal to the duration of the “red light” phase. Fortunately, many of the numerical results affecting the dependence between the model parameters and the optimal solutions for the chosen control strategies can be derived by simple heuristic arguments in good agreement with the numerical results.

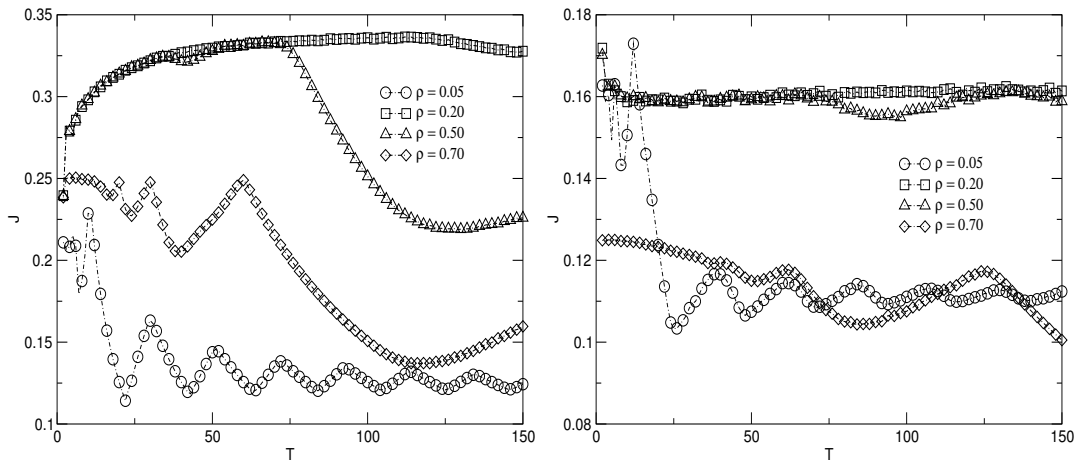


Figure 7.1: The mean flow J of the smallest network segment (one single intersection, $N = 1$) is plotted for different global densities as a function of the cycle length T . In the left plot the randomization parameter is $p = 0.1$ while in the right plot higher fluctuations ($p = 0.5$) are considered. The length of the street is $L = 100$ and the flow is aggregated over 100.000 time-steps.

7.1.1 One Single Street ($N = 1$)

In the following, the smallest possible network topology of the ChSch model is investigated. Obviously, this is a system consisting of only one east-bound and one north-bound street, i.e., $N \times N = 1$, linked by a single intersection. As a further simplification only one of the two directions of this “mini network”, i.e., a single street with periodic boundary conditions and one signalized cell in the middle, is considered. It is obvious that in the case of one single traffic light the term synchronized is a little bit misleading but the relevance of this special case to large networks with “synchronized traffic lights” is discussed later. Figure 7.1 shows the typical dependence between the time periods of the traffic lights T and the mean flow in the system J . For low densities one finds a strong oscillating curve with maxima and minima at regular distances. In the case of a small fluctuation parameter p (left plot) similar oscillations can even be found at very high densities. For an understanding of the underlying dynamics leading to such strong variations in the mean flow the microscopic structure is explored. This allows to formulate a simple phenomenological approach being in good agreement with numerical results. Note that free-flow¹ densities are investigated here, where the vehicles are not constricted by jamming due to the model dynamics but rather by “red” traffic lights. Hence, the free-flow density range shows the largest potential for flow optimization. Later on, the origin of the oscillating flow even at very high densities, which is completely different to the free-flow case, is discussed.

If not stated otherwise, the following parameters are used in this chapter: Street segment length $D = 100$, maximum velocity $v_{\max} = 5$, randomization parameter $p = 0.1$.

¹Here states are denoted as free-flow states if the mean density is smaller than the density corresponding to the maximum flow of the underlying NaSch model.

7.1.2 Low Density – Phenomenological Approach

To give an impression of the influence of the cycle time on the vehicle movement a schematic representation of the observed street is depicted in Fig. 7.2. This picture covers typical dynamical patterns occurring in the system due to vehicles restricted in their movement by the “red light”. Based on these scenarios, a simple phenomenological approach is presented in the following which is able to explain the dependence between vehicle movement and model parameters.

It is assumed that during one traffic light cycle freely moving vehicles organize in an almost stable platoon with a nearly constant width. Furthermore, it is assumed that a phase separation between freely moving and jammed vehicles takes place at high densities. The legitimation for these assumptions is given by the fact that the vehicle movement is triggered by the traffic lights, i.e., vehicles are gathered in front of a signal and hence fluctuations can not spread out.

In the following the focus lies on five scenarios (a)–(e). The cases (a), (b), and (c) describe the derivation of the maxima/minima of the (v, T) -curve, (d) gives a calculation of the mean velocity between maxima and minima, and (e) finally a calculation of the mean velocity between the minima and maxima.

With respect to the cycle time duration, three different cases can be distinguished. The first case considers cycle lengths smaller than the travel time from one intersection to the succeeding which is analyzed in scenario (a). The second case is the most important and realistic one. Here, the cycle length is of the order of the travel time. This is described in the scenarios (b)–(e). Note that all further results in this chapter focus on this case. The third possibility deals with cycle lengths larger than the travel time which are not further investigated since they are unrealistic. Furthermore, it was found that the flow converges fast to its limit $T \rightarrow \infty$. This corresponds to the case where vehicles are free to move on one direction all the time while on the other direction it comes to a complete stop. The flow then is exactly half of the flow found in the underlying NaSch model.

(a) The time a free flowing vehicle requires to move from one intersection to the succeeding one (one full turn on the periodic street) is equal to

$$T_{\text{free}} = \frac{D}{v_{\text{free}}}, \quad (7.1)$$

where $v_{\text{free}} = v_{\text{max}} - p$ is the free-flow velocity of the underlying NaSch model. In Fig. 7.2a a situation is depicted where vehicles organize in a platoon (light grey rectangle) that is able to move ahead all the time. This is only possible if the time for one complete traffic light cycle, i.e., including green and red phase, is equal to the travel time of a vehicle ($T_{\text{free}} = T_{\text{green}} + T_{\text{red}} = 2T$) so that the vehicle platoon arrives at “green light” at the intersection. Obviously, this case is related to a maximum in the flow, whereby the traffic light period is determined by $T = T_{\text{free}}/2$. Additionally, there are further maxima when $T_{\text{free}} = n(T_{\text{green}} + T_{\text{red}})$ with $(n = 0, 1, 2, \dots)$, i.e., within the travel time T_{free} of a vehicle n complete traffic light cycles ($T_{\text{green}} + T_{\text{red}}$) take place. Thus, the traffic light periods corresponding to a maximum in the system flow are given by:

$$T_{\text{max}} = \frac{T_{\text{free}}}{2n}. \quad (7.2)$$

With similar arguments the occurrence of minima can be explained. These minima correspond to situations where the traffic lights switch exactly to red when a vehicle platoon reaches an intersection. It is clear that these assumptions are only valid for very short

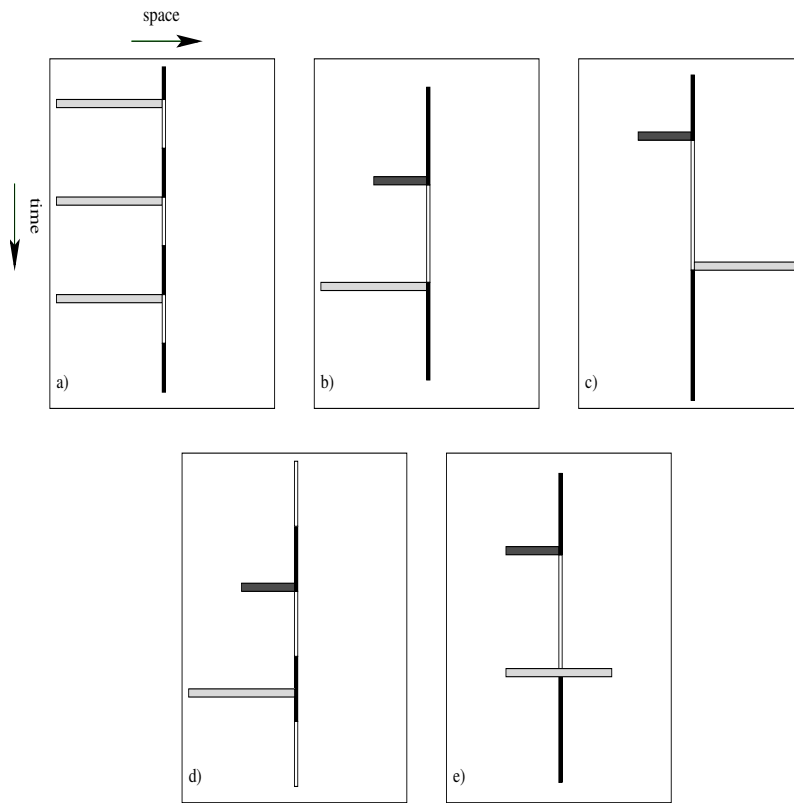


Figure 7.2: Schematic representation of the vehicle movement on an east bound street for different cycle times. Standing cars are represented by dark grey rectangles (x -axis) while moving vehicle platoons are bright grey rectangles. The traffic light is placed in the middle of every figure (time runs along the y -axis). Its state is indicated by the color of the vertical rectangle. “Green light” corresponds to the white colored area of the traffic light while “red light” is painted in dark. At this point one has to take into account that the considered street has periodic boundary conditions and therefore vehicles (light or dark grey rectangle) leaving the right end of every scenario (a)–(e) will return after a certain time on the left side.

cycle times ($2T \leq T_{\text{free}}$) as mentioned above. In the following the focus lies on more realistic larger cycle times of the order of the travel time, i.e., $2T \geq T_{\text{free}}$.

(b) In Fig. 7.2b a situation is shown where vehicles are gathered in front of a “red light”. After the traffic light switches to green the vehicles start moving. Then it switches back to red exactly at the time when the first car of the moving vehicle platoon reaches the intersection again. Now the complete platoon comes to a rest and has to wait until the traffic light switches to green again to continue the movement. Obviously, this case corresponds to a minimum in the flow. The related cycle time is given by the following assumptions. It is sufficient to focus on the first car of the platoon. At the beginning the first vehicle has to accelerate to its maximum velocity. This acceleration process will take on average $T_{\text{acc}} = \frac{v_{\text{max}}}{1-p}$ time-steps. After that, the vehicle has to trespass the remaining part of the street until it reaches the intersection again. The mean velocity on that part

of the road is given by v_{free} . The length of this road segment is given by the length of the street minus the distance that the vehicle has covered during its acceleration phase. Therefore, the time $T_{\text{first}} = \frac{D - T_{\text{acc}}(v_{\text{max}} + 1)/2}{v_{\text{free}}}$ elapses until the intersection is reached. In summary, if the chosen cycle time is equal to

$$T_{\text{min}} = T_{\text{acc}} + T_{\text{first}} + nT_{\text{free}}, \quad (7.3)$$

the system flow is minimal. The last term nT_{free} (with $n = 0, 1, 2, \dots$) takes into account traffic light periods that are larger than the required time to make one turn on a periodic system or to move from one intersection to the succeeding one (for the case $N > 1$). That way the vehicle platoon is able to perform n “turnarounds” before it has to stop immediately in front of the “red light”. These minima at regular distances of T_{free} time-steps can be easily identified in Fig. 7.1.

(c) In accordance with the occurring minima, one also finds maxima at regular distances. These maxima correspond to situations where the length of the green time intervals is sufficiently large so that the last vehicle of a moving platoon is able to pass the intersection before the traffic light switches to red. To derive the cycle times corresponding to this situation one has to focus on the last car of a platoon. Before the traffic light switches to green there are N_{wait} vehicles standing in front of it (dark grey rectangle) (see Fig. 7.2c). After switching to green the last vehicle of the platoon has to wait on average $T_{\text{wait}} = \frac{N_{\text{wait}} - 1}{J_{\text{out}}}$ time-steps before the vehicle in front starts to move (J_{out} is equal to the flow out of a jam). Then further T_{acc} (see case (b)) time-steps are needed for the vehicle to accelerate to its maximum velocity. From then on the vehicle has to reach the first cell (behind the intersection) of the succeeding street within the remaining “green light” interval. The required time to cover this part of the road is given by $T_{\text{last}} = \frac{D + N_{\text{wait}} - T_{\text{acc}}(v_{\text{max}} + 1)/2}{v_{\text{free}}}$. Note that in comparison to case (b) the last vehicle has to cover a slightly larger distance than the first one due to its shifted starting position of about N_{wait} cells. Therefore, the system is in a maximum flow state for the following cycle time:

$$T_{\text{max}} = T_{\text{wait}} + T_{\text{acc}} + T_{\text{last}} + nT_{\text{free}}. \quad (7.4)$$

As in (b) described, the last term nT_{free} takes into account large cycles where the vehicle platoon is able to make n full turns before the pictured situation occurs.

(d) The previous cases (a)–(c) are used as a basis for simple heuristic arguments in order to derive the cycle times corresponding to maximal and minimal mean flow states in the system. Now it is shown that even the complete dependence of the mean velocity on the cycle time can be obtained from phenomenological assumptions. For this purpose it is focused on a situation where the vehicle platoon is able to cross the intersection within the “green light”, i.e., the traffic light does not switch during the time the vehicle platoon occupies the intersection. After the vehicle platoon has passed the intersection, at most n times, the vehicles will come to a rest in front of a “red light” at some times. The remaining waiting time now depends on the chosen cycle time. If the traffic light switches to red immediately before the vehicles reach the intersection, the situation corresponds to the case of minimal flow (see (b)), i.e., the vehicles must wait for the complete cycle time T . In the contrary, if the traffic light switches to green directly after the platoon has trespassed the intersection, this situation corresponds to the case of maximal flow (see (c)), i.e., the vehicle platoon can perform a complete turn within a “red light” phase, and therefore the remaining waiting time becomes minimal. The more general case is given by

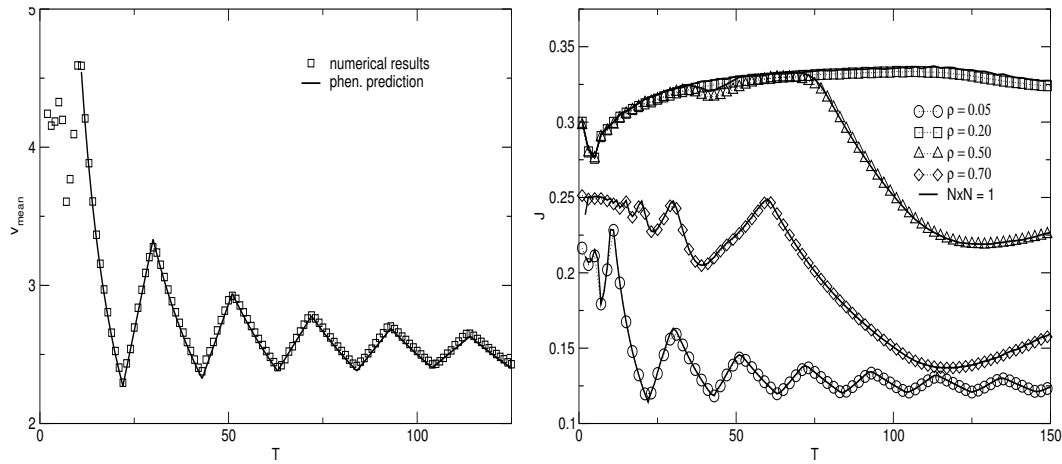


Figure 7.3: **Left:** The mean velocity v_{mean} for a “mini network” $N = 1$ is plotted against the cycle time T . The density on the street is set to $\rho = 0.05$ (free-flow case). One can clearly see that the phenomenological approximation agrees well with the simulation data. **Right:** In order to show how the small network segment with $N = 1$ compares to a large network, a “mini network” is plotted, consisting of one single intersection as well as a relatively large network consisting of $N \times N = 25$ intersections with $2N^2$ street segments.

a situation between maximal and minimal flow, i.e., the vehicle platoon is able to pass the intersection and then after a certain time the traffic light switches to red. To obtain the mean velocity of the vehicles within a complete cycle $T_{\text{cycle}} = 2T$, one neither has to take into account the waiting times of vehicles in the starting phase nor the acceleration process of the vehicles until the maximum velocity is reached. In fact, only the driven distance which is equal to the number of “turnarounds” n for each vehicle must be considered in order to obtain the mean velocity. Note that each vehicle starts its movement out of a certain position in a queue waiting in front of the traffic light and will occupy exactly the same position when it comes again to rest. The mean velocity is given by

$$\bar{v}_{\text{max-min}}(T, n) = \frac{nD}{2T}. \quad (7.5)$$

With Eq. 7.5 it is possible to plot the mean velocity of the system against the traffic light periods only between each n -th maximum and n -th minimum of the curve. The shape of the curve between the n -th minimum and the $(n+1)$ -th maximum is discussed in (e). One should keep in mind that the scenarios (b)–(e) assume $T \geq T_{\text{free}}$, i.e., the cycle times T are in the order of the travel time.

(e) In Fig. 7.2e a situation is pictured where the traffic light switches to “red light” within the time interval at which the vehicle platoon crosses the intersection. As a consequence the fraction of vehicles in front of the traffic light will come to a stop while the rest of the vehicles is able to move on until they reach the traffic light again (periodic boundary conditions). The fact that only a fraction of vehicles is able to complete n cycles whereas the other can complete $n+1$ cycles before they are forced to stop, leads to a simple linear dependence between the mean velocity and the cycle time in this area (see Fig. 7.3).

The left part of Fig. 7.3 points out in what kind the mean velocity of the north bound

street of the considered “mini network” depends on the cycle times. As one can see, the theoretical curve shows an excellent agreement with the simulation data. Not only the positions of the maxima and minima are predicted by theory but also the shape of the curve between the extremals shows a good agreement with the numerical results. Note that the mean velocity on the east bound street shows exactly the same picture. This is not surprising since the duration of the traffic light cycles for both directions is the same. Therefore, the two different directions can be considered as decoupled and independent.

7.1.3 Extension to Large Networks ($N \times N > 1$)

The right part of Fig. 7.3 shows that the results obtained from the observed “mini network” are completely transferable to large networks. Thus, it is stressed here that the assumptions made in (a)–(e) are useful to adjust the optimal cycle times in the ChSch model with “synchronized traffic lights”. The excellent agreement between the small and the large network situation can be ascribed to the “synchronized traffic lights” strategy. In fact, there is no difference for a vehicle approaching an intersection which is a part of a large network or approaching the only existing intersection due to the periodic boundary conditions. The state of the traffic lights is in both cases determined by the “synchronized traffic lights” strategy. Moreover, it is interesting that, although the vehicle movement is stochastic (NaSch model) and the mean density on the streets in the network fluctuates, there is no local concentration of vehicles in the network leading to remarkable deviations in the flow compared to the idealized “mini network” where the density on the streets is conserved. Remind that in the original formulation of the ChSch model the blockage of intersections is allowed. Therefore, fluctuations can lead to a complete breakdown of the flow at high densities where standing vehicles are gathered in different parts of the network. It seems that the signalized intersections of the model interact with the density fluctuations in a way that the vehicles are equally distributed in the network. Although there are extreme fluctuations in the distribution, they do not play an important role in progress of time because the blockage of an intersection due to such fluctuations is excluded here (see Sec. 6.3) so that the density on the roads fluctuates around a mean value. In the following, networks are considered consisting of $N \times N = 25$ intersections.

7.1.4 High Density

So far the free-flow case of the ChSch model was discussed in the scenarios. But also for high densities one can find a strong dependence of the mean flow on the cycle time (see Fig. 7.1). Obviously, for high densities, this dependence is not caused by free flowing vehicle platoons passing or not passing an intersection, but rather due to the movement of large jams gathered in front of the traffic lights. These jams move in opposition to the driving direction.

Starting at densities slightly above the free-flow density (see $\rho = 0.2$ in Fig. 7.3). Here, the mean flow shows no characteristic maxima or minima. The jams in the system are small compared to the cycle times, i.e., the time a jam will block an intersection is negligible small. For small traffic light cycles, large jams are divided into smaller ones by the alternating signal cycles. The mean flow increases with increasing cycle times in this region since the distance between the small jams grows so that the vehicles can accelerate to their maximal velocity. If the cycle time is further increased, the global flow reaches a nearly constant level.

At intermediate densities (see $\rho = 0.5$ in Fig. 7.3) one can find a similar behavior. As for densities about $\rho = 0.2$ the number of jams decreases with increasing cycle times and

the flow grows slightly until it breaks down at a certain value. This breakdown can be explained as follows: At long cycle times only one jam remains between two intersections because the “red light” phase is large enough to gather all vehicles in front of the traffic lights. The breakdown finally occurs when the “red light” phase is even larger than the time needed to conglomerate all vehicles in front of it. As a consequence, the vehicles have to wait considerably longer than they are able to move. Note that the motion at “green light” is hindered because of the fact that for the considered density the jams are relatively large. Therefore, an intersection is blocked when it is reached by the backward moving jam for a long part of the “green light” phase.

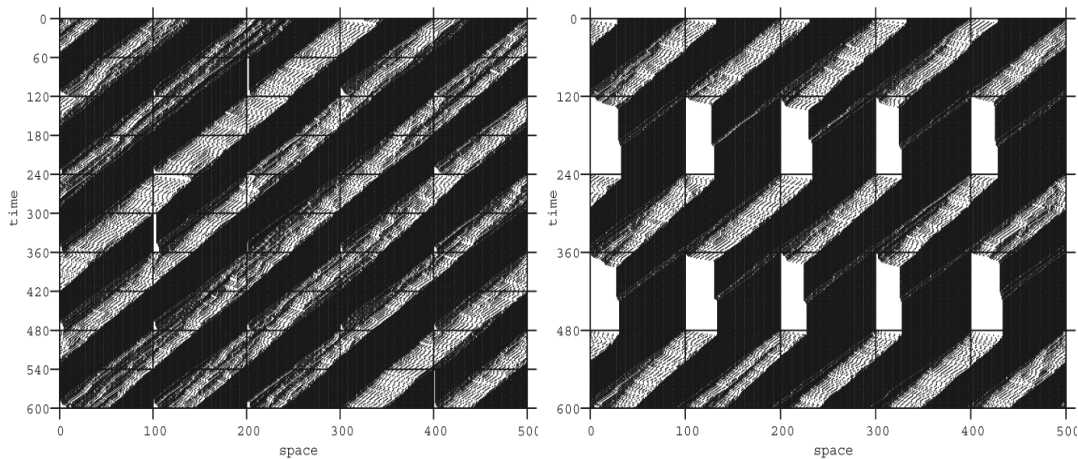


Figure 7.4: In order to give an impression about the origin of the strong oscillations at high densities $\rho = 0.7$, space-time plots are given once for a maximum (left) and once for a minimum (right) flow state. The position of the intersections are represented by the vertical lines. The times corresponding to a switching of a traffic light are represented by the horizontal lines (starting with green traffic lights).

It is interesting that for high densities (see $\rho = 0.7$ in Fig. 7.3) a strong oscillation of the mean flow can be found with characteristic maxima and minima, similar to the free-flow case. This is caused by the fact that at high densities the dynamics of the system is completely determined by the movement of jams. For example, if the length of one cycle (“red light” and “green light”) is chosen in such a way that it is equal to the time the downstream front of a jam needs to move from one intersection to the next one, the large jam will block the intersection when it is red anyway. This corresponds to a maximum in the global network flow and is shown in the left part of Fig. 7.4. It can be seen that the jams are compact and can move nearly undisturbed through the system since the traffic lights at intersections are red when they are blocked by a jam and the time such a jam needs to pass an intersection is in the order of the cycle time. Furthermore, free flowing vehicles can move undisturbed between the jams.

The right part of Fig. 7.4 represents a minimum in the flow. In addition to the “red light” phase also the “green light” phase is mostly blocked by a jam so that the movement at “green light” is hindered.

However, the fraction of time when the “red light” has no influence on the mean flow, because the intersection is blocked by a jam, determines the shape of the curve between the extremals similar to the free-flow scenarios. At this point it must be emphasized that high densities are more difficult to investigate because the jamming in the NaSch model

is strongly determined by the fluctuation parameter. For higher p spontaneous jams can occur even in the outflow region of a jam and therefore jams are not compact anymore. Therefore, at high densities one can see a relatively strong influence of p while in the free-flow case the value of the randomization parameter p does not play an important role.

7.1.5 Optimal Fundamental Diagram

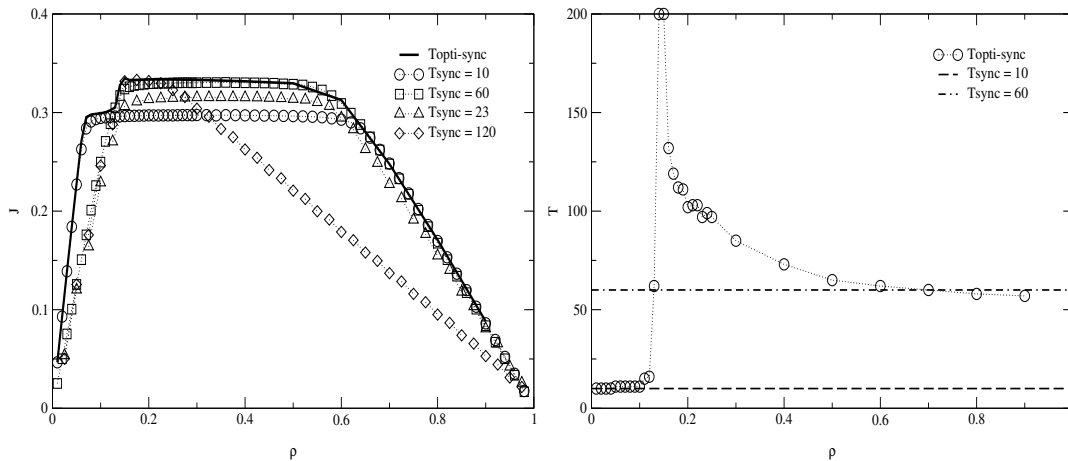


Figure 7.5: The optimal FD for a system with “synchronized traffic lights” is shown in the left plot. The optimal curve (solid line) is obtained by numerical simulations considering cycle times in the interval $T = 0 \dots 200$ for each density. As one can see, the curve can be approximated by the fixed cycle times $T = 10$ and $T = 60$ for different densities. In the right plot the corresponding cycle times are shown. The system parameters are: $N \times N = 25$, $D = 100$, $p = 0.1$, $v_{\text{max}} = 5$.

In Fig. 7.5 (left) the optimal FD for a system operating with “synchronized traffic lights” is plotted. The FD was obtained by systematically scanning the model parameters. More precisely, the curve was obtained by picking the optimal cycle times corresponding to the maximal flow out of plots depicting mean flow vs. cycle time. Therefore, the complete density range was divided into units of $\Delta\rho = 0.01$ and the related plots were analyzed for each density. A mean flow vs. cycle time plot is given in Fig. 7.3 (right) for example.

A wide plateau can be identified in the optimal FD for intermediate densities. This is comparable to other systems with a bottleneck (see Chapter 4). Furthermore, it is noticeable that the upper limit (plateau) for the maximum flow is established at a level about half of the maximum flow of the NaSch model (periodic ring). This circumstance can be ascribed to two facts. First, the directions in the ChSch model are treated equally, and second, the outflow of a jam in the NaSch model self-organizes near to the point of maximum flow. Moreover, the dynamics in the network is determined, for intermediate densities, by vehicles gathered in front of the “red light” (half cycle time) and vehicles moving out of the jam at “green light” (half cycle time). Consequently, the flow in the ChSch model is approximately half of the maximum possible flow of the NaSch model. This is confirmed in Fig. 7.6 where optimal FDs (high densities) are plotted for different street lengths. It can be seen that the maximum flow converges to the half of the maximum flow of the NaSch model, since for large streets (long optimal cycle times) the acceleration processes at the intersections are negligible.

In the right part of Fig. 7.5, the corresponding optimal cycle times are plotted explicitly for

the investigated densities. As one can see, the optimal cycle times for low densities (free-flow) are equal to $T = 10$ and for high densities in the area of $T = 60$. These results are in correspondence with the foregoing argumentations where the optimal free-flow cycle time is described by Eq. 7.1, and for high densities it is assumed that the flow is determined by backwards moving jams². The velocity of such a backwards moving jam is approximately $v_{\text{jam}} \approx (1 - p)$ (see [124]). Assuming that the optimal time for a complete traffic cycle is the travel time $T_{\text{jam}} = \frac{D}{v_{\text{jam}}}$ of the jam between two intersections, the measured cycle time of $T = 60$ in Fig. 7.5 can be explained. Note that the same argumentation holds for systems with different parameters, e.g., larger streets. Therefore, the optimal parameters for the “synchronized traffic lights” strategy can be easily obtained for arbitrary parameter combinations. This can be seen for example in Fig. 7.6 where the optimal FDs for high densities are plotted for different street lengths.

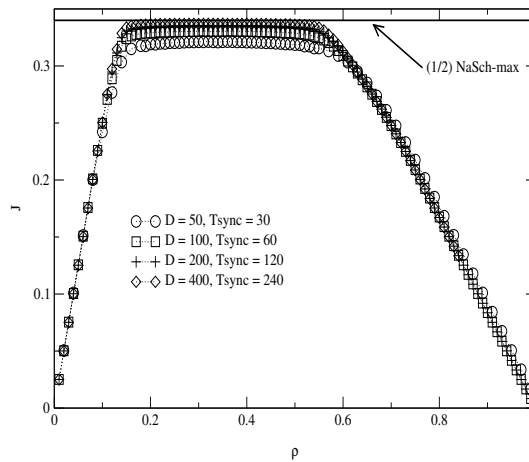


Figure 7.6: Optimal FDs of the ChSch model with “synchronized traffic lights” are plotted for different street lengths. The maximum flow converges to the half of the maximum flow of the NaSch model.

However, at intermediate densities the optimal cycle times are relatively long, accompanied by a sharp transition (see Fig. 7.5 (right)). Fortunately, for this intermediate densities, the global flow is not as sensitive in respect to the chosen cycle times as it is in the case of low or high densities. This can clearly be seen in Fig. 7.3 for $\rho = 0.2$ (no oscillation). Therefore, a simple traffic light control strategy for “synchronized traffic lights” in the ChSch model can be derived, which nearly matches the optimal FD of the system.

The corresponding FDs are plotted for $T = 10$ and $T = 60$ time-steps in (see Fig. 7.5 (left)). It can be seen that the two curves match the optimal FD diagram (solid line). Hence, the following strategy is proposed.

$$T_{\text{approx-sync}} = \begin{cases} \frac{T_{\text{free}}}{2} & \text{for } \rho < \rho_T, \\ \frac{T_{\text{jam}}}{2} & \text{for } \rho > \rho_T. \end{cases} \quad (7.6)$$

The transition density ρ_T is equal to 0.12 for the illustrated case. It is determined by the intersection point of the two curves ($T = 10$, $T = 60$). Note that the plateau of the free-flow FD ($T = 10$) is below the maximum flow.

²For very high densities only a few cells are empty. These cells (holes) move backwards with a velocity of $v_{\text{hole}} = 1 - p$.

Although the optimum can be reached with a simple strategy, some caution is necessary anyhow. As mentioned before, the global flow in the system shows a strong dependence on the chosen cycle times for low (free-flow) as well as for high densities. Therefore, if improper cycle times are used in the simple strategy, strong limitations in the maximal flow can occur. This is also shown in Fig. 7.5 where the FD diagram for two unfavorable cycle times is plotted ($T = 23$, $T = 120$). For $T = 23$, this corresponds to a free-flow minimum (see Fig. 7.1), clearly heavy losses of the flow are noticeable while the flow at intermediate and high densities is unaffected. In the case of $T = 120$ the plateau in the FD almost vanishes, and merge into the half of the FD of the NaSch model. Here the losses in the overall flow are enormous.

7.2 Green Wave Strategy

In the previous section the dependence between traffic light periods and throughput in the ChSch model for “synchronized traffic lights” was discussed. It was shown that the problem can be reduced, for free-flow densities, to an analysis of a single segment (i.e., $N \times N = 1$) of the network. This indicates that synchronizing the traffic lights is an ineffective strategy for free-flow densities, which is not capable to bring an additional gain out of the network topology. Further, it is shown that particularly at free-flow and high densities there are strong oscillations in the throughput (flow) depending on the chosen traffic light periods. Furthermore, at free-flow densities (see Fig. 7.1) the maximal flow (first maxima) is located at a very short cycle time. However, a simple strategy by only considering two different cycle times in respect to a transition density was proposed, leading to the optimum of the ChSch model with “synchronized traffic lights”. In order to improve the flow in the ChSch model, a simple “green wave” strategy is introduced in the following. Besides, the “green wave” is probably the best known traffic light strategy for optimizing city traffic. Therefore, the analysis of its impact onto the overall flow in the ChSch model is of special interest.

7.2.1 Offset Parameter

The traffic lights of the ChSch model are enhanced by an individual offset parameter $\Delta T_{i,j}$ so that they are not enforced to switch simultaneously anymore. In the following the intersections are denoted with indices i, j where $i = 0, 1, \dots, N - 1$ represents the rows and $j = 0, 1, \dots, N - 1$ the columns of the quadratic network. The offset parameter is used to implement a certain time delay T_{delay} between the traffic light phases of two successive intersections. The offset parameter itself can take on the values $\Delta T_{i,j} = 0, \dots, 2T$. Note that a larger $\Delta T_{i,j}$ has no effect because $2T$ corresponds to one complete cycle of a traffic light. The main intention establishing a “green wave” on an intersected street is to keep a platoon of vehicles in motion. It is obvious that the optimal strategy is to adjust the time delay between two successive intersections such that the first vehicle of a moving platoon trespassing an intersection will arrive at the next traffic light exactly at the time when it switches to “green light”. This delay is just the time a free flowing vehicle needs to move from one intersection to the succeeding one, i.e., $T_{\text{free}} = \frac{D}{v_{\text{free}}}$. Thus, this is the optimal time delay T_{delay} between two intersections. Since the interest is in constituting the “green wave” in the whole network, two directions must be taken into account. The intersection at the bottom left corner of the network is the starting point with no time delay $\Delta T_{0,0} = 0$. Then the offset in the first row will be chosen as described, i.e., the time delay between

two successive intersections is in the optimal case equal to T_{free} . After the first row is initialized every intersection in this row will be seen as a new starting point to initialize the corresponding columns. In summary, the offset parameter of the intersections is given by

$$\Delta T_{i,j} = ((i+j)T_{\text{delay}}) \bmod(2T), (i, j = 0, 1, \dots, N-1), \quad (7.7)$$

with the optimal offset parameter $T_{\text{delay}} = T_{\text{free}}$ one gets

$$\Delta T_{i,j} = \left((i+j) \frac{D}{v_{\text{free}}} \right) \bmod(2T), (i, j = 0, 1, \dots, N-1). \quad (7.8)$$

Using this method, a two-dimensional “green wave” strategy can be established in the ChSch model.

7.2.2 Low Densities

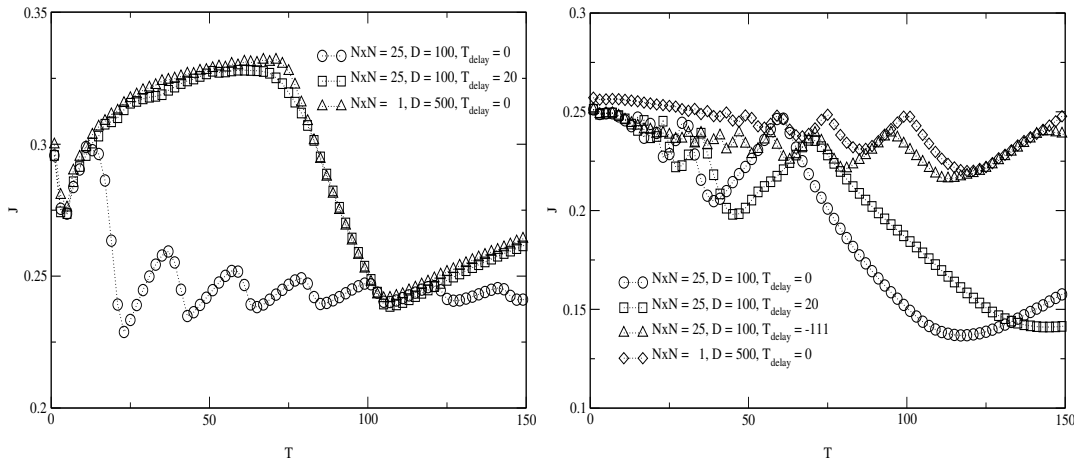


Figure 7.7: In the left plot free-flow densities are considered. The “green wave” strategy ($T_{\text{delay}} = 20$) shows reasonable improvements for the most cycle times over the network with “synchronized traffic lights” ($T_{\text{delay}} = 0$). The right plot shows the influence of the “green wave” strategy in the high-density state. Also for high densities, the performance of the network with “synchronized traffic lights” is exceeded for the most cycle times by the “green wave” strategy.

To quantify the improvement obtained by the “green wave” strategy the overall network flow is plotted against the cycle time in Fig. 7.7 and compared with the “synchronized traffic lights” strategy. The left diagram corresponds to the free-flow case of the system. The density is chosen to $\rho = 0.05$ to ensure that moving vehicles are able to drive from one intersection to the next one without being constricted by jammed cars. Obviously, the “green wave” strategy with a properly chosen offset parameter, i.e., for the considered street length equal to $T_{\text{free}} = T_{\text{delay}} = 20$, shows reasonable improvements over the strategy with “synchronized traffic lights” ($T_{\text{delay}} = 0$). The whole spectrum of plotted cycle times T for the “green wave” strategy exceeds the performance of the network with “synchronized traffic lights” or at least keeps the performance. Moreover, comparing the “green wave” strategy to a network consisting of only one intersection, but with the same total street

length, one finds a remarkable agreement of the curves. Note that every street in the considered network with $N \times N = 25$ is intersected five times. Therefore, it should be stressed here that for free-flow densities in the ChSch model the “green wave” strategy is capable to pipe all vehicles through the streets as if there is only one intersection left. This is due to the fact that the remaining intersections are always green when approached by the vehicle platoon. Further, one should note that similar to the case with a “synchronized traffic lights” strategy the traffic lights interact with the vehicles in such a way that a “green wave” is established in the whole network independent of the initial vehicle distribution or the density fluctuations caused by the internal stochastic part of the model.

Recapitulating, the most important benefits occur at low densities. Here, the “green wave” strategy gives the impression as if the street is intersected only once. Therefore, the optimal cycle time of a traffic light corresponding to the maximal flow is shifted towards realistic values even for small street segment lengths D . One obtains the following equation for the cycle time corresponding to maximal flow (see Eq. 7.2):

$$T_{\max} = \frac{L}{2v_{\text{free}}} = \frac{ND}{2v_{\text{free}}}. \quad (7.9)$$

7.2.3 High Densities – Red Wave

As one can see in the right part of Fig. 7.7 even for high densities the “green wave” strategy shows an incisive impact on the network flow. Although by definition no “green wave” can be established at high densities (for the chosen density of $\rho = 0.7$ no jam free state can exist), an offset in the switching between successive traffic lights can lead anyhow to an improved flow. The origin of this improvement is completely different in comparison to the free-flow case. For low densities the dynamics is driven by vehicles organized in platoons which can move through the streets undisturbed due to the optimal strategy, whereas the dynamics for high densities is governed by the motion of large jams. Large jams move oppositely to the driving direction of the vehicles, from one intersection to the one before. Due to their spatial extension an intersection is blocked for a certain time when trespassed by a jam. Thus, the optimal system state would be reached if a jam moves backward from one intersection to the one before and blocks it while the traffic light is red anyway so that afterwards moving vehicles (outflow of the jam) can take advantage of the green phase as much as possible. In fact, the portion of time that an intersection is blocked by a jam or free determines the system flow at high densities. Note that the time delay at high densities has to be negative since jams move opposite to the driving direction. This is different from the “synchronized traffic lights” case where all lights switch simultaneously so that for high densities only a positive fixed optimal cycle time has to be considered. For a time delay in the order of the optimal time delay of the free-flow case (see Fig. 7.7 (right) for $T_{\text{delay}} = 20$) the curves corresponding to the “green wave” strategy and the “synchronized traffic lights” do not differ much because this T_{delay} is determined by the free vehicle movement. Considering the velocity of a jam instead, which is approximately about $v_{\text{jam}} \approx (1 - p)$ (see [124]), and assuming that the optimal time delay is the travel time $T_{\text{jam}} = \frac{D}{v_{\text{jam}}}$ for the backward motion of a jam between two intersections, the difference to the “synchronized traffic lights” case gets transparent (see Fig. 7.7 (right) for $T_{\text{delay}} = -111$). The “green wave” strategy allows now a reasonable improvement over the “synchronized traffic lights” strategy. Similar to the free-flow density case, the performance of the network with “synchronized traffic lights” strategy is exceeded by the “green wave” strategy for almost all cycle times. Moreover, comparing the “green wave” strategy with an optimal time delay with an idealized “mini network” consisting

of only one intersection, but with an equal total street length, one finds a reasonable agreement between the curves as well. This indicates that for high densities jams can be guided perfectly through the streets by an offset in the switching. This special case of a “green wave”, when jams instead of free flowing vehicles are guided through the network is denoted as “red wave” in the following. Note that the strong oscillations at high densities depend on the statistics of the underlying NaSch model so that the expected gain at these high densities will decrease with increasing p .

7.2.4 Optimal Fundamental Diagram

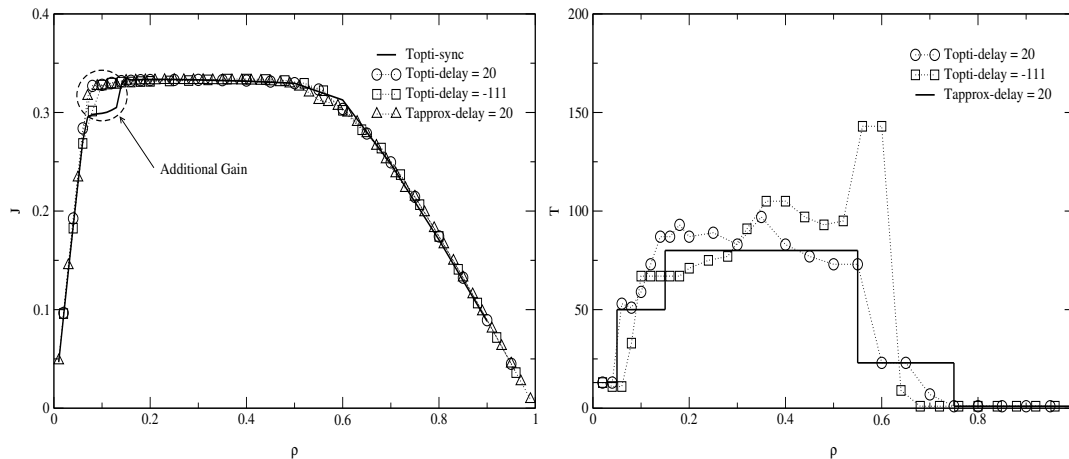


Figure 7.8: Here, the optimal FD for the “green wave” strategy is plotted (left). The optimal adjusted “green wave” is capable to reach the maximal flows of the optimal “synchronized traffic lights” strategy and even outperforms it in a small density region. As well as for the optimal “synchronized traffic lights” strategy, the optimal “green wave” curve is obtained by numerical simulations considering cycle times in the interval from $T = 0 \dots 200$ for each density. In the right plot the corresponding cycle times are shown. The optimal cycle time curve shows a plateau like shape. As can be seen, a simplified cycle time profile (step-function) also fits the FD very well. The system parameters are: $N \times N = 25$, $D = 100$, $p = 0.1$, $v_{\max} = 5$.

The optimal FD for a system operating with a “green wave” strategy is plotted in Fig. 7.8. As for the case of “synchronized traffic” lights, the optimal FD was obtained by systematically scanning the model parameters. This is a hard task, since two different times have to be considered, namely the optimal cycle time as well as the optimal time delay. Furthermore, also for the “green wave” strategy strong oscillations in the flow occur in respect to the cycle times (see Fig. 7.7). Therefore, the optimal cycle times have to be chosen carefully. As expected, the optimal time delays are equal to $T_{\text{delay}} = 20$ and $T_{\text{delay}} = -111$. This is predicted by the heuristic arguments from above. The time delay of $T = 20$ corresponds exactly to the time free flowing vehicles need to reach the next intersection and $T_{\text{delay}} = -111$ to the time a backwards moving jam needs until it reaches the preceding intersection.

Surprisingly, the optimal FD of the “green wave” strategy matches the optimal FD of the “synchronized traffic lights” strategy for almost all densities. Only in a small density area, marked in the plot, the global flow is enhanced about 15%. As a consequence, the optimal FD shows a more elementary shape if compared to the optimal FD operating with the

“synchronized traffic lights” strategy. In the “synchronized traffic lights” case, the optimal FD shows a step in its shape, because it is composed out of two FDs. These are the optimal FD for free-flow ($T = 10$) and the optimal FD for jams ($T = 60$). In the contrary, the two optimal “green wave” FDs match each other although the delay of $T_{\text{delay}} = 20$ is chosen with respect to free-flow while the delay of $T_{\text{delay}} = -111$ is chosen for a proper jam movement. This agreement is due to the fact that two time scales exist for the “green wave” strategy. Even though the time delay is different for the two FDs, the additional degree of freedom with respect to the cycle time leads to the agreement of both curves. However, the upper limit (plateau) for the maximum flow is established at a level about half of the maximum flow of the NaSch model (periodic ring). This upper limit is the same as for “synchronized traffic lights” for the same reason (see Sec. 7.1.5). On the first look, this result may somehow be surprising if expecting an overall improvement by the “green wave” strategy and not only in the small (marked) density area. Especially, when keeping in mind that in the plots where the global flow is plotted versus the cycle time, the flow is improved for almost all cycle times. The reason for this apparent discrepancy is that the flow is in fact improved for the most cycle times, but not the maximum flow. In the right part of Fig. 7.8 the optimal cycle times are plotted for the two time delays considered. The curves both have a plateau like shape, but some differences are also present. The most eye-catching difference is that for densities above $\rho = 0.5$ the optimal cycle time fasten decreases for $T_{\text{delay}} = 20$ while a peak occurs for $T_{\text{delay}} = -111$. As mentioned before, the differences occur due to fact that in both cases the curves have to match the optimum and the cycle time is the only parameter left if the time delay is fixed. The optimal cycle time curve for $T_{\text{delay}} = 20$ is further investigated. The curve is approximated in the following by a step-function in order to give a functional relation for the optimal cycle time for the “green wave” strategy. To illustrate the agreement of the step-function to the optimal curve, the corresponding FD is also plotted in Fig. 7.8 (left). Clearly, the agreement of the approximated step curve to the optimal FD can be seen. The step-function is given by:

$$T_{\text{approx-delay}} = \begin{cases} 13 & \text{for } 0.00 < \rho < 0.05, \\ 50 & \text{for } 0.05 < \rho < 0.15, \\ 80 & \text{for } 0.15 < \rho < 0.55, \\ 23 & \text{for } 0.55 < \rho < 0.75, \\ 1 & \text{for } 0.75 < \rho < 1.00. \end{cases} \quad (7.10)$$

As mentioned before, the global flow in the system shows a strong dependence on the chosen cycle times. Therefore, a lot of caution is necessary, since strong limitations in the reachable flow occur for wrong cycle times. Furthermore, it is quite complicated to obtain the proper cycle times because two different times have to be treated. In the contrary to the “synchronized traffic lights” strategy where a general (including the model parameters) simple strategy can be given, no simple solution exists for the “green wave”. The values used in the suggested step-function can not be easily related to the model parameters. However, despite its disadvantages the “green wave” is capable to enhance the global flow to about 15% in a certain density area.

The most important result is that the optimal FD of the “green wave” strategy matches the system optimum of the ChSch model. This statement is based on the following facts. First of all the positive slope of the FD of the “green wave” strategy corresponds to the free-flow velocity of vehicles. Obviously, higher velocities can not be established. Furthermore, the negative slope (high densities) corresponds to the jam velocity which is a fixed parameter

of the model. And finally, the plateau level can not be trespassed since it corresponds to the maximum flow of the ChSch model for the reasons discussed in (see Sec. 7.1.5). Therefore, the optimal “green wave” FD can be used as a reference point for any traffic light control strategy in order to evaluate its performance. This is done in the next chapter, where the efficiency of local traffic light control strategies is investigated.

7.3 Random Offset

In this section it is demonstrated that switching successive traffic lights with a random shift instead of a fixed one can lead to a more flexible strategy without oscillations. Moreover, it is shown that in contrast to a system with “synchronized traffic lights” a random shift between the intersections can lead for certain cycle times to a remarkable higher global flow. As in the previous section (“green wave” strategy) an offset parameter $\Delta T_{i,j}$ is assigned to every intersection so that the traffic lights are not enforced to switch simultaneously anymore. The offset parameter can take on values between $\Delta T_{i,j} = 0, \dots, 2T$ which are chosen randomly.

To give an insight into the effects induced by the “random offset” strategy, the throughput (flow) in the network is depicted in dependence of the cycle times in Fig. 7.9. The “random offset” strategy is compared to the ChSch model with “synchronized traffic lights” strategy. Obviously, the strong oscillations found in the curves corresponding to the “synchronized traffic lights” strategy are destroyed by the randomness in the switching. Thus, the “random offset” strategy leads to a smoothed curve which is very useful in respect to the applicability when adjusting the optimal cycle times in a network. It is not necessary to pay such strong attention to the cycle times like in systems with “synchronized traffic lights” or “green wave” strategies.

7.3.1 Low Densities

The left part of Fig. 7.9 shows a system with free-flow density $\rho = 0.05$ and a low density of $\rho = 0.2$. The “random offset” strategy outperforms the “synchronized traffic lights” strategy only for relatively short cycle times because unfavorable states (states with minimal global flow) are avoided by the randomness. For longer cycle times, the global flow in a system with “random offset” strategy falls clearly below the global flow in a system with “synchronized traffic lights” strategy. In the case of a system with “synchronized traffic lights” the curve converges in the limit $T \rightarrow \infty$ to the half of the flow found in the NaSch model. This corresponds to the case in which vehicles in the network are free to move in one direction all the time while in the other direction it comes to a complete stop. In contrast, the flow in the “random offset” strategy converges to zero since the switching is not synchronous and therefore the traffic lights along one direction are green or red at random so that all vehicles are gathered in front of the “red light”. Additionally, it must be considered that although the “random offset” strategy is effective for short cycle times, one can obtain remarkable higher flows here with the “green wave” strategy.

7.3.2 High Densities

At high densities ($\rho = 0.5, 0.7$ in Fig. 7.9), the oscillations are suppressed in a similar way as for the low-density case. Hence, as for low densities, this strategy gives an improved flexibility when adjusting optimal cycle times in the network. In addition, the “random offset” strategy outperforms the “synchronized traffic lights” strategy not only for short

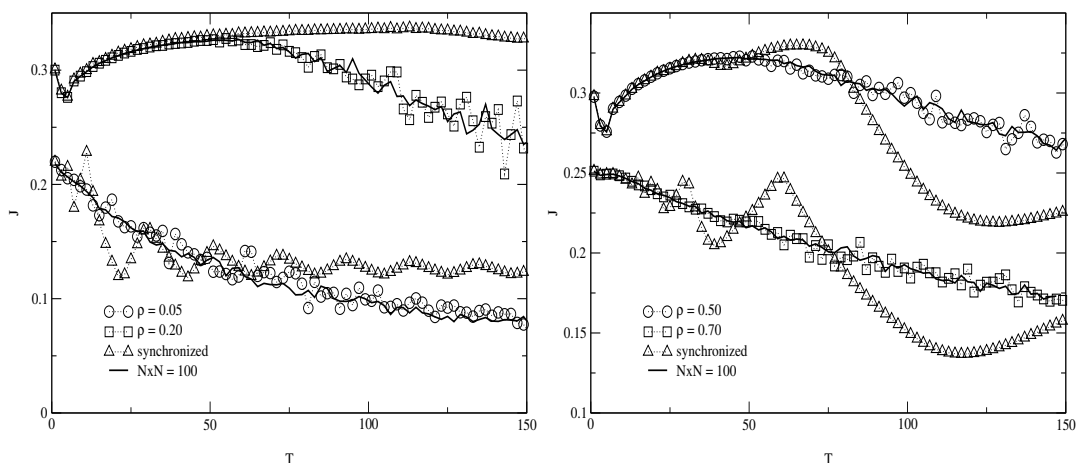


Figure 7.9: The “random offset” strategy is compared to the original ChSch model with “synchronized traffic lights”. The mean flow is plotted versus the traffic light periods for the two different strategies. The network consists of $N \times N = 25$ intersections with $2N^2$ street segments each of length $D = 100$ cells. In the left part of the Figure the flow is plotted for a low density (free-flow, $\rho = 0.05$). It can be seen clearly that the oscillations found in the “synchronized traffic lights” network are suppressed by the “random offset” strategy. Furthermore, in the free-flow density regime the “random offset” strategy shows some advantages over the “synchronized traffic lights” strategy, but only for small cycle times. The oscillations for high densities (right plot) ($\rho = 0.70$) are suppressed in a similar manner as for the low-density case. In addition, the “random offset” strategy seems to outperform the “synchronized traffic lights” strategy in parts of the plotted area. The solid line corresponds to a large network $N \times N = 100$ operating with “random offset” strategy. Here, the curves are more smooth.

cycle times, but also in the whole range plotted in Fig. 7.9 except for some peaks. One possible explanation for the profit out of the randomly switching traffic lights is that parts of the network are completely jammed while in other parts of the network the cars can move nearly undisturbed. However, also here the flow obtained by the “green wave” strategy is still remarkably higher than the flow obtained by the “random offset” strategy. Furthermore, one has to consider that the strong oscillations at high densities depend on the statistics of the underlying NaSch model so that the expected gain at these high densities will decrease with increasing randomization parameter p .

Thus, one can say that among the analyzed global strategies the “green wave” strategy leads to the highest global flow in the network for free-flow densities as well as for high-density states while the “random offset” strategy provides the greatest flexibility since the oscillations are suppressed.

7.3.3 Optimal Fundamental Diagram

In Fig. 7.10 the optimal FD for the “random offset” strategy is plotted. As in the previous cases, the optimal FD was obtained by systematically scanning the model parameters.

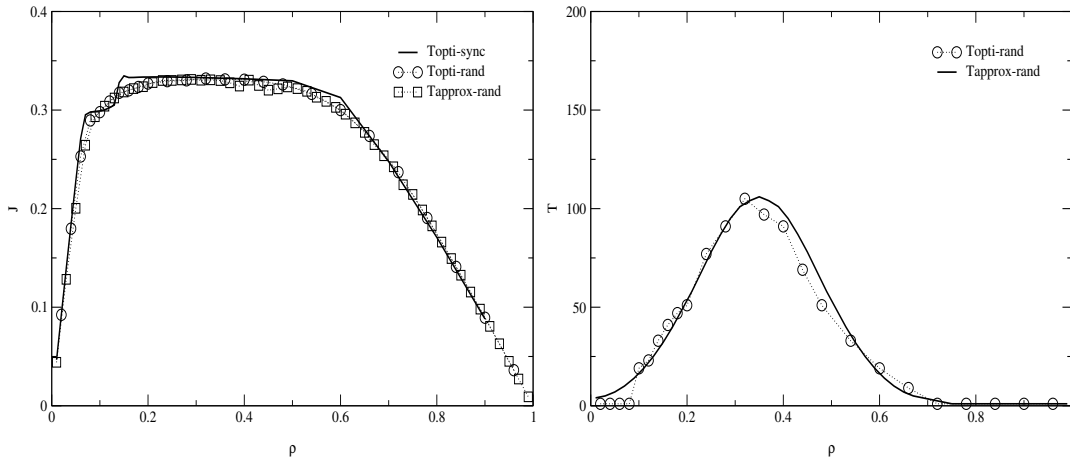


Figure 7.10: The optimal FD for a system with “random offset” strategy is shown in the left plot. In the right plot the corresponding cycle times are shown which seem to be distributed Gaussian. This is confirmed by the test with a Gaussian cycle times profile. The system parameters are: $N \times N = 25$, $D = 100$, $p = 0.1$, $v_{\max} = 5$.

Here, the optimal cycle times can be obtained relatively simple, since the flow vs. cycle time dependence is oscillation free for the “random offset” strategy and only the cycle time has to be considered as the optimization parameter. Remind that in the “green wave” strategy two timescales were considered. As can be seen in the right part of Fig. 7.10, the optimal cycle times corresponding to the maximum flow are relatively low for low as well as for high densities. This is confirmed in Fig. 7.7 where the global flow is plotted against the cycle time. For intermediate densities, the optimal cycle times are increasing up to a density of $\rho = 0.3$ and thereafter decreasing. The optimal cycle times seem to be distributed normally. This is confirmed using the following fit function which reproduces the shape of the points quite accurately.

$$T_{\text{approx-rand}} = 1 + 105e^{-\frac{(\rho-0.35)^2}{3.3}} \quad (7.11)$$

Surprisingly, the “random offset” strategy nearly matches the performance of an optimal “synchronized traffic lights” strategy. Therefore, the “random offset” strategy is not only useful if a flexible strategy (oscillation free) is needed, but also a high throughput in the network can be obtained. However, under consideration of a “green wave” strategy, the flow is still higher for certain densities.

A disadvantage of the “random offset” strategy are the unrealistically short optimal cycle times at low and high densities. This handicap can be avoided by the use of longer cycle times which only leads to a small loss in the global flow since the system is free of oscillation.

Also for the “random offset” strategy the upper limit (plateau) for the maximum flow is established at a level about half of the maximum flow of the NaSch model. This confirms that the limit is universally valid independent from the traffic light strategy used.

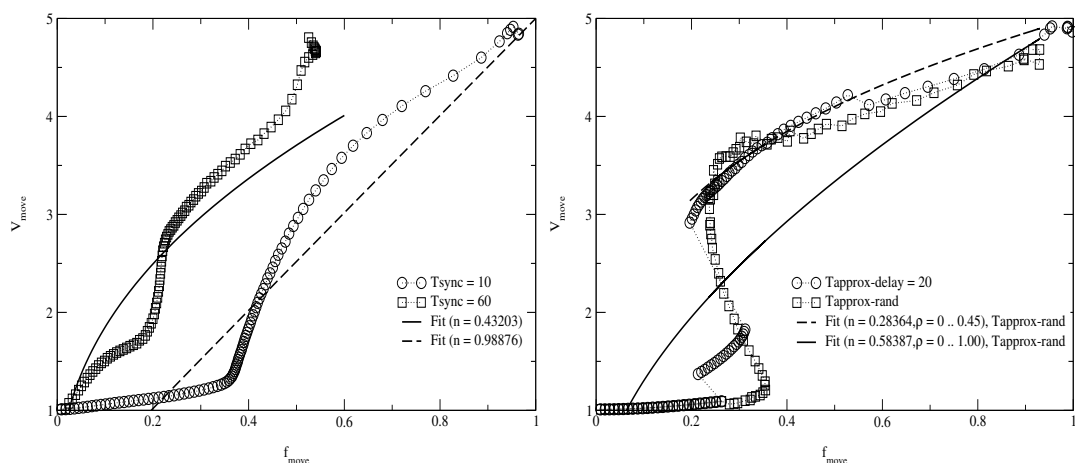


Figure 7.11: The fraction of moving (running) vehicles f_{move} is plotted against their average speed V_{move} . This is done for the “synchronized traffic lights” strategy (left), and for the “green wave” and “random offset” strategy (right). The model parameters considered are: $N \times N = 25$, $L = 100$, $v_{\text{max}} = 5$, $p = 0.1$.

7.4 Comparison with the Two-Fluid Model

In this section, the ChSch model is compared to the two-fluid model from Sec. 6.1. This is done for the different traffic light strategies that are discussed in the previous sections. Therefore, the fraction of moving vehicles f_{move} and the corresponding velocities V_{move} are measured, since these quantities are the starting point of the two-fluid theory. This is done in the left part of Fig. 7.11 for the optimal cycle times of the “synchronized traffic lights” strategy, and for the optimal cycle times of the “random offset” and the “green wave” strategy in the right part of Fig. 7.11. In order to evaluate in how far the curves follow relation Eq. 6.1 which is expected from the two-fluid theory, the best fits to the relation are also given in the figure.

As one can see, the results of the ChSch model systematically deviate from the fitted curves of the two-fluid theory in all cases. This circumstance emphasizes that the dynamics in the ChSch model is by far more complex than predicted by the simple assumptions of the two-fluid theory. The fact that the fraction of standing cars is negligible in the NaSch model until a critical density is trespassed [34] may be one of the main reasons for the deviations. Furthermore, the interplay between the signals and the different driving directions, leading to a plateau in the FD, plays a significant role since global measurements (all streets and directions) are considered here.

In the left part of Fig. 7.11 the results of the comparison are presented for the “synchronized traffic lights” strategy. The cycle times used ($T = 10$, $T = 60$) correspond to the values that match the optimal FD (see Sec. 7.1.5) of the model. The curves can be divided into three approximately linear regimes according to free-flow, plateau, and jammed state of the FD.

In the right part of Fig. 7.11 the results of the “random offset” and the “green wave” strategy are shown. Also here, the parameters that correspond to the optimal flow states are used. The curves can be separated into two different regimes divided by a sharp transition. Furthermore, an artificial curve characteristics is obtained for the “green wave” strategy, reflecting the cycle times vs. density relation (step-function Eq. 7.6). The first of the two fitting curves include all densities. Here, clearly the strong deviations from the numerical

results can be seen which are even stronger than for the “synchronized traffic lights” cases. Note that only the fit curves for the “random offset” strategy are given, since the “green wave” strategy shows a nearly equal behavior. In order to demonstrate that the two-fluid theory can give appropriate results for certain areas, a second fit is given for the “random offset” strategy where only densities below $\rho = 0.45$ are regarded. This corresponds to a system state where the fraction of moving vehicles is greater than $f_{\text{move}} = 0.2$. For this certain area the two-fluid theory matches the ChSch model relatively well.

7.5 Discussion

In this chapter the focus was on global traffic light control strategies in the ChSch model. The main aim of the investigations was to find optimal model parameters in order to maximize the network flow. For this purpose at first the original formulation of the ChSch model where the traffic lights are switched synchronously was considered. It was shown that the global throughput of the network strongly depends on the cycle times, i.e., one finds strong oscillations in the global flow in dependence of the cycle times both for low as well as for high densities. A simple phenomenological approach has been suggested for the free-flow regime in order to determine the characteristics in regard to the model parameters and to obtain a deeper insight into the dynamics in the network. The phenomenological results show a good agreement to numerical data and indicate that the choice of the underlying model for vehicle movement between intersections does not play an important role.

In order to allow a more flexible traffic light control the ChSch model was enhanced by an additional model parameter. This new parameter is assigned to every intersection representing a time offset so that the traffic lights are not enforced to switch simultaneously anymore. A two-dimensional “green wave” was implemented with the help of the new parameter. The “green wave” strategy improves the flow considerably in comparison to the “synchronized traffic lights” strategy at low densities and has even an incisive impact on the throughput at high densities. It was shown that the influence of intersections along a street can be completely avoided by the “green wave” strategy. Although, the “green wave” strategy is capable to give a strong improvement, the dependence between flow and the cycle time found in the original ChSch model remains.

Thus, to avoid this strong oscillations further, a network where traffic lights are switched at random was analyzed. It was shown that the strong oscillations found for a “synchronized traffic lights” strategy and for the “green wave” strategy are completely suppressed by randomness. Thus, the “random offset” strategy can be very useful if a control strategy is required which is not sensitive to the adjustment of the cycle times. Moreover, the “random offset” strategy outperforms the standard ChSch model with the “synchronized traffic lights” strategy at low densities for small cycle times and at high densities for all cycle times. A possible explanation for the profit at high densities in the case of a “random offset” strategy is that vehicles can be distributed inhomogeneous due to the randomness. In fact some parts of the network can be completely jammed while in other parts of the network the cars can move nearly undisturbed.

This additional gain due to the inhomogeneous allocation of vehicles indicates that an autonomous traffic light control based on local decisions could be more effective than the analyzed global schemes as will be discussed in the next chapter.

Furthermore, the optimal cycle times were determined for the three strategies. It was found that the optimal FD of the “green wave” strategy matches the system optimum of

the ChSch model. Therefore, the optimal “green wave” FD can be used as a reference point for any traffic light control strategy in order to judge its performance.

8 Adaptive Traffic Light Control in the ChSch Model

In the previous chapter the ChSch model with global (fixed) traffic light control was analyzed. Since the number of parameters is manageable in the model, the impact of the fixed strategies can be analyzed systematically. This allows to obtain the optimal state under consideration of the chosen strategy, without the use of special optimization algorithms. Furthermore, it was shown by the help of heuristics that the “green wave” strategy is capable to reach the *global* optimum for all densities. The *global* optimum of the ChSch model is given by a FD with a characteristic plateau at intermediate densities. The plateau is established at about half of the flow of the NaSch model. Remind that in the ChSch model vehicles move on the streets according to the NaSch model. Therefore, for low densities (free-flow) the vehicles move with the free-flow velocity given by the NaSch model (positive slope in the FD), not influenced by the intersections. For high densities, the optimum is determined by the backwards movement of holes, these have to be guided unhindered across the intersections (negative slope in the FD). The plateau between the two regions is typical for defect systems (see chapter 4) and reflects the limiting impact of the intersections on the global flow.

In reality, adaptive (decentralized) traffic signal control may be favorable since traffic signals need to react on local conditions. Moreover, global control imposed on the traffic lights cannot always accommodate unforeseeable changes.

In the following, three different adaptive control strategies are suggested for the ChSch model. These are briefly analyzed with the aim to find parameter combinations that match the *global* optimum of the system at its best. Furthermore, the influence of turning and inhomogeneous densities will be investigated in the next chapter in order to demonstrate in how far the adaptive strategies are comparable to the fixed ones under more realistic traffic conditions. Thereby, the knowledge of the *global* optimum derived in the previous chapter is the most important result, since this can serve as a point of reference for all traffic lights strategies.

The adaptive strategies are kept simple in the sense that only parameters are used that can be related easily to measurable quantities in real traffic. Obviously, in reality the control algorithms used are determined by the way the system can sense vehicular traffic. In Germany for example, many traffic signals are equipped with inductive loops, positioned in front of a signal (in the street), which allow to detect passing vehicles, including their velocities.

8.1 Switching Based on Queue Length

The control parameter for a signal to switch is the length of a vehicle queue in front of a red signal. This quantity can be obtained easily from computer simulations but not directly in reality. For example, if the signal is equipped with inductive loops, these can only detect if a vehicle passes the detector but not how many vehicles are queued. Note

that a simple version of “switching based on queue length”, namely a traffic signal switches to green if a vehicle passes the detector in front of the “red light” is quite often used in reality in order to allow the passing of main roads for vehicles on minor roads. However, one can envision an algorithm based on the motion detection of inductive loops that can keep track of approximate queue lengths. The way such an algorithm would compute the queue lengths is as follows. Each detector determines the number of passing vehicles. This variable is updated by adding the number of vehicles passing through the detector of the preceding intersection. In such a control scheme, the communication between neighboring traffic signals is required. An alternative method could be the installation of additional inductive loops in front of the intersection.

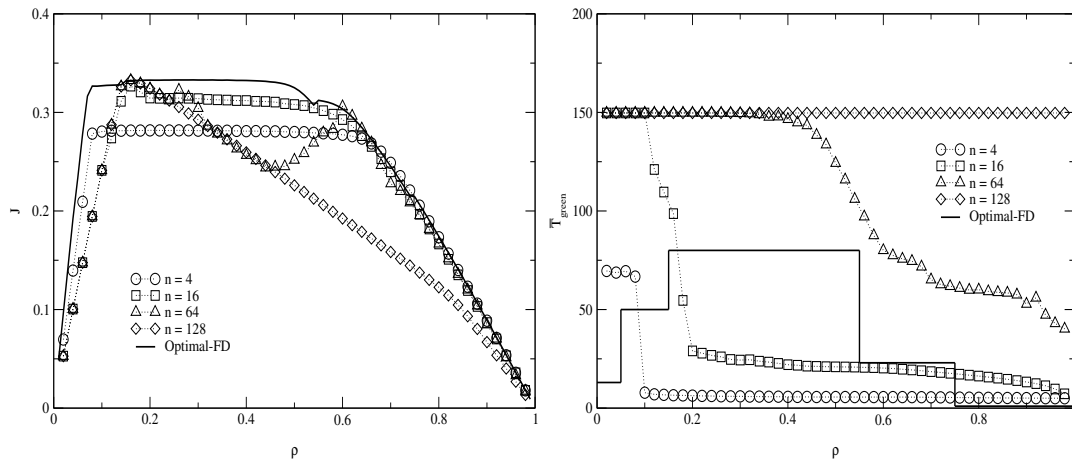


Figure 8.1: The left plot shows FDs for “switching based on queue length” for various queue lengths n . The solid line is obtained by a fixed “green wave” strategy, which represents the *global* optimum. The network consists of 5025 cells. This corresponds to the maximum number of vehicles in the network for $\rho = 1.0$. In the right plot the corresponding mean green-cycle times are depicted.

As mentioned before, the exact queue length can be directly determined in the simulation. The following algorithm is used for “switching based on queue length” in the ChSch model:

- A red signal switches to green if the queue length (number of standing vehicles) in front of the signal is at least equal to n . Furthermore, in order to restrict the investigations to realistic cycle times, a minimum green-cycle time of $T_{\text{min}} = 5$ time-steps, and a maximum green-cycle time of $T_{\text{max}} = 150$ times-steps, is defined. Thus, the signals switch after $T_{\text{max}} = 150$ time-steps even if no queue of length n is formed. Note that the maximum cycle time is equal to the maximum cycle time investigated for the fixed (global) strategies.

The algorithm suggested above is evidently simple regarding the queue length n as the only control parameter. In the left part of Fig. 8.1 FDs for various queue lengths n are plotted. The corresponding mean green-cycle times \bar{T}_{green} are given in the right part of the figure. As mentioned before, the *global* optimum of the system is known from the investigations of the previous chapter. It is represented by the solid black line taken from Sec. 7.2.4. Note, the optimal curve was obtained by the “green wave” strategy which matches the *global* optimum very well. The investigated network here consists of $N \times N = 25$ intersections and streets of a length of $D = 100$ cells. This parameters are used for all further cases if not stated otherwise.

Starting with short queue lengths: The FD for a queue length of $n = 4$ shows some similarities to the FD for “synchronized traffic lights” with a low cycle time of $T = 10$ time-steps (see Fig. 7.5). The curve matches the optimum for low as well as for high densities, but does not reach the maximum flow (plateau) at intermediate densities. The mean green-cycle time takes on a value of $T \approx 75$ time-steps for low densities, i.e., the lights switch before the maximum cycle time is reached. Then by increasing the density it drops to a level of about $T \approx 10$ time-steps.

For a queue length of $n = 16$, the best results are obtained. The curve shows also similarities to the FD of a system with “synchronized traffic lights” for the case with a relatively long cycle time of $T = 60$ time-steps. Here, the curve nearly matches the optimum curve except for low densities. The corresponding mean green-cycle time shows that for low densities the maximum cycle time of $T_{\max} = 150$ is reached, i.e., the traffic lights do not switch due to queuing. However, if higher densities are considered, the cycle time drops at a density of $\rho \approx 0.1$ to a level of about $T \approx 25$ time-steps and then continuously decreases. If the queue length n is further increased, the obtainable flow strongly decreases. For a queue length of $n = 64$ the FD shows a somehow odd shape with a clear minimum in its middle. This shape can be explained considering that for low densities the situation that 64 vehicles are collected in front of a “red light” is barely probable with respect to the street length of $D = 100$. For higher densities, however, it gets more probable that a queue of 64 vehicles is formed, before the maximum cycle time is reached. Given that the large maximum cycle time T_{\max} leads to improper flows. The positive gain out of shorter cycle times at higher densities is reflected by the increasing flow (minimum in the curve). A closer look at the mean cycle times confirms this assumption. Up to relatively high densities, the signals operate at their maximum cycle time of $T_{\max} = 150$ time-steps. However, at high densities, the signal can switch more often due to large queues so that shorter cycle times are established.

Finally, if the queue length n is set to 128 (a value that can never be reached since the street consists of only 100 cells) the signals just switch at the maximum cycle time. This correspond to a fixed strategy with a cycle time of $T = 150$, leading to improper low flows.

It has been shown that despite its simplicity the “switching based on queue length” strategy is capable to get near the *global* optimum. Obviously, the results obtained for the control parameter n have to be seen with respect to the system parameters used, especially the street length D and the limiting cycle times T_{\min} and T_{\max} . It is known from the previous chapter that the global flow strongly depends on the cycle time. Therefore, in order to see the benefits of the strategy, it was checked that T_{\min} and T_{\max} do not correspond to optimal flow states of the model. Remind that the strategy behaves for some densities and for an improper control parameter n like a fixed strategy operating with T_{\max} .

8.2 Switching Based on Waiting Time

For the “switching based on waiting time” strategy, the control parameter is given by the time n that elapses after an intersection has been passed by a vehicle. The aim of this strategy is to enlarge the green phase of a signal, if it is frequently used by vehicles. In the case that no vehicles trespass a green intersection for a certain time n , the signal turns to red. The control parameter n (time elapsed) can be obtained easily in computer simulations as well as in reality since for each event only one single cars has to be detected by an inductive loops for example. Therefore, concerning the applicability to real systems, the “switching based on waiting time” strategy is in advantage over “switching based

on queue length” presented above, where the communication between neighboring traffic signals seems to be required.

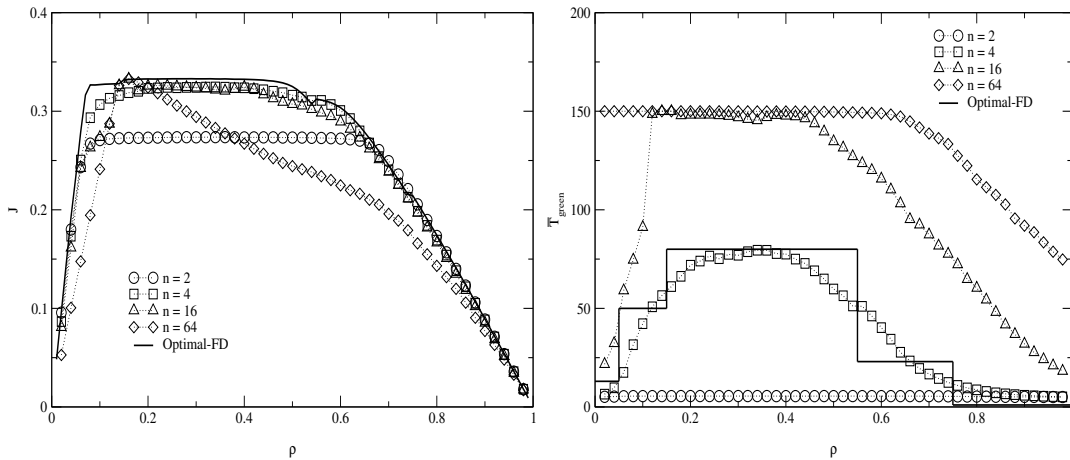


Figure 8.2: In the left plot FDs for various waiting times are depicted while in the right plot the corresponding mean green-cycle times are shown.

The algorithm used for the “switching based on waiting time” strategy in the ChSch model can be formulated as follows:

- A green signal switches to red if in the last n time-steps no vehicle has passed the intersection. As well as in the previous case the cycle times are restricted by a minimum green-cycle time of $T_{\text{min}} = 5$ time-steps and a maximum green-cycle time of $T_{\text{max}} = 150$ times-steps.

The algorithm suggested here is kept simple in the sense that there is only one single control parameter. In the left part of Fig. 8.2, FDs are plotted for various n . The corresponding mean green-cycle times \bar{T}_{green} are depicted in the right part of the figure. As in the previous case, the *global* optimum of the system is represented by the solid line obtained by the “green wave” strategy.

Starting with a waiting time of $n = 2$ time-steps, the following characteristics can be identified in the plots. The maximum flow is limited at about 20% below the system optimum. This can be ascribed to the fact that the waiting time is too short to enlarge the minimum cycle time of $T_{\text{min}} = 5$ time-steps. Even at high densities, where a sufficient amount of vehicles should be present on the streets, the cycle time does not grow above $T_{\text{min}} = 5$ as shown in the right part of Fig. 8.2. The reason for the limitation is obviously two successive car can not trespass an intersection within two time-steps.

The optimal result for “switching based on waiting time” is obtained for $n = 4$ time-steps. The curve then matches the *global* optimum of the system surprisingly well for all densities. This good agreement is quite impressive in regard to the fact that the traffic signals operate autonomously only controlled by one single parameter. Moreover, the corresponding cycle times reveal a further interesting agreement to the optimal curve: For $n = 4$ even the cycle time curve follows the shape of the optimal curve (step-function). Remind that the step-function is used in order to obtain the optimal FD by the “green wave” strategy (see Sec. 7.2.4 for details). Additionally, there is an offset parameter in the switching of the traffic signals (“green wave”) that leads to the *global* optimum. Therefore, one may assume that also in this case an offset in the switching of the signals is established by the autonomous traffic lights since the optimal flow is matched well. However, this point

should be investigated in future in more detail. Nevertheless, it is quite remarkable that with the use of such a simple local strategy the system self-organizes almost in the optimum system state.

If the waiting time is further increased, the obtainable flow decreases, first for low and then for all densities. For a waiting time of $n = 16$ the FD shows also a good agreement to the optimum curve except for a small density area at low densities, where the flow clearly breaks down. As depicted in the right plot of Fig. 8.2, the upper limit for the cycle time of $T_{\max} = 150$ is reached for a wide density area, indicating that the control parameter is too high. However, the fact that the flow is still in a relatively good agreement with the optimum curve indicates that the strategy is not very sensitive in regard to the optimal parameter choice. This fact predestinates the use of the “switching based on waiting time” strategy.

The queue length of $n = 64$ is the highest investigated parameter. Here, the flow clearly falls below the optimum curve for nearly all densities. Furthermore, the cycle time is up to high densities equal to the maximum cycle time. Even for low densities vehicles will pass the intersection within the time interval of $n = 64$. Interestingly, the cycle time decreases for very high densities. This is caused by the fact that for very high densities sometimes vehicles are not able to enter a crossing if it is not assured that it can be left again. This is the case for example, if the street directly behind the crossing is blocked by a jam.

The “switching based on waiting time” strategy seems to be more efficient than the “switching based on queue length” strategy. Despite its simplicity it nearly matches the *global* optimum for the optimal control parameter n . The results obtained have to be seen with respect to the system parameters used, especially the street length D and the limiting cycle times T_{\min} and T_{\max} .

8.3 Switching in Analogy to a Neural Network

In [126] Ohira *et al.* proposed an autonomous traffic signal control algorithm based on an analogy with neural networks. They found self-organizing collective behavior that improves the overall system flow by diffusing congested traffic states (jams). Their investigations were restricted to a single one-dimensional periodic street, whereby the vehicles move according to the rules of the ASEP [96].

Although the system is simple, the strategy is applied to the ChSch model for the following reasons. First of all, there are only a few investigations about the impact of traffic signals in CA models at all. Therefore, it seems interesting in how far the benefits obtained on a simple one-dimensional ring could be transferred to more complex geometries like the ChSch model. Moreover, neural network models have been found to be beneficial for many engineering applications [67].

Comparing the ChSch model to the one-dimensional system investigated by Ohira, the main difference consists of the crossing of traffic streams from vehicles moving along different directions. Furthermore, the vehicles move according to the rules of the NaSch model, which can lead to effects like spontaneous jamming. The signal control algorithm itself can be directly applied to the crossings of the ChSch model.

The cycle time T of an intersection i is determined by the following non-linear, monotonously increasing function:

$$T_i(t) = T_{\min} + T_{\max} \tanh(\beta V_i(t)), \quad (8.1)$$

$$V_i(t+1) = X_i(t). \quad (8.2)$$

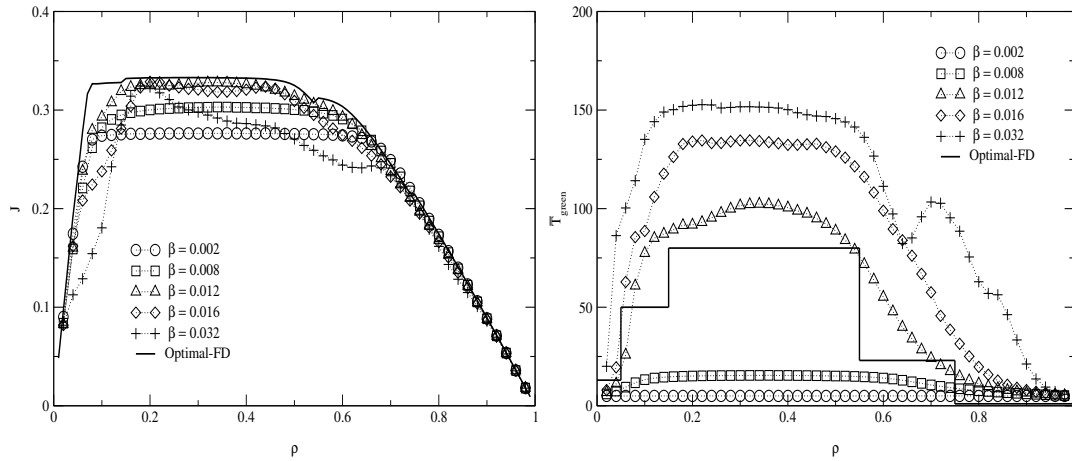


Figure 8.3: The left plot shows FDs for various control parameter β . In the right plot the mean cycle times are depicted.

$V_i(t)$ is a “potential” of the i -th signal at the t -th time-step, thereby $X_i(t)$ is the number of vehicles that crossed the intersection until the t -th time-step while the signal is green. Finally, if the actual time-step t outruns the cycle time $T_i(t)$, the signal switches. Also here, the cycle times are restricted by a minimum green-cycle time of $T_{\min} = 5$ time-steps and a maximum green-cycle time of $T_{\max} = 150$ times-steps. This is included in Eq. 8.1. As mentioned before, the dynamics of such a signal has a correspondence to neural networks. Each signal can be identified with an integrate-and-fire neuron [15, 55, 152], and the traffic going through the intersections can be identified as the neural pulses it receives. The cycle time of the intersection then corresponds to the activity level of the neurons. Note that after each period, the potential V_i and the time-step t is reset to zero just as in the neuron models.

The algorithm described above seems to be more sophisticated than the previous two adaptive strategies. But alike in the other cases only one single input signal is needed. This is the number of vehicles that have crossed an intersection at “green light” until the actual time. The number of trespassed vehicles can be obtained easily in computer simulations as well as in reality by the use of inductive loops for example. The control parameter of the algorithm is given by β , linking the traffic stream with the traffic cycle duration (neuron activity). The impact of β to the overall flow can be seen in the FDs in the left part of Fig. 8.2. The mean cycle times are plotted in the right part of the figure. If a low β is utilized, the cycle times are low since the link to the traffic stream is too weak to enlarge the cycle times adequately. Therefore, the system is not capable to get near the optimal flow. This case is represented in Fig. 8.2 for $\beta = 0.002$, and $\beta = 0.008$.

If the control parameter is set to $\beta = 0.012$, the optimal result is obtained. Here, the FD matches the *global* optimum of the system well for all densities. This agreement is comparable to the optimal case of the “switching based on waiting time” strategy investigated above, since both curves have a similar shape. Also here, it is quite impressive how good the curve compares to the *global* optimum (solid line), although only one single control parameter is used. Furthermore, the mean green-cycle time \bar{T}_{green} for $\beta = 0.012$ approximately follow the shape of the step-function as for the “switching based on waiting time” strategy.

For increasing β furthermore, the obtainable flow decreases and the mean green-cycle time reaches the maximum cycle time for intermediate densities. Since the loss of flow is not

drastic for the focused values of β , the strategy can be assumed to be robust in regard to adjusting a suitable β .

The comparison of “switching based on waiting time” strategy and “switching in analogy to neural networks” reveals some similarities concerning the quantities investigated. Both strategies nearly match the *global* optimum of the system, and the curves shown have a similar shape. Obviously, the similarities can be ascribed to the fact that in both cases the cycle times are determined by the rate of vehicles passing an intersection. Nevertheless, there is an important difference, since in the “switching based on waiting time” strategy the traffic situation is adapted directly by the traffic signals while in the “switching in analogy to neural networks” this interaction is retarded. More precisely, in the “switching in analogy to a neural network” strategy the number of vehicles leading to a certain cycle time can be summarized before this time is reached, i.e., the signal can stay green for a long time although no vehicle arrives. In the contrary, in the “switching based on waiting time” strategy, a signal switches directly to red if a fixed time stamp will be surpassed. However, the impact of this effect is relatively weak, since it is rather improbable that a traffic stream is suddenly interrupted in saturated traffic.

8.4 Discussion

In this chapter the impact of adaptive traffic signal control strategies was analyzed. It has been shown that the adaptive signal control can match the system optimum of the ChSch model even if traffic conditions closer to reality, realized by inhomogeneous densities or turning of vehicles, are considered. The system optimum is known from chapter 7 and serves as a point of reference for the investigated adaptive strategies.

Three different adaptive strategies were introduced. These were kept simple in the sense that only quantities are used that can be obtained easily in real traffic. Furthermore, all strategies only contain one single control parameter. The investigated strategies are; “switching based on queue length”, “switching based on waiting time”, and “switching in analogy to a neural network”.

For the “switching based on queue length” the optimal control parameter was determined. This leads to a flow close to the system optimum.

Also for the “switching based on waiting time” strategy the optimal control parameter was determined, leading to the best results of all investigated adaptive strategies. The FD almost perfectly matches the system optimum. Moreover, even the green-cycle time curve follows the curve of the “green wave” strategy which leads to the system optimum.

The “switching in analogy to a neural network” leads to similar results like the “switching based on waiting time” strategy. It is valuable that the generalization of this algorithm, which was proposed for an one-dimensional system, to the ChSch model retains the benefits.

Summarizing, it was shown that the simple adaptive strategies suggested can lead to a system state close to the system optimum. The results may be beneficial for real networks since the suggested algorithms are simple and the parameters used can easily be obtained in real traffic.

9 Traffic Light Control in the ChSch Model with Inhomogeneous Densities

In the following it is discussed briefly in how far the adaptive strategies presented above compare under more realistic traffic conditions like turning at crossings or fixed inhomogeneous densities.

9.1 Impact of Turning

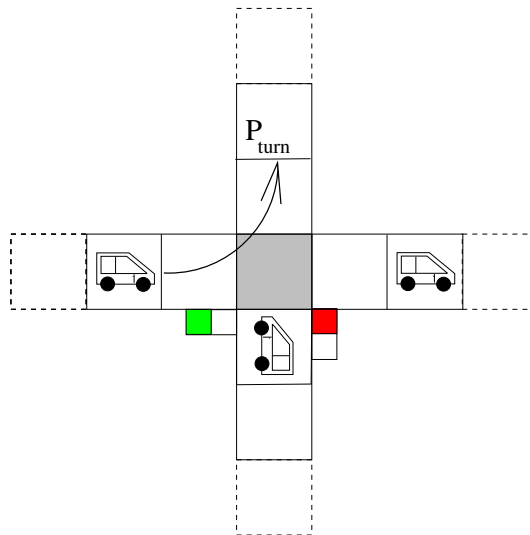


Figure 9.1: Schematic representation of the turning process at a crossing. The illustrated intersection is a segment of a large network. Here, a vehicle changes from west-east direction to south-north direction with probability p_{turn} . Note that the vehicle will keep its direction with probability $1 - p_{\text{turn}}$.

In this section the ChSch model is enhanced by the possibility for vehicles to turn at intersections. The turning allow the vehicles to change their direction and is implemented in a stochastic way. This means that a vehicle crossing an intersection will turn with a specific probability p_{turn} if it is assured that at least the last cell of the chosen road is not occupied. Then the gap to the last car on the new street, i.e., the car ahead, determines the velocity according to *Step 2* of the update rules of the ChSch model (see Sec. 6.3).

In order to demonstrate the impact of the turning process, the fraction of vehicles on the south-north streets $f_{\text{SN}} = N_{\text{SN}}/N^1$ is plotted in Fig. 9.2 for the “synchronized traffic lights” strategy. The fraction of vehicles on the west-east streets is given by $f_{\text{WE}} = 1 - f_{\text{SN}}$.

¹ N_{SN} denotes the number of vehicles driving along the south-north direction. The total number of vehicles is N .

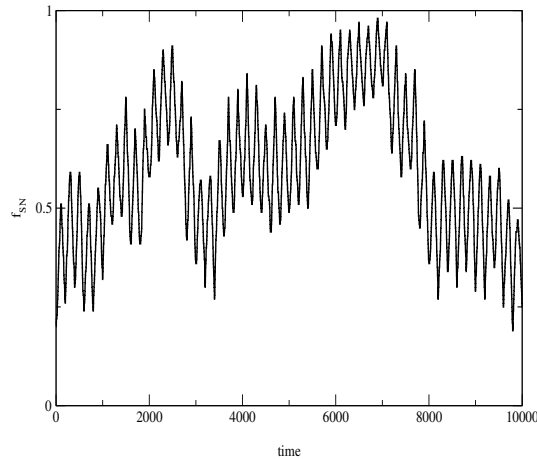


Figure 9.2: The fraction f_{SN} of vehicles in the network moving from south to north is plotted in dependence to the system time. The traffic signals are synchronized (see Sec. 7.1). The turning probability is set to $p_{\text{turn}} = 0.5$.

As can be seen in Fig. 9.2 the fraction of vehicles on the south-north streets f_{SN} fluctuates strongly. On short timescales, the fluctuations are directly related to the cycle time of 100 time-steps. Every time the signals along the west-east direction switch to green, the number of vehicles on the south-north direction increases due to the turning, and then after another 100 time-steps it decreases, since vehicles can now turn back to the west-east direction. Apart from the cycle time based fluctuations, the fraction of vehicles changes more drastically on larger timescales. This effect is related, in addition to the direct signal impact, to the overall system dynamics including topology, vehicle motion, and turning. The underlying dynamics leading to these long ranged fluctuations should be investigated in future more detailed. However, for the analysis in this section it is sufficient to keep in mind that the turning leads to strongly fluctuating densities on the streets in the progress of time. Thus, especially an adaptive strategy should react flexibly to the permanent changing traffic conditions in order to reach the optimal flow.

In the following, the impact of density fluctuations due to turning is briefly investigated for the signal strategies presented so far.

9.1.1 Synchronized Traffic Lights

For the purpose of analyzing the impact of turning events in the ChSch model operating with global (fixed) control strategies, FDs were obtained for different turning probabilities. Thereby the case $p_{\text{turn}} = 1$ forces every vehicle to turn at a crossing if possible. Since the FDs are obtained for an optimal (fixed) cycle time, the dependence of the turning events for other cycle times is furthermore investigated by means of cycle time vs. flow plots.

The optimal solution for the “synchronized traffic lights” is obtained if two different cycle times are considered (see Sec. 7.1.5). These are $T = 10$ time-steps for densities below a certain transition density, and $T = 60$ time-steps for values above. As presented in the left part of Fig. 9.3, turning has almost no influence onto the overall system flow for $T = 10$ time-steps. Only for small densities ($0.05 < \rho < 0.1$) the global flow falls a little bit below the case without turning (\circ). In the right part of Fig. 9.3 the global flow is plotted for a cycle time of $T = 60$ time-steps. Here, the curves show stronger deviations, growing with increasing turning rates compared to the case without turning. The strongest deviations

occur for relatively high densities in the area $0.5 < \rho < 0.7$. In addition also for low densities ($0.05 < \rho < 0.2$) the flow decreases more strongly than for the $T = 10$ time-steps case.

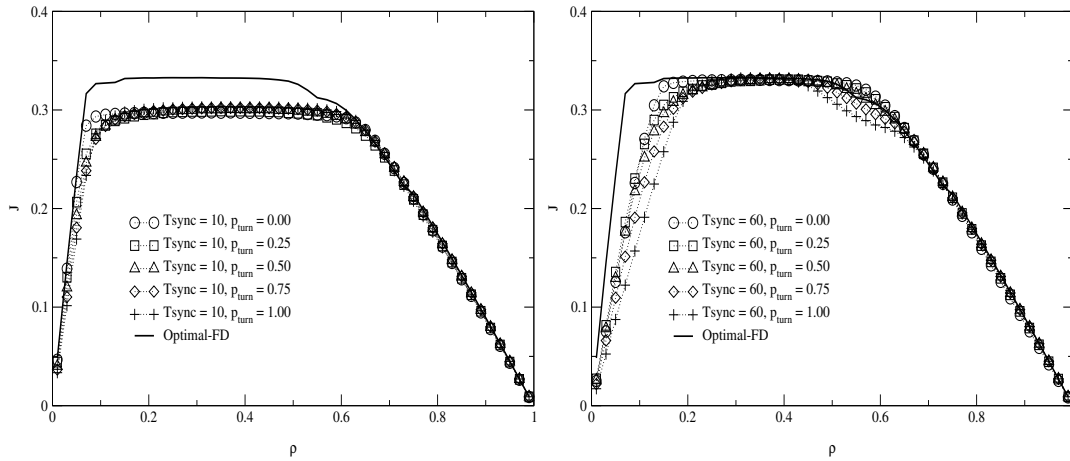


Figure 9.3: In the figure, FDs are plotted for a system operating with “synchronized traffic lights” for different turning probabilities p_{turn} . The left part of the figure corresponds to a cycle time of $T = 10$ time-steps and the right part to a cycle time of $T = 60$ time-steps.

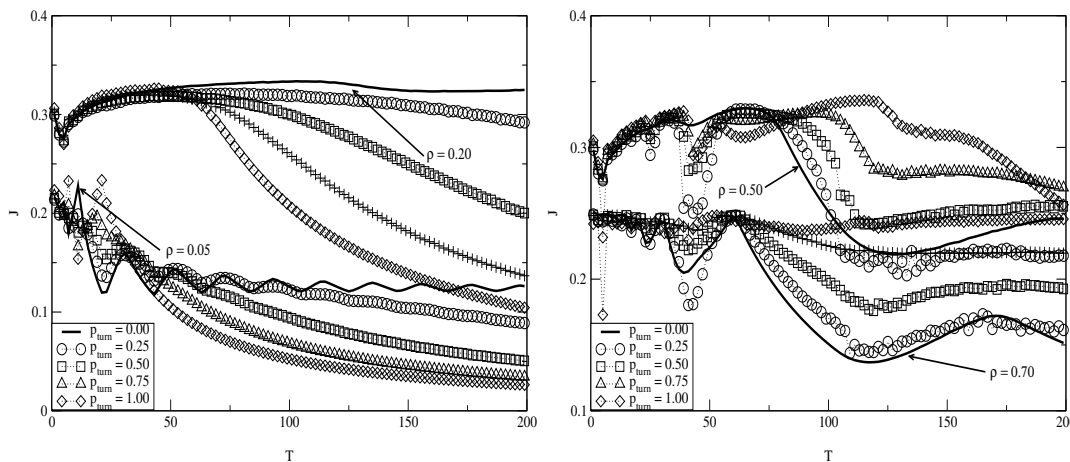


Figure 9.4: The impact of the turning events to the global flow is shown in dependence to the cycle time. The curves display the strong impact of turning events.

In Fig. 9.4 the dependence between the global flow and the chosen cycle time is shown for different turning rates and densities. It can be seen that turning have an immense impact on the global flow for a wide range of cycle times. However, for the fixed cycle times of $T = 10$ and $T = 60$ time-steps, used in Fig. 9.3, the impact is not so distinct. Focusing on high densities, an interesting peculiarity occurs. Here, the global flow is increased for a wide range of cycle times. The reason for this surprising result is quite simple: Improper configurations, e.g., a jam directly in front of an intersection, can be avoided by turning.

The results obtained for the “synchronized traffic lights” show that for the optimal signal cycles the impact of turning is relatively weak in the ChSch model. Nonetheless, turning

has a strong impact for the most of the remaining cycle times. This circumstance is very important in regard to more realistic traffic network geometries. In the most cases it is not possible to obtain an optimal cycle time valid for the whole network because of inhomogeneities like different street lengths. However, the strong impact of turning can also have a positive effect. For high densities, the global flow is increased for long cycle times. Thus, it may be concluded that turning possibilities in dense traffic can be beneficial.

9.1.2 Green Wave

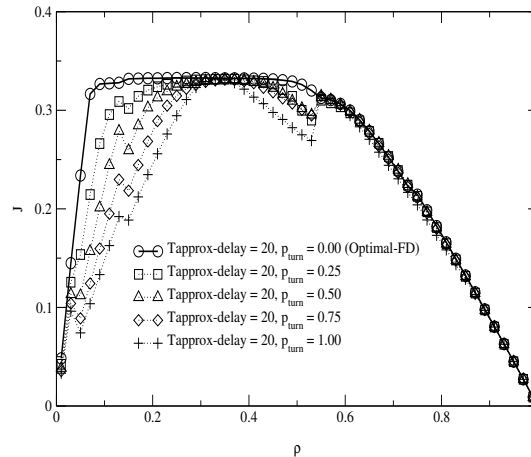


Figure 9.5: The FDs are plotted for the different turning rates. As can be seen in the figure, the loss in the global flow increases with increasing turning rates. Note that the case $p_{\text{turn}} = 0$ leads to the optimal FD of the ChSch model.

The optimal solution for the “green wave” strategy is obtained for density dependent cycle times (step-function). Additionally, there is an offset in the switching between neighboring signals. The corresponding optimal FD matches the *global* optimum of the ChSch model (see Sec. 7.2) for the case without turning.

In the following it is investigated in how far the “green wave” strategy can resist against the impact of turning. Therefore, FDs for the optimal “green wave” algorithm are depicted for different p_{turn} in Fig. 9.5. The FDs reveal a heavy loss of flow as a consequence of the turning events. For low densities the loss in the global flow can be more than 50% for some densities. Furthermore, the FDs have an odd shape with a jump to higher flows at a density of $\rho = 0.55$. A closer examination of the shape reveals that the function used for the cycle times seems to be improper in the presence of turning. However, the strong deviations from the optimal FD could have been expected, given that the “green wave” strategy heavily optimizes the arrival of vehicles at neighboring intersections along a fixed direction. Therefore, the optimization becomes redundant if a large amount of vehicles turns.

Figure 9.6 confirms the strong impact of turning to the global flow. Here, the dependence of the global flow on the cycle time is shown for various turning rates and densities. The low-density cases are illustrated in the left plot and the high-density cases in the right one. Remind that in addition to the cycle time there is an offset of $\Delta T = 20$ time-steps between succeeding crossings.

In the “synchronized traffic lights” case discussed above, the optimal cycle times are situated at uncritical positions ($T = 10$, $T = 60$). In the contrary, the optimal cycle times

(step-function) for the “green wave” strategy are situated at critical positions, leading to a lower flow. Moreover, it can be seen in Fig. 9.6 that in the most cases for low densities the optimal system flow can not be achieved anymore even if another cycle time would be chosen. One aspect which also occurs for “synchronized traffic lights” is the increased flow for high densities.

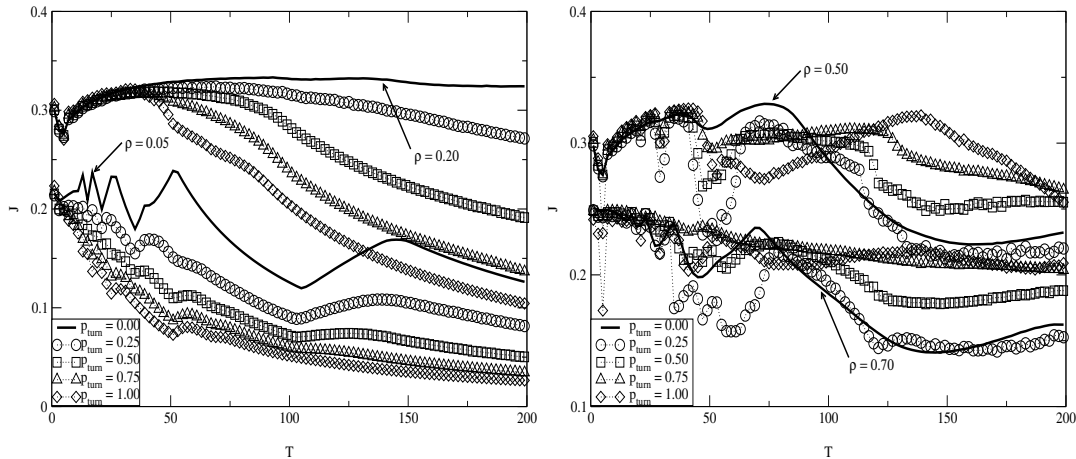


Figure 9.6: The impact of the turning events to the global flow is plotted in dependence to the cycle time. Note that for high densities the global flow is increased by turning for a wide range of cycle times.

The results stress that the “green wave” strategy is an improper candidate if turning of vehicles is allowed. Especially for low densities the flow is up to 50% lower than in a system without turning. Furthermore, the FDs show an artificial shape caused by the cycle time relation used. Even like for the “synchronized traffic lights” case, it may be concluded that turning possibilities in dense traffic can be beneficial since for high densities the flow is increased by turning.

9.1.3 Random Offset

For the “random offset” strategy the impact of turning is negligible small. This can be seen in the FDs in Fig. 9.7 (left). The FDs are almost equal. The origin for the robustness against turning is given by the optimal cycle time curve obtained in Sec. 7.3.3 (Gaussian). This incorporate factors as topology or mean velocity of vehicles, but does not coordinate the switching between the intersections. Instead, the switching events between intersections are determined by a random offset. Therefore, it barely plays a role if a vehicle changes the direction in order to approach the next intersection or not. The weak impact of turning is also confirmed in the right part of Fig. 9.7 where the cycle time is plotted against the global flow. It can be seen that the curves representing the events with turning, follow the solid curve (no turning) with just some small deviations.

Hence, it can be stated here that the “random offset” strategy is flexible and applicable. This is confirmed by the results of the previous chapter, where the “random offset” strategy seems to be the most flexible one. However, it must be reminded that the FD of the “random offset” strategy does not match the system optimum.

In the following, the impact of turning is analyzed with the focus to the adaptive strategies presented. Note that for the global strategies fixed cycle times are given from the outside, while for the adaptive signals the cycle times are determined flexibly due to the internal

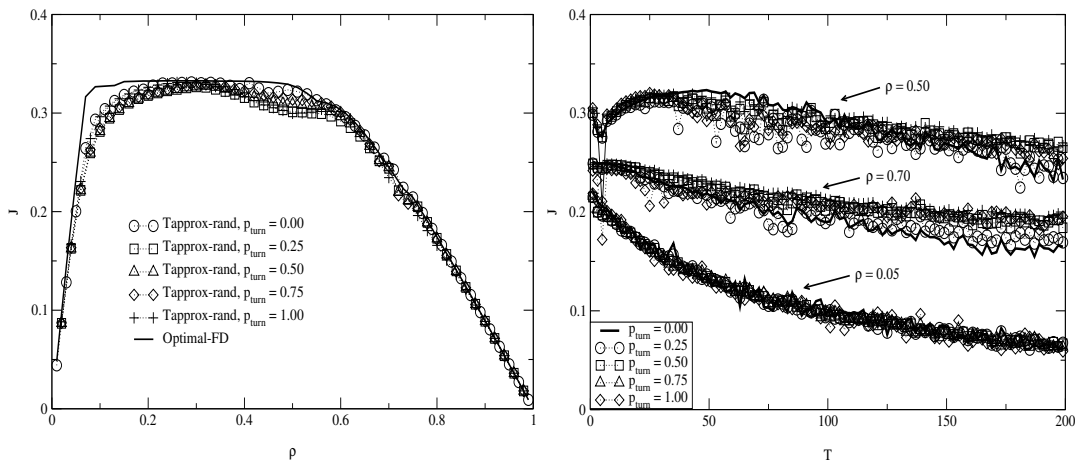


Figure 9.7: The impact of turning is almost negligible for the “random offset” strategy as can be seen in the FD (left) and cycle time vs. global flow dependence (right).

signal algorithm. Therefore, the impact of the turning process was shown for the global strategies by the dependence of the global flow on the chosen cycle time, while for the adaptive strategies the impact to the cycle times can be analyzed directly as will be shown further below.

9.1.4 Switching Based on Queue Length

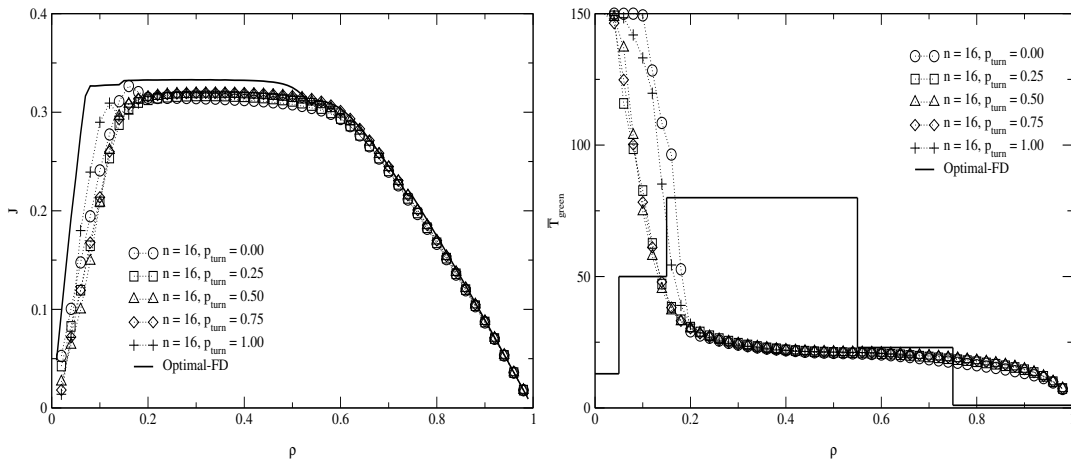


Figure 9.8: For the “switching based on queue length” strategy, the impact of turning is relatively low.

In the case of “switching based on queue length”, the impact of turning seems also negligible as in the case of a “random offset”. The deviations are, compared to the FD without turning (\circ), relatively small. A little curiosity occurs for a turning rate of $p_{\text{turn}} = 1$. Here, for small densities the flow becomes even a little bit higher than for the case without turning. Also the mean green-cycle time curves keep the same shape, almost independent of turning. This can be seen in Fig. 9.8 (right). The only difference is the transition area between high and short cycle times which is shifted in respect to the turning rate. Note that the mean green-cycle time is plotted vs. the global density. The mean green-cycle time originates out of the adaptive algorithm reacting to the traffic conditions. Remind

that this presentation is different from the cases where global strategies with a fixed cycle time are considered.

Consequently, it can be stated that the “switching based on queue length” reacts flexible to the fluctuating densities without heavy losses of the flow. However, one should keep in mind that the flow achievable is clearly below the system optimum, represented by the solid line.

9.1.5 Switching Based on Waiting Time

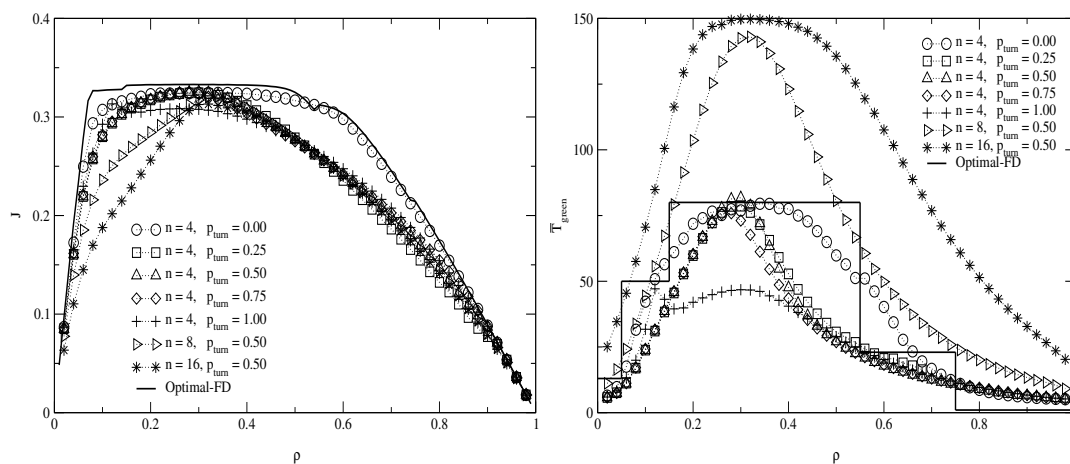


Figure 9.9: The FDs (left) reveal a strong impact of turning to the overall flow. This can be seen by the immense flow loss for densities above $\rho = 0.3$.

In the contrary to the previous case, turning strongly influences the system if the signals operate according to the “switching based on waiting time” strategy. The corresponding FDs (see Fig. 9.9) reveal a strong loss of flow especially for high densities. There is only a small density area at $\rho = 0.3$ where the flow stays nearly uninfluenced.

For the case without turning, the switching events along one direction self-organize into an optimal state similar to the “green wave” strategy (see Sec. 8.2). Therefore, the strategy is almost capable to reach the system optimum. If turning is allowed, the system optimum can not be obtained anymore. The right plot of Fig. 9.9 shows that the mean green-cycle time decreases, especially for densities above $\rho = 0.3$. This decrease can be explained considering that the mean gap between the vehicles, driving across an intersection, gets larger due to vehicles that have turned off. Therefore, the probability for n vehicle to pass the next intersection within a given time (control parameter of the strategy), is considerably lowered. In order to test in how far the results may be improved by larger waiting times, comparable curves are given for $n = 8$ and $n = 16$. In accordance to the case without turning, the global flow is not improved but rather declined with increasing n .

The “switching based on waiting time” strategy reacts sensitive on density fluctuations caused by turning. Nevertheless, the strategy is very usable for densities below $\rho = 0.3$, and moreover even capable to reach the system optimum in the case without turning.

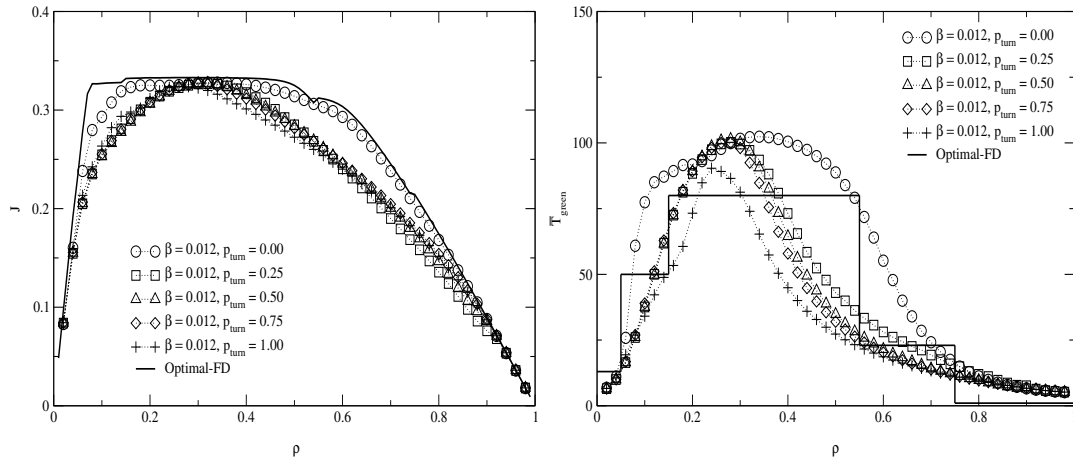


Figure 9.10: The FDs obtained for signals operating in analogy to a neural network are comparable to the “switching based on waiting time” case. Clearly, one can see the heavy loss of flow at densities around $\rho = 0.3$.

9.1.6 Switching in Analogy to a Neural Network

Considering the “switching in analogy to a neural network” strategy, similar results to the “switching based on waiting time” strategy discussed above are obtained. This can be seen in Fig. 9.10 (left) where the negative impact of turning becomes visible by the loss of flow at densities around $\rho = 0.3$. Moreover, for the “switching in analogy to a neural network” strategy, the flow loss is even larger especially for low densities. Remind that already the case without turning pointed out that there are some similarities between the strategies.

The main difference to the “switching based on waiting time” strategy is the retarded interaction between passing vehicles and the cycle time (see Sec. 8.3 for details). This delay leads to an additional loss of flow. In the right part of Fig. 9.10 the mean green-cycle time is given for the investigated turning rates. Here, the cycle time decreases at densities around $\rho = 0.3$, which is in totally agreement to the case of “switching based on waiting time”.

Similar to the results obtained before, it must be stressed here that the “switching in analogy to a neural network” is very sensitive in regard to density fluctuations caused by turning, even for low densities.

9.2 Inhomogeneous Densities

In the following section the impact of inhomogeneous densities along the two directions of the network is investigated. This situation is somehow comparable to real city networks which are mostly build out of main streets or directions with a higher density, and minor ones with a lower density. While in the ChSch model both directions and moreover all streets are treated equally, in the following different densities are initialized and turning is disabled. This leads to different densities along the south-north and the west-east direction.

Obviously, this case can not be compared with the fluctuating density caused by turning. Although the turning events can lead to different densities on short time-scales, these

differences are statistical and fade out on long time-scales. Note that the case of fixed different densities along the directions may be more realistic than the case of fluctuating densities due to turning events, since in the last case all drivers act totally uncoordinated (randomly) without any route choice, while in reality obviously preferred routes exist.

9.2.1 Synchronized Traffic Lights

In the following the impact of inhomogeneous densities is investigated for “synchronized traffic lights”. Remind that for the global strategies the green-cycle time T_{green} is equal to the red-cycle time T_{red} . Therefore, the two directions can be assumed to be completely independent (decoupled). This was discussed in chapter 7. Consequently, the result for the whole network is given by the superposition of the results from the two directions. The consequence thereof is that the impact of inhomogeneous densities can be derived directly from the homogeneous case. Therefore, among the global strategies only the “synchronized traffic lights” case is exemplarily analyzed.

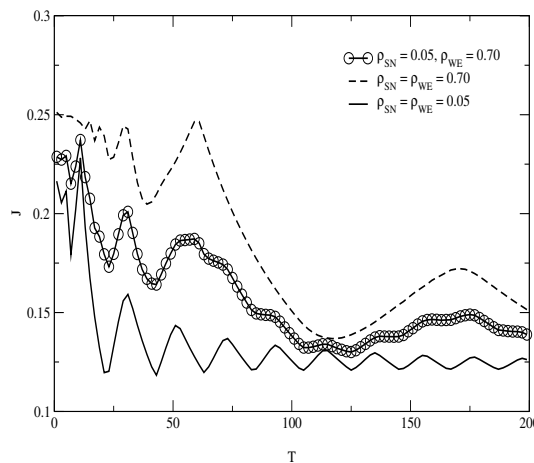


Figure 9.11: The global flow (\circ) is given as a combination of the flows along the two directions.

In Fig. 9.11 the global flow (\circ) as well as the flow for each direction is plotted in dependence to the cycle time. It can clearly be seen that the global flow combines from the flows on the two different directions.

In order to constitute an inhomogeneous density in the network, the density along the south-north direction was fixed to certain values for the analysis. FDs for the different fixed densities are depicted in Fig. 9.12. These are obtained by varying the density on the west-east direction. The starting point is a low fixed density of $\rho_{\text{SN}} = 0.05$. Obviously, the minimum global density for this case is equal to $\rho = 0.025$ and the maximum global density is reached at $\rho = 0.525$. Therefore, the corresponding FD is compressed in regard to the density, i.e., the FDs are only capable to cover a part of the possible densities between 0 and 1.

In the FDs, two different cycle times ($T = 10$, $T = 60$) leading to the optimal result for the “synchronized traffic lights” strategy were used. Thereby, the left part of Fig. 9.12 represents the case $T = 10$ time-steps, while in the right part a cycle time of $T = 60$ time-steps is used. For the low fixed density of $\rho_{\text{SN}} = 0.05$ in both cases a plateau is formed with a flow clearly below the flow that is obtained in a system with homogeneous density (solid line). The flow decrease is caused by the fact that the direction with the low density can not contribute enough to the overall flow. A similar picture is obtained

for the fixed density of $\rho_{SN} = 0.7$. Here, the portion to the overall flow is also too low, since the flow on the south-north streets is low due to the high density (jamming). For intermediate fixed densities, the plateau is established at the same level as for the system with homogenous densities. However, the width of these plateaus is considerably smaller.

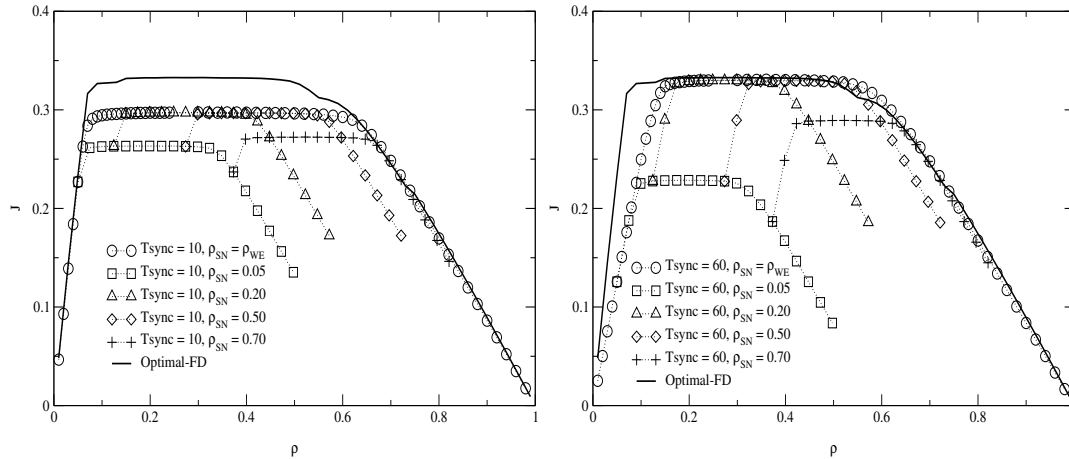


Figure 9.12: The FDs for different fixed densities along the south-north direction are shown. Thereby the left part of the figure corresponds to the case with a cycle time of $T = 10$ time-steps and the right part to a cycle time of $T = 60$ time-steps.

It was shown that an inhomogeneous density distribution leads to heavy flow losses (global flow) if the signals operate with the “synchronized traffic lights” strategy. Only a few data points match the flow of the corresponding homogeneous system. Note that it is not necessary to check in how far different cycle times could be beneficial, e.g., shorter green-cycles on the minor roads, since the used cycle times ($T = 10$, $T = 60$) are the optimal ones independent of the density (see chapter 7.1.5).

9.2.2 Switching Based on Queue Length

For the adaptive strategies, the green- and red-cycle times are not forced to be equal as for the global strategies. Therefore, the algorithms may assign different green-cycles to the signals in respect to the directions. One would expect that this leads to some benefits over the global strategies in the case of inhomogeneous densities, since the streets with a higher traffic demand can be preferred.

The FDs taken from a system operating with “switching based on queue length” strategy are shown in Fig. 9.13 (left). The control parameter n is set to 16 in correspondence to the optimal solution which was derived in the beginning of this chapter. Obviously, as in the case of “synchronized traffic lights”, the obtainable global densities are restricted by the fixed density along the south-north direction.

Focusing on the low fixed density of $\rho_{SW} = 0.05$, a clear difference to the “synchronized traffic lights” case can be seen, namely that no plateau is formed. This shape is similar to a FD of a system without defect. For the other fixed densities, a plateau is formed. The corresponding curves show, in comparison to the “synchronized traffic lights” case, a higher flow for low densities (before the plateau), while the flow decreases faster for high densities (behind the plateau).

In the right plot of Fig. 9.13 the mean green-cycle time is given once for the streets with varied density (main plot), and once for the streets with fixed density (inset). Note that

for both cases the mean cycle time is plotted against the global density. As can be seen in the figure, for a low fixed density of $\rho_{SN} = 0.05$ the mean green phase for the west-east direction stays at the maximum level of $T = 150$ time-steps, whereas the green phase for the south-north direction (inset) early drops to a relatively low level. This can be explained as follows: The mean green-cycle times are established from a competition between the queues formed at red signals along both directions. In the case of a low fixed density, the traffic signals along the south-north direction are barely forced to switch to green. Therefore, the green-cycle time along the south-north direction is established at a low, and along the west-east direction at a high level. However, for higher fixed densities the cycle times are mostly organized at a relatively low level for both directions since switching due to the formation of queues is possible along both directions.

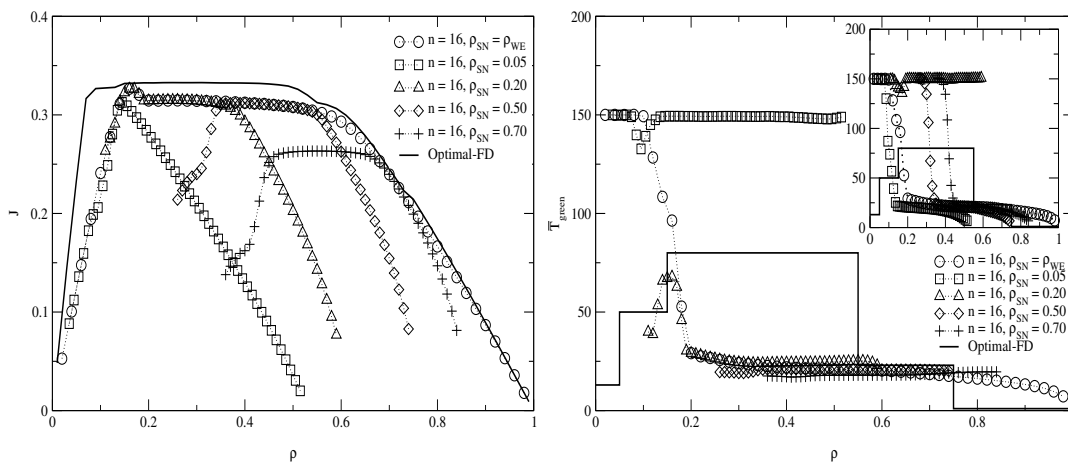


Figure 9.13: FDs of a system with inhomogeneous densities operating with “switching based on queue length” algorithm are shown in the left plot. The corresponding green-cycle times are given in the right plot.

Recapitulating, the “switching based on queue length” strategy does not lead to better results if compared to the synchronized signals strategy. Only for the low $\rho_{SN} = 0.05$ a higher flow can be obtained for some densities. For the remaining fixed densities the queues, formed in front of the signals, are large enough to force the signals to switch along both directions.

9.2.3 Switching Based on Waiting Time

Among the adaptive strategies, the “switching based on waiting time” strategy leads to the best results for inhomogeneous densities. As can be seen in the left plot of Fig. 9.14, most of the data points are situated on the optimal curve (solid line). Remind that the optimal curve for “switching based on waiting time” nearly matches the system optimum. In case of a low fixed density ($\rho_{SN} = 0.05$), the FD shows a triangular shape. This is similar to the previous case, but here the overall flow is noticeably higher.

If the density on the south-north streets is increased to $\rho_{SN} = 0.2$, the flow is fixed for all densities at a level corresponding to the maximum flow of the optimal FD (solid line). This result is different from the previous two cases where relatively small plateaus are observed, and additionally a region with a positive slope for low densities and a negative slope for high densities. Therefore, it can be stated that the “switching based on waiting time” strategy organizes the system in an optimal way, at least for $\rho_{SN} = 0.2$. Moreover, for high densities the flow is even a little bit higher than for the case without turning.

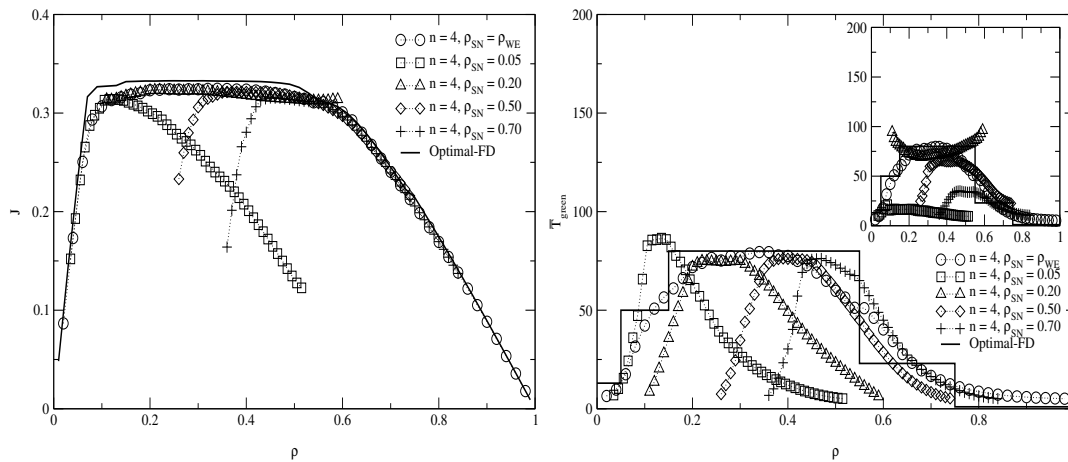


Figure 9.14: For the “switching based on waiting time” strategy almost all data points match the optimal solution. This can be seen in the left plot of the figure where FDs for different fixed densities are given. The corresponding mean green-cycle time (right) shows that the strategy reacts flexibly to the traffic conditions.

In the remaining two cases $\rho_{SN} = 0.5, 0.7$, the plateaus formed are smaller. However, the data points behind the plateau (negative slope) are situated on the optimal curve. This is also different from the “switching based on queue length” strategy where considerable lower flows are obtained for the higher densities. Note that for high fixed densities the flow along the south-north direction is relatively low since the fixed density always corresponds to the jammed state² of the system. Therefore, the data points before the plateau must be situated below the optimal curve.

The corresponding mean green-cycle times are given in Fig. 9.14 (right). It can be seen that the green-cycle time curves along the west-east direction (varied density) retain their shape compared with the optimal curve (solid line), but they are more narrow and their maximum is shifted from lower to higher densities. This underlines that the cycle times are flexibly adjusted to the traffic conditions in order to obtain an optimal result. Moreover, for the south-north direction (fixed density) the mean green-cycle time curves (inset) can even take on a completely different shape, as can be seen in the case of $\rho_{SN} = 0.2$. Here, the green-cycle times curve has a complete contrary orientation if compared to the optimal curve (solid line); it is concave instead of convex.

The results stress that the “switching based on waiting time” strategy is predestinated for networks with inhomogeneous density distributions on the streets (major and minor roads). The algorithm reacts flexibly on varying traffic conditions, as can be seen on the wide range of cycle times for the different fixed densities. Furthermore, the algorithm even matches the optimal solution in the most cases.

9.2.4 Switching in Analogy to a Neural Network

The results for “switching in analogy to a neural network” are comparable to the previous case. This is not further surprising since the mechanisms extending the green-cycle times are similar in both cases, i.e., passing vehicles extend the cycle times. The good agreement

²The flow in the jammed state of the NaSch model is given by $J \approx (1 - \rho)p$ (see Sec 2.3.1).

can be seen in Fig. 9.15.

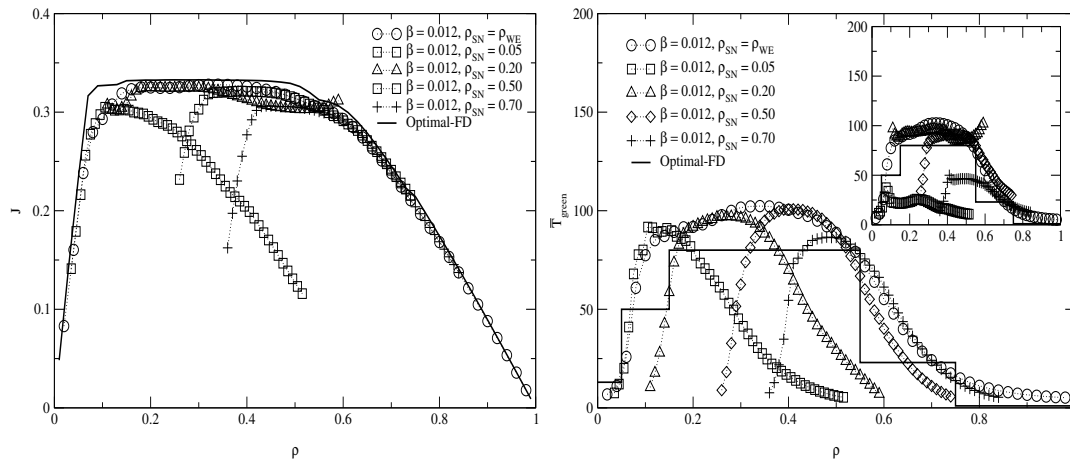


Figure 9.15: As can be seen in the FDs (left), a large part of the data points matches the optimal curve (solid line). The corresponding mean green-cycle times are given in the right plot.

Also like in the previous case, the FD shows a simple triangular shape (no plateau) for $\rho_{SN} = 0.05$. The corresponding maximum flow is a little bit lower than for the “switching based on waiting time” strategy.

Furthermore, for $\rho_{SN} = 0.2$ the flow stays almost fixed independent from the global density, and nearly all data points are situated on the optimal curve.

For the two remaining cases $\rho_{SN} = 0.5, 0.7$, the plateau level does not reach the maximum flow. However, in the region of the FD where the slope is negative all data points are situated on the optimal curve again. Remind that the optimal curve of the neural network strategy is a little bit below the system optimum.

A look at the corresponding mean green-cycle times in Fig. 9.15 (right) reveals that also here the cycle times are flexibly adjusted. In comparison to the optimal curve (solid line) it can be seen that the curves are more narrow and shifted towards smaller or larger densities. Moreover, similar to the “switching based on waiting time” case, the cycle time curves along the south-north direction (inset) can take on a completely different orientation.

The “switching in analogy to a neural network” seems to be an useful strategy for systems with an inhomogeneous density distribution since it leads to relatively good results. However, compared with the “switching based on waiting time” strategy (previous section) it is a little bit inferior.

9.3 Discussion

In order to provide a more realistic vehicle distribution in the network, the ChSch model was firstly enhanced by a stochastic turning of vehicles. The turning leads to strongly fluctuating densities on the streets.

It has been found that turning can have a strong impact to the system state. This was checked for the fixed strategies, presented in the previous chapter, as well as for the adaptive strategies. In the most cases the global flow is situated below the flow of the corresponding scenario without turning. The deviations from the optimal FD are caused by the fact that most of the strategies optimize the movement of vehicles along a fixed

direction. Therefore, the optimization gets worse if a large amount of vehicles change their direction. However, in some cases, e.g., the standard ChSch model (“synchronized traffic lights”), the negative impact is surprisingly weak or even negligible as in the case of the “random offset” strategy. For the “random offset” strategy the influence of turning is almost negligible since no fixed directions are optimized, i.e., the switching between intersections is coordinated randomly.

Unfortunately, the adaptive strategies, especially the “switching based on waiting time” and the “switching in analogy to a neural network”, are not capable to prevent the system from the negative impact of the fluctuating traffic states.

A surprising result was found for the fixed strategies, here turning can increase the global flow for high densities and large cycle times. Thus, it may be concluded that turning possibilities in dense traffic can lead to positive effects.

Furthermore, the impact of inhomogeneous densities along the two directions in the ChSch model was investigated. This was done in order to mimic the inhomogeneous traffic demand (major and minor roads) in real city networks, since the case of inhomogeneous densities due to random turning seems to be unrealistic.

For the global strategies it has been shown that the global flow is given as the superposition of the flows along the two directions, since these are independent. Therefore, the global flow is strongly determined by unfavorable traffic states even if occurring only along one direction.

The adaptive signal control algorithms lead to good results for the case of inhomogeneous densities. It has been found that the algorithms, especially the “switching based on waiting time” and “switching in analogy to a neural network” strategy, react flexibly on the inhomogeneous densities. The results are close to the optimal solution almost for all densities.

This result is quite important given that the case of inhomogeneous densities seems to be more realistic than the case of fluctuating densities due to turning, since in the case of turning all drivers act totally uncoordinated while in reality preferred routes exist.

10 Summary and Outlook

The intention of this thesis has been to provide insight into the phenomena of traffic jams in terms of cluster formation in cellular automata (CA) models for traffic flow.

In chapter 1 an introduction to this thesis was given. The second chapter reviewed the most important empirical observations as well as the basic modelling concepts in that field. The first part of the thesis covered the VDR (velocity-dependent randomization) model for highway traffic. Based on random walk theory an analytical approach to the dynamics of single jam clusters in the VDR model was suggested in chapter 3. This approach has been capable to determine important characteristic quantities of jams as resolving probabilities or lifetimes. It was shown that the random walk approach renders the jamming dynamics of the model very well. In consideration of the fact that recent CA models (see Sec. 2.3.2) use the VDR slow-to-start rule for the generation of wide phase separated jams it can be concluded that the results are generic.

In addition to the jamming dynamics, determined by internal model rules, it is further important to understand the impact of external forces. Therefore, the influence of local defects to the jamming dynamics of the VDR model was analyzed in chapter 4. It turned out that a new phase occurs at the defect which shows similarities with “stop-and-go” traffic. The fact that such a system state is absent in the model without defect underlines its strong influence.

Finally, the VDR model was analyzed with open boundary conditions in chapter 5. The aim has been to provide a completer insight to the impact of external forces since open boundaries are known to strongly influence the system dynamics. It turned out that a new insertion strategy had to be defined in order to prepare the high-flow states occurring in the model. Several new results were obtained. First of all it was shown that an extremal current principle suggested by Kolomeisky *et al.* [92] is fulfilled for the VDR model. This is a surprising result since the principle was intended to be only valid for models that show only one single maximum in the fundamental diagram like the NaSch model. Furthermore, a completely new phase, denoted as JO (jam outflow) phase where metastable high-flow states can exist in finite systems, was revealed. From a practical point of view a flow optimization strategy, followed, for example, in the Lincoln- and the Holland-Tunnels in New York, was reproduced with the help of the new high-flow phase.

The second part of the thesis covered the Chowdhury-Schadschneider (ChSch) model for city traffic. Here, an additional factor exerts influence on the formation of jams, namely the impact of red traffic lights. The main focus laid on the optimization of the throughput in the network.

Therefore, in chapter 7 global traffic light control strategies were considered. It was shown that for synchronized traffic lights the global throughput of the network strongly depends on the cycle times, i.e, one finds strong oscillations. These oscillations were explained, in good agreement to numerical results, by the help of a simple phenomenological approach. In order to allow a more flexible traffic light control, the ChSch model was enhanced by

an additional model parameter (offset) so that the traffic lights are not enforced to switch simultaneously anymore. One application for the offset parameter was the implementation of a two-dimensional “green wave” strategy in the network. It was shown that the optimal FD of the “green wave” strategy matches the *global* optimum of the ChSch model so that it can be used as a reference point for the other traffic light strategies investigated. In this context a new effect was presented denoted as “red wave”. A “red wave” describes a system at a high density where the traffic lights are adjusted in a way just that jams can be guided unhindered through the network. Although, the “green wave” strategy improves the flow considerably the strong oscillations remain. Thus, in order to avoid these strong oscillations the offset parameter was further used to allow a random switching between the traffic lights (“random offset”).

The investigations concerning the ChSch model were extended in chapter 8 by the use of adaptive traffic signal control. Therefore, three different adaptive strategies were introduced. The corresponding optimal control parameters were determined and the strategies were compared with the global (fixed) ones. It was shown that the simple adaptive strategies can lead to a state close to the system optimum. This result may be beneficial for real networks since the suggested algorithms are simple and the parameters used can easily be obtained in real traffic.

The motivation of introducing an adaptive signal control was to provide robust strategies that match the system optimum even if traffic conditions closer to reality are considered. In order to model such conditions inhomogeneous vehicle distributions in the network were assumed in chapter 9. These were realized by a stochastic turning of vehicles, which leads to strongly fluctuating densities on the streets, and on the other hand by fixed inhomogeneous densities along the two directions of the network. For the case of stochastic turning a strong impact to the system was obtained. The global flow was mostly situated below the corresponding case without turning for the global as well as for adaptive strategies. However, in some cases, e.g., for the “random offset” strategy, the influence of turning is weak. The case of fixed inhomogeneous densities along the two directions should mirror the inhomogeneous traffic demand (major and minor roads) in reality. This seems to be more realistic than the case of fluctuating densities due to turning since the drivers act totally uncoordinated while in reality preferred routes exist. It turned out that the adaptive signal control can lead to good results, outperforming the global fixed strategies. Especially, the “switching based on waiting time” strategy, where a green signal switches if it is not used for a certain time, was found to react flexibly on inhomogeneous densities. The results obtained in this case are close to the *global* optimum of the ChSch model almost for all densities.

Recapitulating, the results presented provide an extensive insight into the jamming dynamics in CA models for traffic flow, both for highway as well as for city traffic. In particular, the impact of external forces, realized by defects, boundary conditions, or traffic lights, was analyzed. These external elements can be related to restricting elements of real traffic. Therefore, the results may be beneficial for the simulation of realistic traffic scenarios. However, the results also raised some questions that could motivate new research.

First of all, an important element of congestion in stochastic CA models, which was not considered in this work, is the occurrence of spontaneous jams. In the VDR model jams can emerge out of the metastable high-flow states due to local velocity fluctuations. Consequently, such fluctuations determine the stability and lifetime of the high-flow states. The understanding of this process is useful for realistic traffic simulations since the stability of a traffic state is one of the most important elements for a proper traffic forecast. There-

fore, the phenomenon of spontaneous jamming in the VDR model should be investigated in future. Moreover, only the slow-to-start case ($p \ll p_0$) of the VDR model was considered in this thesis. It is known that the fluctuation parameters p_0, p also exhibit a strong impact to the jamming dynamics in addition to the influence concerning the occurrence of spontaneous jams. Therefore, especially the transition from the VDR model to the NaSch model ($p \Rightarrow p_0$) should be investigated since both models show a totally different jamming dynamics (see Sec. 2.3.1).

Another point concerns on- and off-ramps. These are assumed to be the origin of a variety of different traffic states observed empirically. It was realized that for the NaSch model [30] as well as for the VDR model [129] local defects are comparable to on-ramps. In this context, the behavior of local defects should be studied in more detailed CA traffic models [83, 89]. This seems to be promising since already in the VDR model a phase was observed with a wide jam passing a localized congested region consisting of small compact jams. Similar traffic states were also observed in real traffic [76, 77, 83, 90] and related to the more detailed models. However, it is important to determine which of the effects found in the empirical observations can be related with the enhanced dynamics of the models and which effects are related with the defect (the analogue to on-ramps) itself.

A further question arises concerning the stripped microscopic jam pattern occurring in the VDR model with open boundaries. A comparable state was recently interpreted [83] as a sign for the “pinch effect” appearing in real traffic (see chapter 2) in the vicinity of on- and off-ramps. It seems to be useful to compare the phase diagrams obtained in chapter 5 with the empirical findings. In particular, it could be beneficial to compare the phase diagram with more detailed models, e.g., BL model (see Sec. 2.3.2), in order to validate the dynamics.

As already discussed in chapter 6 no theoretical framework exists for the description of city traffic, in the contrary to highway traffic. In cities traffic is mainly determined by the traffic lights and the topology of the network. Therefore, the results of the ChSch model are of rather theoretical nature. Nonetheless, due to the basic structure of the model some of the results seem to be universal and might be transferable to real traffic. Besides the assignability to reality many further questions arose during the analysis of the ChSch model. In regard to the simple “Manhattan” geometry of the model it seems to be useful to analyze how the traffic light strategies compare, if inhomogeneous street lengths are considered. Moreover, it could be useful to analyze in how far observable of individual vehicles like stop-times or travel-times compare to the *global* optimum. In this context, it should be investigated how the strategies succeed if cars are advised to follow fixed routes, i.e., turning is not random anymore. From a practical point of view one is interested to questions like: How many traffic lights have to be equipped with an adaptive signal control in order to improve the traffic flow?

Bibliography

- [1] ANTAL, T., AND SCHÜTZ, G. M. Asymmetric exclusion process with next-nearest-neighbor interaction: Some comments on traffic flow and a nonequilibrium reentrance transition. *Phys. Rev. E* 62 (2000), 83–89.
- [2] APPERT, C., AND SANTEN, L. Boundary induced phase transitions in driven lattice gases with metastable states. *Phys. Rev. Lett.* 86 (2001), 2498–2501.
- [3] BAK, P., TANG, C., AND WIESENFELD, K. Self-organized criticality. *Phys. Rev. A* 38 (1988), 364–374.
- [4] BANTAY, P., AND JANOSI, I. M. Avalanche dynamics from anomalous diffusion. *Phys. Rev. Lett.* 68 (1992), 2058–2061.
- [5] BARLOVIĆ, R. Metastabile Zustände in Zellularautomatenmodellen für den Straßenverkehr. *Diplomarbeit, Gerhard-Mercator Universität Duisburg, Germany* (1998).
- [6] BARLOVIĆ, R., ESSER, J., FROESE, K., KNOSPE, W., NEUBERT, L., AND SCHRECKENBERG, M. Online traffic simulation with cellular automata. In *Traffic and Mobility* (Berlin, 1999), W. Brilon, F. Huber, M. Schreckenberg, and H. Walentowitz, Eds., Springer, pp. 117–134.
- [7] BARLOVIĆ, R., HUISINGA, T., SCHADSCHNEIDER, A., AND SCHRECKENBERG, M. Open boundaries in a cellular automaton model for traffic flow with metastable states. *Phys. Rev. E* 66 (2002), 046113.
- [8] BARLOVIĆ, R., SANTEN, L., SCHADSCHNEIDER, A., AND SCHRECKENBERG, M. Metastable states in CA models for traffic flow. In *Traffic and Granular Flow '97* (Singapore, 1998), M. Schreckenberg and D. Wolf, Eds., Springer, pp. 335–340.
- [9] BARLOVIĆ, R., SANTEN, L., SCHADSCHNEIDER, A., AND SCHRECKENBERG, M. Metastable states in cellular automata for traffic flow. *Eur. Phys. J. B* 5 (1998), 793–800.
- [10] BARLOVIĆ, R., SCHADSCHNEIDER, A., AND SCHRECKENBERG, M. Random walk theory of jamming in a cellular automaton model for traffic flow. *Physica A* 294 (2001), 525–538.
- [11] BENJAMIN, S. C., JOHNSON, N. F., AND HUI, P. M. Cellular automata models of traffic flow along a highway containing a junction. *J. Phys. A* 29 (1996), 3119–3127.
- [12] BIELEFELDT, C., AND BUSCH, F. Motion - a new on-line traffic signal network control system. *IEE Conference on Road Traffic Monitoring and Control* 391 (1994), 55–59.
- [13] BIHAM, O., MIDDLETON, A. A., AND LEVINE, D. Self-organization and a dynamical transition in traffic-flow models. *Phys. Rev. A* 46 (1992), R6124–R6127.

- [14] BRUNET, L. G., AND GONCALVES, S. Cellular automaton block model of traffic in a city. *Physica A* 237 (1997), 59–66.
- [15] CHERRY, C., Ed. *Information theory*. Butterworths Washington, 1961.
- [16] CHEYBANI, S., KERTÉSZ, J., AND SCHRECKENBERG, M. The nondeterministic Nagel-Schreckenberg traffic model with open boundary conditions. *Phys. Rev. E* 63 (2001), 016108.
- [17] CHEYBANI, S., KERTÉSZ, J., AND SCHRECKENBERG, M. Stochastic boundary conditions in the deterministic Nagel-Schreckenberg traffic model. *Phys. Rev. E* 63 (2001), 016107.
- [18] CHOPARD, B., AND DROZ, M., Eds. *Cellular automata modelling of physical systems*. Cambridge University Press, 1998.
- [19] CHOPARD, B., LUTHI, P. O., AND QUELOZ, P. Cellular automata model for car traffic in a two-dimensional street network. *J. Phys. A* 29 (1996), 2325–2336.
- [20] CHOWDHURY, D., SANTEN, L., AND SCHADSCHNEIDER, A. Statistical physics of vehicular traffic and some related systems. *Physics Reports* 329 (2000), 199–329.
- [21] CHOWDHURY, D., AND SCHADSCHNEIDER, A. Self-organization of traffic jams in cities: effects of stochastic dynamics and signal periods. *Phys. Rev. E* 59 (1998), R1311–R1314.
- [22] CHUNG, K. H., HUI, P. M., AND GU, G. Q. Two-dimensional traffic flow problems with faulty traffic lights. *Phys. Rev. E* 51 (1995), 772–774.
- [23] CREMER, M., AND LUDWIG, J. A fast simulation model for traffic flow on the basis of boolean operations. *Math. and Comp. in Sim.* 28 (1986), 297–307.
- [24] CSAHOK, Z., AND VICSEK, T. Traffic models with disorder. *J. Phys.: Condensed Matter* 27 (1994), L591–L596.
- [25] CSANYI, G., AND KERTÉSZ, J. Scaling behaviour in discrete traffic models. *J. Phys. A* 28 (1995), L427–L432.
- [26] CUESTA, J. A., MARTÍNEZ, F. C., MOLERA, J. M., AND SÁNCHEZ, A. Phase transition in two-dimensional traffic-flow models. *Phys. Rev. E* 48 (1993), R4175–R4178.
- [27] DAGANZO, C. F., CASSIDY, M. J., AND BERTINI, R. L. Possible explanations of phase transitions in highway traffic. *Transp. Res. B* 33 (1999), 365–379.
- [28] DE GIER, J., AND NIENHUIS, B. Exact stationary state for an asymmetric exclusion process with fully parallel dynamics. *Phys. Rev. E* 59 (1999), 4899–4911.
- [29] DIEDRICH, G. Numerische Untersuchung zur Phasenseparation in Zellularautomaten für den Strassenverkehr. *Diplomarbeit, Universität zu Köln, Germany* (1999).
- [30] DIEDRICH, G., SANTEN, L., SCHADSCHNEIDER, A., AND ZITTARTZ, J. Effects of on- and off-ramps in cellular automata models for traffic flow. *Int. J. of Mod. Phys. C* 11 (2000), 335–345.

-
- [31] DOMB, C., AND LEBOWITZ, J., Eds. *Phase Transition and Critical Phenomena*, vol. 17. Academic Press, New York, 1995.
- [32] DOMB, C., AND LEBOWITZ, J. L., Eds. *Phase Transition and Critical Phenomena*, vol. 19. Academic Press, New York, 2000.
- [33] EDIE, L. C., AND FOOTE, R. S. Traffic flow in tunnels. *Highway Research Board, Proc. Annu. Meet.* 37 (1958), 334–344.
- [34] EISENBLÄTTER, B., SANTEN, L., SCHADSCHNEIDER, A., AND SCHRECKENBERG, M. Jamming transition in a cellular automaton model for traffic flow. *Phys. Rev. E* 57 (1998), 1309–1314.
- [35] EMMERICH, H., AND RANK, E. Investigating traffic flow in the presence of hindrances by cellular automata. *Physica A* 216 (1995), 435–444.
- [36] ESSER, J. Simulation von Stadtverkehr auf der Basis zellulärer Automaten. *Doktorarbeit, Gerhard-Mercator Universität Duisburg, Germany* (1997).
- [37] ESSER, J., AND SCHRECKENBERG, M. Microscopic simulation of urban traffic based on cellular automata. *Int. J. of Mod. Phys. C* 8 (1997), 1025–1036.
- [38] EVANS, M. R. Bose-Einstein condensation in disordered exclusion models and relation to traffic flow. *Europhys. Lett.* 36 (1996), 13–18.
- [39] EVANS, M. R. Exact steady states of disordered hopping particle models with parallel and ordered sequential dynamics. *J. Phys. A* 30 (1997), 5669–5685.
- [40] EVANS, M. R., RAJEWSKI, N., AND SPEER, E. R. Exact solution of a cellular automaton for traffic. *J. Stat. Phys.* 95 (1999), 45–96.
- [41] FELLER, W. *An Introduction to Probability Theory and Its Applications*. Wiley Series, 1968.
- [42] FREUND, J., AND PÖSCHEL, T. A statistical approach to vehicular traffic. *Physica A* 219 (1995), 95–114.
- [43] FUKUI, M., AND ISHIBASHI, Y. Effect of delay in restarting of stopped cars in a one-dimensional traffic model. *J. Phys. Soc. Jpn.* 66 (1997), 385–387.
- [44] FUKUI, M., OIKAWA, H., AND ISHIBASHI, Y. Flow of cars crossing with unequal velocities in a two-dimensional cellular automaton model. *J. Phys. Soc. Jpn.* 65 (1996), 2514–2517.
- [45] GARDNER, M. The fantastic combinations of john conway’s new solitaire game “life”. *Sc. American* 220 (1970), 120–123.
- [46] GARTNER, N. H. Opac: Strategy for demand-responsive traffic signal control. *IFAC-IFIP-IFORS Conference on Control, Computers, Communications in Transportation* 6 (1989), 499–503.
- [47] GERWINSKY, M., AND KRUG, J. Analytic approach to the critical density in cellular automata for traffic flow. *Phys. Rev. E* 60 (1999), 188–196.
- [48] GREENBERG, H., AND DAOU, A. The control of traffic flow to increase the flow. *Op. Res.* 8 (1960), 524.

- [49] GREENSHIELDS, B. D. A study of traffic capacity. In *Proceedings of the Highway Research Board* (Washington, D.C., 1935), vol. 14, Highway Research Board, pp. 448–477.
- [50] GU, G. Q., CHUNG, K. H., AND HUI, P. M. Two-dimensional traffic flow problems in inhomogeneous lattices. *Physica A* 217 (1995), 339–347.
- [51] GUPTA, H., AND RAMASWAMY, R. Backbones of traffic jams. *J. Phys. A* 29 (1996), L547–L553.
- [52] HAGER, J. S., KRUG, J., POPKOV, V., AND SCHÜTZ, G. M. Minimal current phase and universal boundary layers in driven diffusive systems. *Phys. Rev. E* 63 (2001), 056110.
- [53] HALL, F. L. Traffic stream characteristics. In *Traffic Flow Theory – A state-of-the-art report*, <http://www-cta.ornl.gov/cta/research/trb/tft.html> (Washington D.C., 1992), T. R. Board, Ed., Transp. Res. Board.
- [54] HALL, F. L., ALLEN, B. L., AND GUNTER, M. A. Empirical analysis of freeway flow-density relationships. *Transp. Res. A* 22 (1986), 45–46.
- [55] HANSON, S., Ed. *Advances in Neural information processing systems*. Morgan Kaufmann San Mateo, 1993.
- [56] HECK, H. M. Sigma - Entwicklung eines heuristischen Modells zur koordinierten Lichtsignalsteuerung. *Heureka: Optimierung in Verkehr und Transport* (1987), 187–208.
- [57] HELBING, D. Modeling multi-lane traffic flow with queuing effects. *Physica A* 242 (1997), 175–194.
- [58] HELBING, D. *Verkehrsdynamik*. Springer, Berlin, 1997.
- [59] HELBING, D. Traffic and related self-driven many-particle systems. *Rev. Mod. Phys.* 73 (2001), 1067–1141.
- [60] HELBING, D., HENNECKE, A., AND TREIBER, M. Phase diagram of traffic states in the presence of inhomogeneities. *Phys. Rev. Lett.* 82 (1999), 4360–4363.
- [61] HELBING, D., HERRMANN, H., SCHRECKENBERG, M., AND WOLF, D., Eds. *Traffic and Granular Flow '99* (Heidelberg, 2000), Springer.
- [62] HELBING, D., AND TREIBER, M. Gas-kinetic-based traffic model explaining observed hysteretic phase transition. *Phys. Rev. Lett.* 81 (1998), 3042–3045.
- [63] HENRY, J., AND FARGES, J. On-line parameter estimation for urban traffic control. In *IFAC-IFIP-IFORS Conference on Control, Computers, Communications in Transportation* (Headington Hill Hall, 1989), vol. 6, Pergamon Press, pp. 505–507.
- [64] HERMAN, R., AND GARDELS, K. Vehicular traffic flow. *Sc. American* 6 (1963), 35–43.
- [65] HERMAN, R., AND PRIGOGINE, I. A two-fluid approach to town traffic. *Science* 204 (1979), 148.

-
- [66] HERRMANN, M., AND KERNER, B. S. Local cluster effect in different traffic flow models. *Physica A* 255 (1998), 163–188.
- [67] HOPFIELD, J. J. Neural networks and physical systems with emergent collective computational abilities. *Proc. Natl. Acad. Sci. USA* 79 (1982), 2554–2558.
- [68] HORIGUCHI, T., AND SAKAKIBARA, T. Numerical simulations for traffic-flow models on a decorated square lattice. *Physica A* 252 (1998), 388–404.
- [69] HUANG, D. Noise properties in the Nagel-Schreckenberg traffic model. *Phys. Rev. E* 64 (2001), 036108.
- [70] HUISINGA, T., BARLOVIĆ, R., KNOSPE, W., SCHADSCHNEIDER, A., AND SCHRECKENBERG, M. A microscopic model for packet transport in the internet. *Physica A* 294 (2001), 249–256.
- [71] HUISINGA, T., BARLOVIĆ, R., KNOSPE, W., SCHADSCHNEIDER, A., AND SCHRECKENBERG, M. Microscopic modeling of packet transport in the internet. In *Traffic and Granular Flow '01* (Heidelberg, 2003), M. Fukui, Y. Sugiyama, M. Schreckenberg, and D. Wolf, Eds., Springer.
- [72] JANOWSKY, S. A., AND LEBOWITZ, J. Finite-size effects and shock fluctuations in the asymmetric simple-exclusions process. *Phys. Rev. A* 45 (1992), 618–625.
- [73] JANOWSKY, S. A., AND LEBOWITZ, J. L. Exact results for the asymmetric exclusion process with a blockage. *J. Stat. Phys.* 77 (1994), 35–51.
- [74] KERNER, B. S. Experimental features of self-organization of traffic flow. *Phys. Rev. Lett.* 81 (1998), 3797–3800.
- [75] KERNER, B. S. Traffic flow: Experiment and theory. In *Traffic and Granular Flow '97* (Singapore, 1998), M. Schreckenberg and D. E. Wolf, Eds., Springer, pp. 239–267.
- [76] KERNER, B. S. The physics of traffic. *Physics World* 8 (1999), 25–30.
- [77] KERNER, B. S. Experimental features of the emergence of moving jams in free traffic flow. *J. Phys. A* 33 (2000), 221–228.
- [78] KERNER, B. S. Phase transitions in traffic flow. In *Traffic and Granular Flow '99* (Heidelberg, 2000), D. Helbing, H. Herrmann, M. Schreckenberg, and D. Wolf, Eds., Springer, pp. 253–282.
- [79] KERNER, B. S. Complexity of synchronized flow and related problems for basic assumptions of traffic flow theories. *Network and Spatial Economics* 1 (2001), 35–76.
- [80] KERNER, B. S. Empirical macroscopic features of spatial-temporal traffic patterns at highway bottlenecks. *Phys. Rev. E* 65 (2002), 046138.
- [81] KERNER, B. S. Three phase traffic theory. In *Traffic and Granular Flow '01* (Heidelberg, 2003), M. Fukui, Y. Sugiyama, M. Schreckenberg, and D. Wolf, Eds., Springer.

- [82] KERNER, B. S., KLENOV, S. L., AND KONHÄUSER, P. Asymptotic theory of traffic jams. *Phys. Rev. E* 56 (1997), 4200–4216.
- [83] KERNER, B. S., KLENOV, S. L., AND WOLF, D. E. Cellular automata approach to three-phase traffic theory. *J. Phys. A* 35 (2002), 9971–10013.
- [84] KERNER, B. S., AND REHBORN, H. Experimental features and characteristics of traffic jams. *Phys. Rev. E* 53 (1996), R1297–R1300.
- [85] KERNER, B. S., AND REHBORN, H. Experimental properties of complexity in traffic flow. *Phys. Rev. E* 53 (1996), R4275–R4278.
- [86] KERNER, B. S., AND REHBORN, H. Experimental properties of phase transitions in traffic flow. *Phys. Rev. Lett.* 79 (1997), 4030–4033.
- [87] KNOSPE, W. Synchronized traffic: Modeling and empirical observations. *Doktorarbeit, Gerhard-Mercator Universität Duisburg, Germany* (2002).
- [88] KNOSPE, W., SANTEN, L., SCHADSCHNEIDER, A., AND SCHRECKENBERG, M. Disorder effects in cellular automata for two-lane traffic. *Physica A* 265 (1999), 614–633.
- [89] KNOSPE, W., SANTEN, L., SCHADSCHNEIDER, A., AND SCHRECKENBERG, M. Towards a realistic microscopic description of highway traffic. *J. Phys. A* 33 (2000), L477–L485.
- [90] KNOSPE, W., SANTEN, L., SCHADSCHNEIDER, A., AND SCHRECKENBERG, M. Human behavior as origin of traffic phases. *Phys. Rev. E* 65 (2002), 015101(R).
- [91] KNOSPE, W., SANTEN, L., SCHADSCHNEIDER, A., AND SCHRECKENBERG, M. Single-vehicle data of highway traffic: Microscopic description of traffic phases. *Phys. Rev. E* 65 (2002), 056133.
- [92] KOLOMEISKY, A. B., SCHÜTZ, G. M., KOLOMEISKY, E. B., AND STRALEY, J. P. Phase diagram of one-dimensional driven lattice gases with open boundaries. *J. Phys. A* 31 (1998), 6911–6919.
- [93] KOSHI, M., IWASAKI, M., AND OHKURA, I. Overview on vehicular flow characteristics. In *Proc. 8th International Symposium on Transportation and Traffic Theory* (Toronto, 1983), University of Toronto Press, pp. 403–426.
- [94] KRAUSS, S. Microscopic Modelling of Traffic Flow: Investigation of collision free vehicle dynamics. *Doktorarbeit, Universität zu Köln, Germany* (1997).
- [95] KRAUSS, S., WAGNER, P., AND GAWRON, C. Metastable states in a microscopic model of traffic. *Phys. Rev. E* 55 (1997), 5597–5602.
- [96] KRUG, J. Boundary-induced phase transitions in driven diffusive systems. *Phys. Rev. Lett.* 67 (1991), 1882–1885.
- [97] KRUG, J. Platoon formation as a critical phenomenon. In *Traffic and Granular Flow '97* (Singapore, 1998), M. Schreckenberg and D. E. Wolf, Eds., Springer, pp. 285–301.

-
- [98] KRUG, J., AND FERRARI, J. Phase transitions in driven diffuse systems with random rates. *J. Phys. A* 29 (1996), 465–471.
- [99] KÜHNE, R., AND IMMES, S. Freeway speed distribution and acceleration noise – calculations from a stochastic continuum theory and comparison with measurements. In *Proceedings of the 10th International Symposium on Transportation and Traffic Theory* (New York, 1987), N. H. Gartner and N. H. M. Wilson, Eds., Elsevier, pp. 119–137.
- [100] LANDAU, L. D., AND LIFSCHITZ, E. M. *Lehrbuch der theoretischen Physik, Bd.5, Statistische Physik*. Harri Deutsch, Ffm., 1991.
- [101] LEE, H., LEE, H., AND KIM, D. Origin of synchronized traffic flow on highways and its dynamic phase transition. *Phys. Rev. Lett.* 81 (1998), 1130–1133.
- [102] LEE, H., LEE, H., AND KIM, D. Dynamic states of a continuum traffic equation with on-ramp. *Phys. Rev. E* 59 (1999), 5101–5111.
- [103] LÜBECK, S., SCHRECKENBERG, M., AND USADEL, K. D. Density fluctuations and phase transition in the Nagel-Schreckenberg traffic flow model. *Phys. Rev. E* 57 (1998), 1171–1174.
- [104] MACDONALD, J. T., AND GIBBS, J. H. Kinetics of biopolymerization on nucleic acid templates. *Biopolymers* 7 (1969), 707.
- [105] MARRO, J., AND DICKMAN, R., Eds. *Nonequilibrium Phase Transitions in Lattice Models*. Cambridge University Press, 1999.
- [106] MAURO, V., AND TARANTO, C. D. Utopia. In *IFAC-IFIP-IFORS Conference on Control, Computers, Communications in Transportation* (Paris, France, 1989), vol. 6, AFCET Proceedings, pp. 575–597.
- [107] MIKA, H. S., KREER, J. B., AND YUAN, L. S. Dual-mode behaviour of freeway traffic. *Highway Research Record* 279 (1969), 1–13.
- [108] MUSHA, T., AND HIGUCHI, H. The $1/f$ fluctuation of a traffic current on an expressway. *Jpn. J. Appl. Phys.* 15 (1976), 1271–1275.
- [109] MUSHA, T., AND HIGUCHI, H. Traffic current fluctuation and the burgers equation. *Jpn. J. Appl. Phys.* 17 (1978), 811–816.
- [110] NAGATANI, T. Anisotropic effect on jamming transition in traffic flow model. *J. Phys. Soc. Jpn.* 62 (1993), 2656–2662.
- [111] NAGATANI, T. Jamming transition in the traffic-flow model with two level crossing. *Phys. Rev. E* 48 (1993), 3290–3294.
- [112] NAGATANI, T. Jamming transition induced by a stagnant street in a traffic-flow model. *Physica A* 198 (1993), 108–116.
- [113] NAGATANI, T. Power-law distribution and $1/f$ noise of waiting time near traffic-jam threshold. *J. Phys. Soc. Jpn.* 62 (1993), 2533–2536.
- [114] NAGATANI, T. Effect of jam-avoiding turn on jamming transition in twodimensional traffic flow model. *J. Phys. Soc. Jpn.* 63 (1994), 1228–1231.

- [115] NAGATANI, T. Self-organization in 2d traffic flow model with, jam-avoiding drive. *J. Phys. Soc. Jpn.* *64* (1995), 1421–1430.
- [116] NAGATANI, T. Kinetics of segregation in a two-lane highway traffic flow. *J. Phys. A* *29* (1996), 6531–6542.
- [117] NAGATANI, T. Phase transition and scaling in the generalized traffic flow model. *Physica A* *246* (1997), 460–470.
- [118] NAGEL, K. Life-times of simulated traffic jams. *Int. J. of Mod. Phys. C* *5* (1994), 567–580.
- [119] NAGEL, K., AND HERRMANN, H. J. Deterministic models for traffic jams. *Physica A* *199* (1993), 254–269.
- [120] NAGEL, K., KAYATZ, C., AND WAGNER, P. Breakdown and recovery in traffic flow models. In *Traffic and Granular Flow '01* (Heidelberg, 2003), M. Fukui, Y. Sugiyama, M. Schreckenberg, and D. Wolf, Eds., Springer.
- [121] NAGEL, K., AND PACZUSKI, M. Emergent traffic jams. *Phys. Rev. E* *51* (1995), 2909–2918.
- [122] NAGEL, K., AND SCHRECKENBERG, M. A cellular automaton model for freeway traffic. *J. Physique I* *2* (1992), 2221–2229.
- [123] NAMAZI, A., EISSFELDT, N., WAGNER, P., AND SCHADSCHNEIDER, A. Boundary-induced phase transitions in a space-continuous traffic model with non-unique flow-density relation. *Eur. Phys. J. B* *30* (2002), 559–571.
- [124] NEUBERT, L., LEE, H. Y., AND SCHRECKENBERG, M. Density waves and jamming transition in a cellular automaton of traffic flow. *J. Phys. A* *32* (1999), 6517–6525.
- [125] NEUBERT, L., SANTEN, L., SCHADSCHNEIDER, A., AND SCHRECKENBERG, M. Single-vehicle data of highway traffic: a statistical analysis. *Phys. Rev. E* *60* (1999), 6480–6490.
- [126] OHIRA, T. Autonomous traffic signal control model with neural network analogy. In *the proceedings of InterSymp'97: 9th International Conference on Systems Research, Informatics and Cybernetics, Baden-Baden, Germany* (1997).
- [127] POPKOV, V., SANTEN, L., SCHADSCHNEIDER, A., AND SCHÜTZ, G. M. Empirical evidence for a boundary-induced nonequilibrium phase transition. *J. Phys. A* *34* (2001), L45–L52.
- [128] POPKOV, V., AND SCHÜTZ, G. M. Steady-state selection in driven diffusive systems with open boundaries. *Europhys. Lett* *48* (1999), 257–263.
- [129] POTTMEIER, A. Einfluss lokaler Defekte auf die Dynamik von Zellularautomaten-Modellen für den Straßenverkehr. *Diplomarbeit, Gerhard-Mercator Universität Duisburg, Germany* (2000).
- [130] POTTMEIER, A., BARLOVIĆ, R., KNOSPE, W., SCHADSCHNEIDER, A., AND SCHRECKENBERG, M. Localized defects in a cellular automaton model for traffic flow with phase separation. *Physica A* *308* (2002), 471–482.

-
- [131] PRESTON, K., AND DUFF, M., Eds. *Modern Cellular Automata: Theory and Applications*. Plenum, 1984.
- [132] PRIGOGINE, I., AND HERMAN, R. *Kinetic Theory of Vehicular Traffic*. American Elsevier, New York, 1971.
- [133] RICKERT, M. Simulationen zweispurigen Autobahnverkehrs mit Zellularautomaten. *Diplomarbeit, Universität zu Köln, Germany* (1994).
- [134] ROBERTSON, D., AND BRETHERTON, R. Optimizing networks of traffic signals in real time - the scoot method. *IEEE Transactions on Vehicular Technology* 40 (1991), 11–15.
- [135] ROTERS, L., LÜBECK, S., AND USADEL, K. D. Critical behavior of a traffic flow model. *Phys. Rev. E* 59 (1999), 2672–2676.
- [136] SANTEN, L. Numerical investigations of discrete models for traffic flow. *Doktorarbeit, Universität zu Köln, Germany* (1999).
- [137] SASVARI, M., AND KERTÉSZ, J. Cellular automata models of single lane traffic. *Phys. Rev. E* 56 (1997), 4104–4110.
- [138] SCHADSCHNEIDER, A. Analytical approaches to cellular automata for traffic flow: Approximations and exact solutions. In *Traffic and Granular Flow '97* (Singapore, 1998), M. Schreckenberg and D. Wolf, Eds., Springer.
- [139] SCHADSCHNEIDER, A. The Nagel-Schreckenberg model revised. *Eur. Phys. J. B* 10 (1999), 573–582.
- [140] SCHADSCHNEIDER, A., CHOWDHURY, D., BROCKFELD, E., KLAUCK, K., SANTEN, L., AND ZITTARTZ, J. A new cellular automata model for city traffic. In *Traffic and Granular Flow '99* (Heidelberg, 2000), D. Helbing, H. Herrmann, M. Schreckenberg, and D. Wolf, Eds., Springer.
- [141] SCHADSCHNEIDER, A., AND SCHRECKENBERG, M. Traffic flow models with 'slow-to-start' rules. *Ann. Phys.* 6 (1997), 541–551.
- [142] SCHRECKENBERG, M., BARLOVIĆ, R., KNOSPE, W., AND KLÜPFEL, H. Statistical physics of cellular automata models for traffic flow. In *Computational Statistical Physics: From Billiards to Monte Carlo* (New York, 2002), Springer, pp. 113–126.
- [143] SCHRECKENBERG, M., SCHADSCHNEIDER, A., NAGEL, K., AND ITO, N. Discrete stochastic models for traffic flow. *Phys. Rev. E* 51 (1995), 2939–2949.
- [144] SCHRECKENBERG, M., AND WOLF, D., Eds. *Traffic and Granular Flow '97* (Singapore, 1998), Springer.
- [145] SIMON, P. M., AND NAGEL, K. Simplified cellular automaton model for city traffic. *Phys. Rev. E* 58 (1998), 1286–1295.
- [146] SIMS, A. G., AND FINLAY, A. B. Scats: Splits and offsets simplified (sos). *ARRB Proceedings* 14 (1984), 17–33.
- [147] STAUFFER, D. Computer simulations of cellular automata. *J. Phys. A* 24 (1991), 909–927.

- [148] STAUFFER, D., AND AHARONY, A. *Introduction to Percolation Theory*. Taylor and Francis, London, 1992.
- [149] TAKAYASU, M., AND TAKAYASU, H. 1/f-noise in a traffic flow model. *Fractals 1* (1993), 860–866.
- [150] TRANSIMS. Transportation Analysis and Simulation System, Los Alamos National Laboratory, Los Alamos. <http://www-transims.tsasa.lanl.gov>.
- [151] TREITERER, J. Investigation of traffic dynamics by aerial photogrammatic techniques. *The Ohio State University, Technical Report PB-246094* (1975).
- [152] v. FOERSTER, H., AND ZOPF, G. W., Eds. *Principles of self-organization*. Pergamon Press, New York, 1962.
- [153] VAN KAMPEN, N. *Stochastic Processes in Physics and Chemistry*. North-Holland, 1992.
- [154] VILAR, L. C. Q., AND DE SOUZA, A. M. C. Cellular automata models for general traffic conditions on a line. *Physica A 211* (1994), 84–92.
- [155] VINCENT, R. A., MITCHELL, A. I., AND ROBERTSON, D. I. User guide to transyt. *TRRL Laboratory Report No.888 8* (1980).
- [156] VON NEUMANN, J., AND BURKS, A. W. *Theory of Self-Reproducing Automata*. Univ. of Illinois Press, Urbana, IL, 1966.
- [157] WAHLE, J., BAZZAN, A. L., KLÜGL, F., AND SCHRECKENBERG, M. The impact of real-time information in a two-route scenario using agent-based simulation. *Transp. Res. C* (2001), 399–417.
- [158] WAHLE, J., CHROBOK, R., POTTMEIER, A., AND SCHRECKENBERG, M. A microscopic simulator for freeway traffic. *Networks and Spatial Economics 2* (2002), 371–386.
- [159] WAHLE, J., NEUBERT, L., AND SCHRECKENBERG, M. A cellular automaton traffic flow model for online simulation of traffic. *Parallel Comp. 27* (2001), 719–735.
- [160] WANG, B. H., WOO, Y. F., AND HUI, P. M. Improved mean-field theory of two-dimensional traffic flow models. *J. Phys. A 29* (1995), L31–L35.
- [161] WEBPAGE. Physics of Transport and Traffic, University Duisburg-Essen(Standort Duisburg). In <http://www.traffic.uni-duisburg.de>, *Several projects concerning large scale cellular automata modelling of transportation networks are presented here*.
- [162] WILLIAMS, J. C., MAHMASSANI, H. S., AND HERMAN, R. Sampling strategies for two-fluid model parameter estimation in urban networks. *Transp. Res. A 29A* (1995), 229.
- [163] WOLF, D., SCHRECKENBERG, M., AND BACHEM, A., Eds. *Traffic and Granular Flow* (Singapore, 1996), World Scientific.
- [164] WOLFRAM, S. *Theory and Applications of Cellular Automata*. World Scientific, Singapore, 1986.

- [165] WOLFRAM, S. *A New Kind of Science*. Wolfram Media, Inc, Illinois, USA, 2002.
- [166] YUKAWA, S., KIKUCHI, M., AND TADAKI, S. Dynamical phase transition in one dimensional traffic flow model with blockage. *J. Phys. Soc. Jpn.* 63 (1994), 3609–3618.

Zusammenfassung und Ausblick

In der vorliegenden Arbeit wurde die “Clusterbildung” (Staubildung) in Zellulären Automaten (ZA) für den Straßenverkehr untersucht, mit der Zielsetzung einen Einblick in das Phänomen des Verkehrsstaus zu geben.

Das erste Kapitel führte in die Thematik dieser Arbeit ein. Im zweiten Kapitel wurden grundlegende empirische Befunde und Simulationsmodelle vorgestellt.

Der erste Teil dieser Arbeit befasste sich mit dem VDR (Velocity-Dependent Randomization) Modell für den Autobahnverkehr. Auf der Basis der “Random Walk” Theorie konnte eine analytische Beschreibung der Dynamik einzelner Staus präsentiert werden (Kapitel 3). Diese Beschreibung gibt Zugang zu wichtigen Größen der Staudynamik, wie der Lebenszeit oder der Auflösewahrscheinlichkeit und zeigt eine gute Übereinstimmung mit numerischen Ergebnissen. Dabei lassen sich die Ergebnisse auch auf andere ZA Modelle übertragen.

Neben der Dynamik einzelner Staus ist es gerade im Hinblick auf realitätsnahe ZA Simulationen wichtig, den Einfluss äußerer Faktoren zu untersuchen. Deshalb wurde in Kapitel 4 der Einfluss lokaler Störstellen auf die Staudynamik des VDR Modells untersucht. Es stellte sich heraus, dass ein völlig neuer Verkehrszustand an der Störstelle entstehen kann, der Ähnlichkeiten zum “Stop and Go” Verkehr aufweist. Die Tatsache, dass ein solcher Verkehrszustand nicht im VDR Modell ohne Störstellen existiert, unterstreicht den enormen Einfluss äußerer Faktoren auf die Staudynamik.

Um die Untersuchungen bezüglich des Einflusses äußerer Faktoren auf die Staudynamik zu vervollständigen, wurde in Kapitel 5 das VDR Modell mit offenen Randbedingungen betrachtet. Es zeigte sich, dass eine neue Einfüllstrategie eingeführt werden musste um die Hochflusszustände des Modells erzeugen zu können. Eines der wichtigsten Ergebnisse des Kapitels war, dass ein von Kolomeisky *et al.* [92] vorgeschlagenes “Maximalstrom Prinzip” auch für das VDR Modell erfüllt ist. Dieses Ergebnis ist überraschend, da ursprünglich angenommen wurde, dass das Prinzip nur gültig ist für Modelle mit einem Maximum im Fundamentaldiagramm wie z.B. dem NaSch Modell. Als weiteres Ergebnis zeigen sich zwei neue Stauphasen, die aus kompakten Staus bestehen. Zusätzlich konnte die Existenz einer neuen Hochflussphase präsentiert werden. Mit Hilfe dieser Hochflussphase wurde eine Optimierungsstrategie nachgestellt, wie sie beispielsweise im Lincoln- und Hollandtunnel in New York angewendet wird.

Der zweite Teil dieser Arbeit befasste sich mit dem Chowdhury-Schadschneider (ChSch) Modell für den Stadtverkehr. In diesem üben Verkehrsampeln den Haupteinfluss auf die Staudynamik aus. Die Untersuchungen zur “Clusterbildung” im ChSch Modell konzentrierten sich auf die Flussoptimierung im Straßennetzwerk anhand von Verkehrsampeln. Kapitel 7 befasste sich mit den Auswirkungen globaler (fester) Ampelschaltungen. Im Falle von synchronisierten Ampeln zeigte sich eine starke Abhängigkeit des Flusses von den Ampelzyklen anhand starker Oszillationen. Diese Oszillationen konnten mit Hilfe einer phänomenologischen Näherung in guter Übereinstimmung zu den numerischen Resultaten erklärt werden. Mit der Zielsetzung flexiblere Ampelschaltungsstrategien zu ermöglichen,

wurde das ChSch Modell um einen weiteren Parameter, dem so genannten "Offset", erweitert. Eine Anwendung des "Offsets" war die Etablierung einer zwei-dimensionalen "Grünen Welle" im Netzwerk. Es stellte sich heraus, dass das optimale FD der "Grünen Welle" mit dem *globalen* Optimum des ChSch Modells übereinstimmt, sodass dieses als Referenz für die anderen Strategien diene. In diesem Zusammenhang konnte ein weiterer neuer Effekt präsentiert werden. Bei hohen Dichten bestand die Möglichkeit Staus störungsfrei durch das Netzwerk zu lotsen. Dieser Effekt führte zu einer erheblichen Flusserhöhung und wurde als "Rote Welle" bezeichnet, da die Rotphasen der Ampeln an die Bewegung der Staus angepasst wurden. Obwohl die "Grüne Welle" zu deutlichen Flusssteigerungen führte, blieben die starken Oszillationen erhalten. Deshalb wurde der "Offset" in einer weiteren Strategie eingesetzt um ein zufälliges Umschalten zwischen den Verkehrsampeln zu realisieren. Damit konnten die Oszillationen vollständig unterdrückt werden.

In Kapitel 8 wurde das ChSch Modells um adaptive Ampelschaltungen erweitert. Es wurden drei adaptive Ampelstrategien vorgestellt und untersucht, wobei das optimale FD der "Grünen Welle" den Bezugspunkt für die jeweiligen Strategie bildet. Es zeigte sich, dass die adaptiven Strategien in der Lage sind, sich selbstständig nahe an das *globale* Optimum zu organisieren. Diese Ergebnisse könnten für reale Anwendungen von Nutzen sein, da die Algorithmen sehr einfach und die verwendeten Meßgrößen leicht zu bestimmen sind.

Die Hauptmotivation hinter der Einführung adaptiver Ampelschaltungen im ChSch Modell war, robuste Strategien zur Verfügung zu stellen, die auch unter realitätsnahen Verkehrsbedingungen zu hohen Flüssen führen. Dazu wurde das Modell in Kapitel 9 um inhomogene Fahrzeugverteilungen erweitert. Diese wurden zum einen durch ein zufälliges Abbiegen der Fahrzeuge an den Ampeln realisiert und andererseits durch ungleiche (feste) Dichten auf den beiden Richtungen des Netzwerkes. Im Falle des Abbiegens wurde eine starke Abhängigkeit des Flusses festgestellt. Dieser stellte sich meistens unterhalb des *globalen* Optimums ein. Der zweite Fall mit ungleicher Dichteverteilung sollte den Umstand nachstellen, dass reale Stadtnetze aus Haupt- und Nebenstraßen aufgebaut sind. Diese Art der Dichteinhomogenität erscheint realitätsnäher als ein zufälliges Abbiegen, da Verkehrsteilnehmer in der Realität feste Routenvorstellungen besitzen und nicht willkürlich an beliebigen Punkten im Straßennetz abbiegen. Für den Fall der festen Dichteinhomogenitäten führten die adaptiven Ampelstrategien zu einem Resultat nahe am *globalen* Optimum und übertrafen die globalen Strategien.

Zusammenfassend kann man sagen, dass die vorgestellten Ergebnisse einen umfassenden Einblick in die Staudynamik von ZA Modellen für den Autobahnverkehr sowie den Stadtverkehr gewähren. Der Hauptteil dieser Arbeit befasste sich mit dem Einfluss äußerer Faktoren auf die Staudynamik. Diese äußeren Faktoren können mit entsprechenden flusslimitierenden Elementen des realen Straßenverkehrs in Verbindung gebracht werden. Daher sind die Erkenntnisse aus dieser Arbeit insbesondere nützlich für realitätsnahe Verkehrssimulationen.

Im Verlauf dieser Arbeit kristallisierten sich viele neue Fragen heraus, die weitere Untersuchungen motivieren.

So stellte sich beispielsweise die Frage nach dem Einfluss der spontanen Staubildung (Stau aus dem Nichts). Dieses wichtige Element der Stauentstehung wurde in der vorliegenden Arbeit nicht berücksichtigt. Im VDR Modell können aufgrund von lokalen Geschwindigkeitsfluktuationen Staus spontan aus den metastabilen Hochflusszuständen entstehen. Infolgedessen bestimmen die Fluktuationen die Stabilität und die Lebensdauer der Hochflusszustände (staufrei). Ein Verständnis der Stauentstehung ist gerade im Hinblick auf realitätsnahe Verkehrssimulationen wichtig, da die Stabilität eines Verkehrszustandes ele-

mentar ist für die Verkehrsvorhersage. Deshalb sollte in zukünftigen Arbeiten die spontane Staubildung im VDR Modell genauer analysiert werden. Des Weiteren nehmen auch die Fluktuationsparameter p_0, p einen wesentlichen Einfluss auf die Staudynamik des VDR Modells. In dieser Arbeit wurde der “slow-to-start” Fall mit $p \ll p_0$ untersucht. Insbesondere sollte in einer zukünftigen Arbeit der Übergang des VDR Modells zum NaSch Modell $p \Rightarrow p_0$ analysiert werden da die beiden Modelle eine vollkommen unterschiedliche Staudynamik aufweisen (siehe Kapitel 2).

Bezüglich der lokalen Störstellen könnten die Gemeinsamkeiten zu Auf- und Abfahrten untersucht werden, da letztere eine bedeutende Ursache für eine Vielzahl existierender Verkehrszustände zu sein scheinen. Es wurde festgestellt, dass lokale Störstellen im NaSch Modell [30] als auch im VDR Modell [129] durchaus Ähnlichkeiten zu Szenarien mit Auf- und Abfahrten aufweisen. In diesem Zusammenhang könnte der Einfluss lokaler Störstellen auf die Dynamik von realitätsnahen ZA Modellen wie z.B. dem BL Modell [89] untersucht werden. Diese Untersuchungen erscheinen vielversprechend in Anbetracht der Tatsache, dass schon im VDR Modell die Koexistenz von großen Staus und kleinen, an die Störstelle gepinnten Staus gezeigt werden konnte. Vergleichbare Zustände wurden auch in empirischen Untersuchungen beobachtet und in Verbindung zu realitätsnahen Verkehrsmodellen gebracht, die die Fahrzeugdynamik sehr detailliert beschreiben [76, 77, 83, 90]. Hier erscheint es besonders wichtig zu verstehen, welche der beobachteten Effekte der Fahrzeugdynamik zuzuschreiben sind und welche der Störstelle.

Eine weitere wichtige Frage stellt sich im Hinblick auf die kompakten Staus, die in der Stauphase des VDR Modells unter Einfluß offener Randbedingungen entstehen. Ein vergleichbarer Verkehrszustand wurde kürzlich mit dem “Pinch Effect” (siehe Kapitel 2) in Verbindung gebracht, der vorzugsweise in der Umgebung von Auf- und Abfahrten beobachtet wird [83]. Es erscheint daher naheliegend, die in Kapitel 5 präsentierten Phasenraumdiagramme mit den empirischen Befunden zu Vergleichen um mögliche Übereinstimmungen aufzuzeigen. Zusätzlich sollten auch Phasenraumdiagramme anderer Modelle, wie z.B. dem BL Modell zum Vergleich herangezogen werden um deren Dynamik zu validieren.

In Kapitel 6 wurde schon herausgestellt, dass keine umfassende theoretische Beschreibung der Verkehrszustände des Stadtverkehrs existiert. Der Verkehr wird hier, anders als auf Autobahnen, hauptsächlich durch die topologische Struktur des Straßennetzes und die angewendeten Ampelschaltungen bestimmt. Deshalb sind die Ergebnisse des ChSch Modells eher theoretischer Natur. Dennoch erscheinen die Resultate aufgrund der einfachen Struktur des Modells, zumindest in einigen Fällen, qualitativ auf reale Verkehrssituationen übertragbar zu sein. Neben der Übertragbarkeit auf reale Verkehrsszenarien kamen im Verlauf der Untersuchungen einige neue Fragen auf, die in zukünftigen Arbeiten untersucht werden könnten. Zuerst stellt man sich aufgrund der einfachen “Manhattan” Geometrie des Straßennetzes im ChSch Modell die Frage, welchen Einfluss abweichende Geometrien auf die vorgestellten Ampelschaltstrategien hätten. Man würde erwarten, dass die adaptiven Strategien besser abschneiden, da diese flexibler auf die veränderten Verkehrsbedingungen reagieren. Des Weiteren erscheint es sinnvoll Meßgrößen individueller Fahrzeuge, wie z.B. Standzeiten oder Wartezeiten mit dem *globalen* Optimum zu Vergleichen. Aus praktischer Sicht interessieren Fragestellungen wie: Wieviele Ampeln müssten mit adaptiven Systemen ausgestattet werden, um den Verkehrsfluß zu verbessern?

Kurzfassung

Zellularautomaten (ZA) Modelle ermöglichen eine effektive Implementierung umfangreicher Verkehrsszenarien und erfreuen sich deshalb einer wachsenden Popularität. In den letzten Jahren wurden zahlreiche Modellierungsansätze auf ZA Basis vorgeschlagen.

Die vorliegende Arbeit teilt sich in zwei Bereiche. Der erste Teil befasst sich mit der Staudynamik des VDR (Velocity-Dependent Randomization) Modells, einer Verallgemeinerung des bekannten Nagel-Schreckenberg (NaSch) Modells. Das VDR Modell eignet sich besonders gut für die Analyse der Staudynamik da hier kompakte phasenseparierte Staus auftreten. Auf der Grundlage der "Random Walk" Theorie wird eine analytische Beschreibung der Staudynamik präsentiert. Die Ergebnisse aus dem Ansatz zeigen eine gute Übereinstimmung mit Computersimulationen und sind auf andere ZA Modelle für den Straßenverkehr übertragbar. Des Weiteren wird der Einfluss lokaler Störstellen auf die Staudynamik des VDR Modells untersucht. Es stellt sich heraus, dass in Abhängigkeit der Stärke der Störstelle "Stop and Go" Verkehr entstehen kann, der in dem Modell ohne Störstelle nicht auftritt. Abschließend wird der Einfluss offener Randbedingungen im VDR Modell untersucht. Mit Hilfe von Monte-Carlo Simulationen werden die Phasenraumdiagramme bestimmt. Es zeigen sich zwei neue Stau-Phasen die aus kompakten kleinen Staus bestehen. Zusätzlich bildet sich eine neue Hochflussphase in endlichen Systemen aus.

Der zweite Teil dieser Arbeit betrachtet das Chowdhury-Schadschneider (ChSch) ZA Modell für den Stadtverkehr. Bezüglich der Staubildung beeinflussen zwei Faktoren die Staudynamik des ChSch Modells. Zum einen werden die Staus an den roten Ampeln der Kreuzungen erzeugt und andererseits wird deren Dynamik durch das NaSch Modell bestimmt. Ausgangspunkt der Untersuchungen sind globale (feste) Ampelschaltstrategien. Hier findet man eine starke Abhängigkeit des Flusses von den Ampelphasen, die sich anhand von Oszillationen manifestiert. Im weiteren Verlauf der Arbeit wird dann der Einfluss adaptiver Ampelschaltstrategien untersucht. Es zeigt sich hier, dass die adaptiven Ampeln in der Lage sind, das System an einen Zustand nahe des Optimums zu führen. Mit der Zielsetzung eine realistischere Fahrzeugverteilung im Straßennetz zu erzeugen, wird das ChSch Modell mit inhomogenen Dichteverteilungen untersucht. In diesem Fall zeigen die adaptiven Strategien eine bessere Effektivität als die globalen.

Danksagung

Mein herzlicher Dank gilt den vielen Menschen, die zum Gelingen dieser Arbeit beigetragen haben.

Der allererste Dank geht an Prof. Dr. Michael Schreckenbergr für die Betreuung der Arbeit, die wertvollen Anregungen und Diskussionen und für die Schaffung idealer Arbeitsbedingungen.

An dieser Stelle möchte ich PD Dr. Andreas Schadschneider für die hervorragende freundschaftliche und fachliche Zusammenarbeit danken.

Dass mir die am “Lehrstuhl von Physik und Verkehr” verbrachten Jahre in guter Erinnerung bleiben werden, ist nicht zuletzt der Verdienst der Mitarbeiterinnen und Mitarbeiter während dieser Zeit. Mein Dank geht an: Roland Chrobok, Birgit Dahm, Jörg Esser, Kai Fröse, Sigudur Havstein, Torsten Huisinga, Oliver Kaumann, Hubert Klüpfel, Wolfgang Knospe, Florian Mazur, Tim Meyer-König, Lutz Neubert, Andreas Pottmeier, Andre Stebens, Joachim Wahle, Nathalie Waldau, Matthias Woltering und falls ich jemanden vergessen habe natürlich auch an Ihn.

Insbesondere möchte ich an dieser Stelle Torsten Huisinga erwähnen, der mich während des Studiums, der Diplomarbeit und Doktorarbeit begleitet hat und zu einem lieben Freund geworden ist. Das gleiche gilt für Wolfgang Knospe der mir auch im Laufe der Jahre ans Herz gewachsen ist.

Mein besonderer Dank geht an Torsten Huisinga, Hubert Klüpfel, Andreas Pottmeier, PD Dr. Andreas Schadschneider und Matthias Woltering für das Korrekturlesen.

Meiner Freundin Ina Topeters danke ich für die Verständnisbereitschaft und Unterstützung während der Verwirklichung dieser Arbeit.

Der größte Dank gebührt meinen Eltern Ivan und Stefića und meiner Schwester Danijela für die stete Unterstützung nicht nur während meiner Ausbildung.

Lebenslauf

Persönliche Daten

Name: Robert Barlović
Geburtsdatum: 12.01.1974
Geburtsort: Mönchengladbach
Familienstand: ledig
Staatsangehörigkeit: deutsch

Schul- und Ausbildung

1984 – 1990 Kath. Hauptschule Neuwerk, Mönchengladbach
Mai 1990 Fachoberschulreife
1990 – 1993 Ausbildung zum Industriemechaniker, A. Monforts GmbH
und Co, Mönchengladbach
Mai 1993 IHK Prüfungszeugnis
1991 – 1993 Berufliche Schulen für Technik, Mönchengladbach
Mai 1993 Fachhochschulreife (Abendform)

Hochschulstudium

Okt. 1993 Immatrikulation an der Gerhard-Mercator Universität Duisburg, Studiengang Physik (DII)
Sep. 1995 Vordiplom, Erwerb der fachgebundenen Hochschulreife aufgrund bestandener Brückenkurse
April 1998 Abschluß der Diplomarbeit bei Prof. Dr. Michael Schreckenberg
seit Juli 1998 Anfertigung der vorliegenden Dissertation unter Anleitung von Prof. Dr. Michael Schreckenberg

Arbeitsverhältnisse

April 1996 – Juni 1998 Studentische Hilfskraft am Lehrstuhl Physik von Transport und Verkehr der Gerhard-Mercator Universität Duisburg
seit Juli 1998 Wissenschaftlicher Angestellter am Lehrstuhl Physik von Transport und Verkehr der Gerhard-Mercator Universität Duisburg

Erklärung

Ich versichere, dass ich die von mir vorgelegte Dissertation selbständig angefertigt, die benutzten Quellen und Hilfsmittel vollständig angegeben und die Stellen der Arbeit – einschließlich der Abbildungen –, die anderen Werken im Wortlaut oder dem Sinn nach entnommen sind, in jedem Einzelfall als Entlehnung kenntlich gemacht habe; dass diese Dissertation noch keiner anderen Fakultät oder Universität zur Prüfung vorgelegen hat; dass sie – abgesehen von unten angegebenen Teilpublikationen – noch nicht veröffentlicht worden ist sowie, dass ich eine solche Veröffentlichung vor Abschluß des Promotionsverfahrens nicht vornehmen werde. Die Bestimmungen dieser Promotionsordnung sind mir bekannt. Die von mir vorgelegte Dissertation ist von Herrn Professor Dr. Michael Schreckenberg betreut worden.

Duisburg, den 11. März 2003

Teilpublikationen

R. Barlović, T. Huisinga, A. Schadschneider, and M. Schreckenberg, Open boundaries in a cellular automaton model for traffic flow with metastable states, *Phys. Rev. E* 66 (2002), 046113

R. Barlović, E. Brockfeld, A. Schadschneider, and M. Schreckenberg, Optimal traffic states in a cellular automaton model for city traffic, in *Traffic and Granular Flow 01*, M. Fukui, Y. Sugiyama, M. Schreckenberg, D. E. Wolf (2003)

A. Pottmeier, R. Barlović, W. Knospe, A. Schadschneider, and M. Schreckenberg, Localized defects in a cellular automaton model for traffic flow with phase separation, *Physica A* 308 (2002), 471-482

E. Brockfeld, R. Barlović, A. Schadschneider, and M. Schreckenberg, Optimizing traffic lights in a cellular automaton model for city traffic, *Phys. Rev. E* 64 (2001), 056132

R. Barlović, A. Schadschneider, and M. Schreckenberg, Random walk theory of jamming in a cellular automaton model for traffic flow, *Physica A* 294 (2001), 525-538

R. Barlović, L. Santen, A. Schadschneider, and M. Schreckenberg, Metastable states in CA models for traffic flow, in *Traffic and Granular Flow 97*, M. Schreckenberg and D. E. Wolf (1998), 335-340

R. Barlović, L. Santen, A. Schadschneider, and M. Schreckenberg, Metastable states in cellular automata for traffic flow, *Eur. Phys. J. B* 5 (1998), 793-800